

REVIEWS OF TOPICAL PROBLEMS

PACS numbers: 52.25.Xz, 94.30.C –, 95.30.Qd

100th ANNIVERSARY OF THE BIRTH OF V L GINZBURG

Thin current sheets: from the work of Ginzburg and Syrovatskii to the present day

L M Zelenyi, H V Malova, E E Grigorenko, V Yu Popov

DOI: https://doi.org/10.3367/UFNe.2016.09.037923

Contents

Abstract. We outline the history and development of the theory of thin current sheets in a collisionless space plasma from the early ideas of V L Ginzburg and S I Syrovatskii to the present day. We review the key achievements of the quasi-adiabatic theory, which provided insight into the fine structure of thin current sheets and enabled a comparison with experiment. This comparison showed the quasi-adiabatic approach to be more effective than the classical MHD approximation. With the development of the quasi-adiabatic theory in the last two decades, the existence of a number of new thin current sheet features, such as multi-scaling, metastability, and embedding, has been predicted and subsequently confirmed in situ; the role of individual particle populations in the formation of the current sheet fine structure has also been investigated. The role of nonadiabatic effects in accelerating plasma beamlets interacting with current sheets is examined. Asymmetry mechanisms in thin current sheets in the presence of a magnetic shear component are described. A study is carried out of current sheet self-organization processes leading to the formation of a shear magnetic component consistent with currents flowing in the plasma. It is demonstrated that the ongoing development of the theory of thin current structures is a logical continuation of Syrovatskii's and Ginzburg's ideas on cosmic rays and reconnected current sheets in the solar corona.

Keywords: collisionless space plasma, thin current sheets, quasi-adiabatic theory, acceleration and scattering of plasma particles, beamlets

L M Zelenyi Space Research Institute, Russian Academy of Sciences, ul. Profsoyuznaya 83/32, 117342 Moscow, Russian Federation; Moscow Institute for Physics and Technology (State University), Institutskii per. 9, 141700 Dolgoprudnyi, Moscow region, Russian Federation
E-mail: lzelenyi@iki.rssi.ru
H V Malova Space Research Institute, Russian Academy of Sciences, ul. Profsoyuznaya 83/32, 117342 Moscow, Russian Federation; Lomonosov Moscow State University, Skobel'tsyn Institute of Nuclear Physics, Leninskie gory 1, str. 2, 119991 Moscow, Russian Federation
E-mail: hmalova@yandex.ru
E E Grigorenko Space Research Institute, Russian Academy of Sciences, ul. Profsoyuznaya 83/32, 117342 Moscow, Russian Federation
E-mail: elenagrigorenko2003@yandex.ru
V Yu Popov Lomonosov Moscow State University, Faculty of Physics, Leninskie gory 1, str. 2, 119991 Moscow, Russian Federation; Space Research Institute, Russian Academy of Sciences, ul. Profsoyuznaya 83/32, 117342 Moscow, Russian Federation; National Research University Higher School of Economics, ul. Myasnitskaya 20, 101000 Moscow, Russian Federation
E-mail: masterlu@mail.ru

Received 19 September 2016
Uspekhi Fizicheskikh Nauk **186** (11) 1153 – 1188 (2016)
DOI: 10.3367/UFNr.2016.09.037923
Translated by S D Danilov; edited by A M Semikhatov

1. Thin current sheets. History of the question

1.1 Ginzburg's and Syrovatskii's ideas on the origin of cosmic rays and their interaction with cosmic magnetic fields. Syrovatskii's ideas on reconnecting current sheets

Over his long and creative life in science, Ginzburg made masterly studies devoted to an extraordinarily wide spectrum of problems: from astrophysics and optics of crystals [1–3] (see also the references therein) to superconductivity and superfluidity [4–6]. In particular, he was interested in questions related to the origin and acceleration mechanisms of cosmic rays (CRs). Ginzburg (either alone or together with Syrovatskii) wrote three review articles for *Physics–Uspekhi* [7–9] on the origin of CRs, and, several decades later, in 1993, yet another review summarizing the research in this area over four decades [10]. Notably, Ginzburg's idea on the galactic origin of CRs then received experimental verification.

In monograph [9], Ginzburg and Syrovatskii noted that galactic cosmic rays (GCRs) represent streams of high-energy particles capable of interacting with magnetic fields in space, possibly modifying their structure. In turn, magnetic fields in space may affect the characteristics of cosmic rays, in particular, the observed energy spectra. The Solar System is permeated, in addition to GCRs, by so-called solar cosmic rays (SCRs) — particles of lower energy than GCRs, originating from flare processes on the Sun and in the solar wind. Deeper knowledge of the origin of SCRs and the transformation accompanying their propagation in the interplanetary space was necessary for developing ideas on plasma processes and structures that serve as sources of SCRs or interact with SCRs along their propagation path. Prompted by Ginzburg, theoretical and laboratory studies on reconnection processes in current sheets [11–14] were initiated at the Lebedev Physical Institute of the USSR Academy of Science (Russian Academy of Science, RAS) (FIAN) in the 1960s. These studies were intended to answer the question of the origin of solar flares as the sources of SCRs. Ginzburg was certain of the utmost importance of research carried out by Syrovatskii on reconnection processes in current sheets, and always called for the coordination of research related to solar flares with regard to results from theory and laboratory experiments [15]. This idea now has a continuation. The results of laboratory modeling carried out by A G Frank and colleagues are compared with direct measurement results pertaining to similar phenomena in cosmic plasma [16].

According to the scenario proposed by Syrovatskii [15, 17], the energy of solar flares is first accumulated in current sheets and then released in an explosive way on their breakup or disruption.

Later on, with further progress in experimental observations in near-terrestrial space (in particular, through the Cluster multi-satellite mission launched in 2000), the ideas that relatively thin current sheets, several proton gyroradii in thickness [18], playing a role of magnetic energy reservoirs, can spontaneously break up, releasing a large amount of energy by developing instabilities (see Ref. [19] and the references therein), were brilliantly confirmed for Earth's magnetosphere [20–22].

It was shown that similar metastable structures can form in space predominantly at the boundaries between magnetic fields of different directions [19]. The assumed range of scales can be very broad: from magnetospheres of the Solar System planets [23, 24] and magnetic loops in the solar corona [25] to magnetic fields of astrophysical objects with strong magnetic fields — pulsars [26]. After intense debates lasting years within the international scientific community [27–30], theoretical stability analysis of thin current sheets (TCSs) culminated in the theory of metastable current sheets [19, 31], and the concept of magnetic reconnection in current sheets is now generally accepted [22, 32–34].

We note that TCSs have long been regarded as infinitely thin magnetohydrodynamical (MHD) discontinuities, and their description was carried out mainly in the MHD framework [13–15, 35]. Today, based on numerous observations in space, it has become clear that TCSs have a small but finite thickness; they are characterized by a fine structure and special, quasi-adiabatic [36] (see Section 2.1) dynamics of plasma particles. As a consequence, kinetic models [19] turn out to be very efficient in describing TCSs; they allow us to construct and explore a new type of plasma equilibria and their dynamics, find how their structure depends on boundary and initial conditions, and also reveal kinetic nonadiabatic effects related to the small thickness of TCSs and plasma particle dynamics (so-called beamlets [37]) (see Section 2.4). In this review, we discuss the main recent advances in research pertaining to the structure of TCSs and the embedded particle dynamics.

1.2 Beginning of experimental observations of thin current structures in the solar corona, in the magnetospheres of planets, and in shock waves. Importance of the Syrovatskii model for explaining solar flares

The formation of current sheets (CSs) and magnetic reconnection inside them constitute the most important physical processes responsible for the transport and acceleration of cosmic plasma. The scales of these processes lie in the range from the size of planetary magnetospheres to astrophysical and galactic scales [38–40]. Some spiral galaxies host anomalously long-lived structures with oppositely directed magnetic fields with a lifetime comparable to the time of the existence of the galaxy itself [41]. These magnetic configurations can form as a result of nonlinear evolution of physical fields in which wide regions with slow field variations are separated by small-volume regions characterized by a sharp gradient of the magnetic field and frequent field sign reversals (so-called internal transitional layers). Studying and modeling processes enabling the formation of such structures and their evolution plays an important role in clarifying the mechanisms related to the generation, development, and decay of astrophysical and geophysical magnetic fields [42].

Theoretical studies devoted to the models of magnetospheres of accreting neutron stars led to solutions in the form of axisymmetric CSs that support disk-shaped magnetic structures around stars in a self-consistent way [43]. By exploring accreting magnetic stars, it has been shown that not only flat (disk-shaped) but also cylindrical current structures with poloidal and toroidal currents can form in their magnetospheres [44]. Notably, such CSs represent long-lived configurations [45].

Progress in the satellite monitoring of cosmic plasma as well as in methods of local and remote analysis of its characteristics in electromagnetic frequency bands that are not accessible from the ground contributed to broadening the knowledge on the structure and dynamics of CSs in the magnetospheres of Earth and planets as well as in the vicinity of the Sun. For example, it has been shown that CSs in the

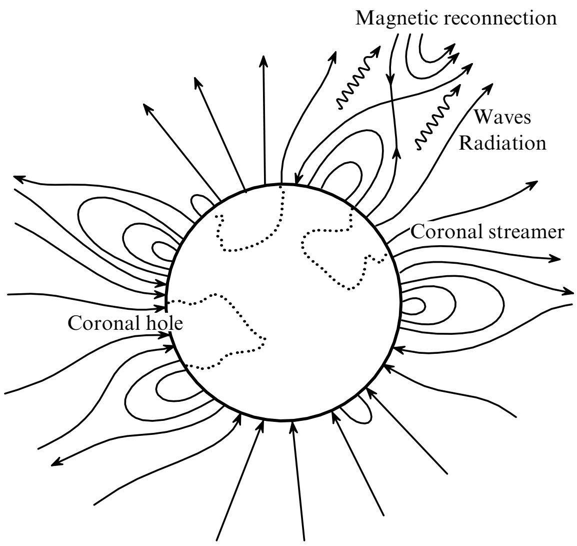

Figure 1. Schematic of the solar corona, its magnetic field loops, streamers, and coronal holes (regions with reduced density and temperature of plasma). Flares occur in the vicinity of magnetic reconnection regions, the X-lines, and are accompanied by waves and turbulence.

solar corona can form in places where magnetic loops either intersect or come close to one another [13, 14, 35, 36]. Vertical banded CSs can also be located inside helmet-shaped magnetic structures (streamers) stretching radially from the Sun's surface [46]. Instabilities developing in these current structures can initiate processes of reconnection and dissipation spawning solar flares. In the vicinity of neutral magnetic regions — X-lines — energy is released in the form of heated and accelerated streams of matter and wave activity (solar flares are clearly seen in the X-ray and gamma ranges) (Fig. 1). Large-scale matter ejections can also occur from the solar corona (so-called coronal mass ejections, CMEs) [46–49].

Solar flares, being powerful manifestations of solar activity (the energy release can reach 10^{32} erg for 10^3 s) affect the state of Earth's atmosphere, planets, and plasma surrounding them in the most direct way. An important feature of flares is that a large portion of energy is released in a nonthermal form, i.e., as ejected matter, accelerated particles, and hard electromagnetic radiation [50]. For this reason, studies of flares play a key role in clarifying general mechanisms for generating high-energy particles and cosmic rays in the solar wind.

Three phases in the evolution of current sheets in the solar corona are identified in [50]. The initial phase lasts from several to several dozen hours and encompasses the formation and expansion of a current sheet. The mechanism of Coulomb plasma heating by a strong current in the sheet dominates through this phase, whereas the current sheet itself can be considered a quasistationary structure. Most interesting for research is the second, explosive, phase during which enormous energy stored in the sheet is released within a time interval of about 10 s.

The main stages of energy transformation comprise hydrodynamical motion (sheet disruption), thermal heating resulting from anomalous resistance in the disruption region, and the generation of streams of accelerated plasma particles. During the third, 'hot', phase of the flare, a hot coronal region is forming where the main energy dissipation mechanism is in all probability due to turbulent heating. The theoretical problem of exploring current sheets in the solar corona naturally breaks into two parts: internal and external. The first includes an explanation of the physics behind the explosive energy release in a bounded spatial region, which takes a necessary step toward clarifying the nature of flare events. Unfortunately, such information can only be retrieved indirectly, by analyzing the effect of flare activity on the interplanetary space and Earth. The second problem deals with the analysis of the effect of energy ejections on the heliosphere as a whole and on the near-terrestrial space in particular.

Studies by Syrovatskii were instrumental in solving the problem of the nature of solar flares [51]. His simple and elegant model (the Syrovatskii model) of a current sheet in a high-conductivity plasma [15, 16, 35], which treats the CS as a surface of MHD discontinuity separating oppositely directed magnetic fields, proved its efficiency in explaining the physics of solar flares. Further advances in MHD modeling [52–54] contributed in an efficient way to uncovering the physics of nonstationary processes on the Sun [55–57].

Owing to satellite-based studies of recent decades, current sheets were also discovered in the solar wind, as the flow of particles with a frozen magnetic field, traveling radially from the Sun at a supersonic speed [52]. Invariably observed there is a heliospheric current sheet (HCS) — a quasi-stationary, relatively thin (about 10^4 km in thickness) current structure, located predominantly in the equatorial belt of the Sun and separating oppositely directed magnetic fields [58]. Far from the star, because of the nonalignment of solar magnetic and rotational axes, the HCS takes the folded form of a ballet tutu and, as a result, at a distance of 1 astronomical unit (a.u.) (1 a.u. $\approx$ 215 solar radii is the distance between Earth and the Sun), the interplanetary magnetic field (IMF) comes to Earth with a prevailing north or south component. Furthermore, the structure of the equatorial current can be rather complex: numerous TCSs can be present around the HCS, arising either at boundaries of differing plasma flows in the solar wind or as a result of layering of the HCS in nonstationary conditions of the solar wind.

We note that despite the available observational data, the theoretical understanding of the fine structure of CSs, in particular, in the corona and solar wind, is still insufficiently complete. Loud noise accompanying measurements of atomic and ion spectral lines hinders measurements of the fine structure of current configurations and related magnetic fields in the solar chromosphere and corona [59]. Only relatively thick current structures within the CMEs are typically accessible through measurements [60, 61]. As a consequence, the current structures in the vicinity of the Sun are basically a subject of theoretical and model research [58–60].

Compared to solar CSs, much better explored are the CSs in magnetospheres of Earth and other planets of the Solar System, whether possessing their own magnetic field (Mercury, Jupiter, Saturn, Uranus, and Neptune) or lacking it (Venus and Mars). It is natural that Earth's magnetosphere is the best explored one.

After the first data on Earth's magnetic field from space became available, Ness proposed in 1962 [62] that Earth's magnetosphere on the night side, instead of being dipole-shaped, has the shape of a highly stretched conical tube that broadens with the distance from Earth and, in analogy with comets, is called the 'magnetotail'. The surface of the tail where Earth's magnetic field is separated from the solar wind

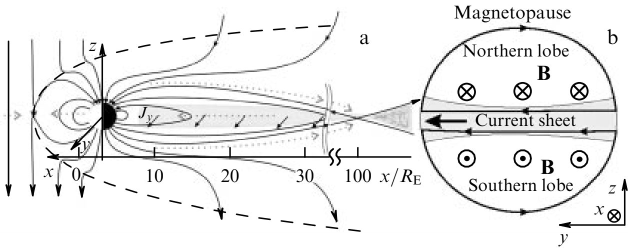

Figure 2. Schematic of magnetosphere sections by the planes (a) xz and (b) yz. A current with a density J_y flows in the tail neutral region. The CS is located between the northern and southern lobes of the magnetosphere filled with a rarefied plasma. The magnetospheric magnetic field lines reconnect at the magnetopause (the dashed line in panel a) with the interplanetary magnetic field. The dashed arrows in panel a show the direction of large-scale convection of magnetic field lines to the nocturnal side where at a distance on the order of $100R_E$ a reverse reconnection of magnetospheric and interplanetary magnetic fields takes place. At even further distances, the transverse magnetic field B_z becomes turbulent, but the configuration with field reversal is preserved.

is called the magnetopause. The solar wind flow along Earth's dipole magnetic field is the factor explaining why such an elongated configuration of the magnetosphere forms on the nocturnal side of Earth [63]. The speed of the solar wind ranges from 300 to 1000 km s^{-1} in Earth's orbit, the temperature of plasma particles is from 10 to 50 eV, and their density is between 1 and 10 cm^{-3}. For the southward direction of the interplanetary magnetic field, favorable conditions are created for the reconnection between the solar wind and magnetosphere field lines; the reconnected lines are then transported by the solar wind to the tail. The reverse reconnection of magnetic field lines takes place at a distance of about $100R_E$ from Earth ($R_E \approx 6400$ km is Earth's radius), where the far neutral line forms. The reconnected field lines on Earth's side move with the convective flow to the planet, and the lines staying in the solar wind are blown away from Earth together with the solar plasma.

Figure 2 shows a schematic of Earth's magnetosphere in two sections xz and yz. For the uniformity of exposition, here and below we use the traditional geocentric solar magnetospheric (GSM) reference frame, with the x axis directed from the center of Earth to the Sun, the z axis lying in the plane passing through the x axis and the axis of the geomagnetic dipole, and the y axis, completing them to a right-hand reference frame, in the dawn–dusk direction. The large-scale current J_y crosses the tail from the dawn side to the dusk side, maintaining oppositely directed magnetic fields in the northern and southern lobes of the magnetosphere. This current branches at the magnetopause and closes along it, forming a giant current system resembling a theta-pinch, as shown in Fig. 2b.

In the neutral sheet of a CS, the sign of the B_x component of the magnetic field reverses; at the ends of a CS, close to the magnetopause, it reaches $\sim 20-30$ nT, whereas the component B_z, normal to the sheet (with a magnitude of the order of 1–2 nT) is continuous and positive ($B_z > 0$) in the part of the tail that is close to Earth. The cause of this behavior is a generic connection between the B_z component and the field of Earth's magnetic dipole directed northward in the equatorial plane. The other, alternating-sign magnetic field component B_x is supported in a self-consistent way by the current flowing transverse to the tail. At distances of the order of or greater than $100R_E$, the influence of Earth's magnetic field weakens such that the normal component practically disappears on average, the field fluctuates, and the configuration becomes turbulent. Nevertheless, the CS of Earth's magnetotail preserves its structure with antiparallel field lines at distances up to 1.5 million km from Earth, and possibly even further. The CS thickness in the tail is not constant: it depends on both the location in space (the closer to Earth, the stronger the influence of the planetary dipole field is and the greater the thickness of the CS under quiet conditions) and global magnetospheric perturbations — substorms, during which the CS thickness can vary substantially.

Magnetic substorms are caused by the interaction between the solar wind and Earth's magnetic field [64]. The solar wind is a flow of hot proton–electron plasma with small (up to 5%) inclusions of helium nuclei and heavy ions with a frozen interplanetary magnetic field (IMF) having a sectorial structure. In its motion in the ecliptic plane, Earth alternately enters sectors with an oppositely directed magnetic field (predominantly northward or southward in the GSM reference plane). The southward IMF creates favorable conditions in the head part of Earth's magnetosphere for active reconnection of magnetic field lines of the solar wind and Earth's magnetosphere. The reconnected field lines are carried downstream to the magnetotail region, which is accompanied by a sharp increase in the magnetic flux in the tail, tail contraction, and amplification of the large-scale magnetic field E_y inside it. Plasma drift in the direction toward the neutral plane with a velocity $\mathbf{v}_d \sim \mathbf{E}_y \times \mathbf{B}_z$ can lead to the formation of a particularly thin CS with the thickness from 200 to 2000–3000 km [20–22, 33]. Under quiet conditions, the CS thickness in this region is $(1-2)R_E$ on average.

The main characteristics of TCSs differ essentially from those of CSs under quiet conditions in the magnetosphere. Satellite measurements provide the following main characteristics of TCSs (see review [36]): (1) the small sheet thickness $L \sim \rho_i \sim 250-1000$ km (ρ_i is the ion gyroradius); (2) the high current density 10 nA m^{-2}, which is an order of magnitude higher than the transverse current through the tail under quiet conditions; (3) a small ratio of the normal and tangent magnetic field components at the sheet edges, $B_z/B_x \sim 0.1$; (4) embedding of TCSs into a broader plasma sheet and noncoincidence of their profiles [20, 66]; (5) anisotropy of the longitudinal–transverse distribution in plasma velocities (as a rule, with $v_\parallel^2 > v_\perp^2$); (6) transfer of a substantial current by ions in open orbits [called Spacer orbits (see Section 1.3)] [36, 68]; (7) bifurcated (split) current profile in the TCSs; (8) frequent asymmetry of the profile with respect to the neutral plane [22, 69].

The formation of TCSs from a thick configuration takes from 30 min to 2 h, which means that this process can be viewed as a quasistationary evolution [70]. A TCS is characterized by an excess of free energy, which can be released through the development of plasma instabilities. These instabilities arise spontaneously; they are accompanied by local disruption in the CS, while the processes of energy dissipation bears an explosive character [31]. As a result of TCS disruption, a large amount of energy is rapidly released (within a time interval of the order of several dozen seconds) in the form of energy of accelerated particles, heated plasma streams, and radiated waves [29]. After long debates, the scientific community embraced the idea that the main type of instability responsible for the disruption of TCSs is the so-called tearing mode [71, 72], leading to the splitting of CSs into separate current threads with the formation of large-scale plasmoids — closed plasma 'bubbles'. The tearing mode helped to explain the processes leading to the formation of X-lines in TCSs, which are detected by satellites. The tearing mode is supposed to trigger a chain of substorm plasma processes at all levels [65], from microscales to meso- and global scales in Earth's magnetosphere.

Further stages of substorm development are studied sufficiently well: the streams of plasma head to the high-latitude ionosphere following the reconnected field lines of southern and northern lobes of the magnetosphere, giving rise to polar auroras. Simultaneously, a giant plasmoid is formed in the magnetotail of Earth's magnetosphere (with the length along the x axis being from $10R_{\mathrm{E}}$ to several dozen R_{E}), which moves away from Earth, carrying a fraction of the high-energy plasma [63].

Summarizing this section, it can be argued that TCSs are universal magnetic plasma structures in the global hierarchy of cosmic systems, from galactic to stellar and planetary systems. TCSs can be key contributors to the formation of quasistationary magnetic configurations such as internal transitional layers in spiral galaxies, disk magnetic structures in neutron stars, and current sheets on the Sun and in planetary magnetospheres. It is recognized at present that TCSs can play the role of reservoirs of magnetic energy that can be released in an explosive manner; this, in turn, governs the dynamics of many plasma processes in space, in particular, plasma transport and heating.

1.3 Stages in the development of the theory of current equilibria

The task of finding plasma equilibria in kinetic theory reduces to solving the Vlasov–Maxwell system of equation for the magnetic and electric fields and the plasma distribution function in a CS:

$$\mathbf{v}\,\frac{\partial f_\alpha}{\partial \mathbf{r}}+\frac{q}{m}\left(\mathbf{E}+\frac{1}{c}\,\mathbf{v}\times\mathbf{B}\right)\frac{\partial f_\alpha}{\partial \mathbf{v}}=0\,,\qquad \alpha=\mathrm{i},\mathrm{e}\,,\tag{1}$$

$$\operatorname{rot}\mathbf{B}=\frac{4\pi}{c}\sum_{\alpha=\mathrm{i,e}}\int \mathbf{v}f_\alpha(\mathbf{v},\mathbf{r})\,\mathrm{d}\mathbf{v}\,,\tag{2}$$

$$\operatorname{div}\mathbf{E}=4\pi\sum_{\alpha=\mathrm{i,e}}\int e f_\alpha(\mathbf{v},\mathbf{r})\,\mathrm{d}\mathbf{v}\,.\tag{3}$$

Here, $\mathbf{E}=-\operatorname{grad}\varphi$ is the electric field, φ is the electrostatic potential, the derivative $\partial B/\partial t=0$, and hence phenomena considered here are stationary, and the plasma density is

$$n_\alpha(z)=\int f_\alpha(z,\mathbf{v})\,\mathrm{d}\mathbf{v}\,,\qquad \frac{1}{2}\sum_{\alpha=\mathrm{e,i}} n_\alpha(z)\Big|_{z\to\pm\infty}=n_0\,.$$

The boundary conditions for the fields $B_x(z)|_{z\to\pm\infty}=B_0$; $\varphi(z)|_{z\to\pm\infty}=0$ are determined by the geometry of the system under consideration and the plasma density n_0 at infinity. The indices $\alpha=\mathrm{i,e}$ correspond to ions and electrons. We assume that at the distances of interest ($\sim\rho_{\mathrm{i}}$), the plasma can be considered as quasi-neutral, i.e., $n_{\mathrm{i}}\approx n_{\mathrm{e}}$.

Solving the full system of equations (1)–(3) presents a rather difficult computational task; hence, as a rule, strongly simplified current configurations that allow analytic or semi-analytic solutions are considered. Simple one- or two-dimensional plasma equilibria are commonly considered, whereas the plasma distribution function is whenever possible taken as a function of the integrals of motion of plasma particles [73] [according to the Liouville theorem, such a distribution function is constant in the entire space, which makes solving system (1)–(3) substantially easier]. Also, when solving magnetospheric problems, the longitudinal (along current lines) y-components of the magnetic and electric fields are routinely ignored, i.e., it is assumed that $B_y=0$ and $E_y=0$.

Even several decades ago, when satellite observations in the magnetotail were less abundant, it was a common practice to conceive the current sheet in the tail as a relatively thick, quasi-equilibrium plasma configuration several dozen ion gyroradii in thickness with an isotropic plasma distribution maintained by plasma pressure gradients in the direction toward Earth. This configuration is being constantly destroyed in an explosive way during substorms, i.e., is unstable. One of the first and simplest one-dimensional models of such 'thick' equilibrium was the kinetic model by Harris [74], which is still being used to analyze and interpret the research results related to Earth's magnetosphere.

In the Harris model [74], the plasma distribution function depends on two integrals of motion of the particles: the total energy $W_0=m_\alpha v^2/2$ and the generalized momentum $P_y=m_\alpha v_y+(e/c)A_y(z)$, whereas the self-consistent tangent component of the magnetic field B_x, the current density j_y, and the plasma density n depend only on the coordinate z that is transverse to the current. Then, as a result of simplifications, system (1)–(3) reduces to the following one [75]:

$$\begin{aligned}
&f_\alpha(W_0,P_y)=\mathrm{const}\,,\\
&\operatorname{rot}\mathbf{B}_x=\frac{4\pi}{c}\sum_{\alpha=\mathrm{i,e}}\int \mathbf{v}f_\alpha(\mathbf{v},z)\,\mathrm{d}\mathbf{v}\,,\\
&\sum_{\alpha=\mathrm{i,e}} q_\alpha n_\alpha=0\,,\quad \varphi=0\,.
\end{aligned}\tag{4}$$

The distribution function in the Harris model is taken as

$$f_\alpha=n_0\left(\frac{m_\alpha}{2\pi T_\alpha}\right)^{3/2}\exp\left(-\frac{W_0}{T_\alpha}+\frac{n_\alpha P_y}{T_\alpha}-\frac{m_\alpha V_{\alpha y}^2}{2T_\alpha}\right),\tag{5}$$

where T_α is the temperature of α-type particles ($\alpha=\mathrm{i,e}$), m_α is the mass, and $V_{\alpha y}$ is the stream velocity (quasineutrality requires that $V_{\mathrm{i}y}/T_{\mathrm{i}}=-V_{\mathrm{e}y}/T_{\mathrm{e}}$).

The equilibrium solutions for the tangent magnetic field $B_x(z)$ and the plasma density $n(z)$ take the form [74]

$$\begin{aligned}
&B_x(z)=B_0\tanh\frac{z}{L}\,,\\
&n(z)=\frac{n_0}{\cosh^2(z/L)}\,.
\end{aligned}\tag{6}$$

The half-width of CSs is determined by the temperatures and density of plasma components (protons and electrons) and their relative velocity [29]:

$$L=\frac{c}{V_{\mathrm{i}y}-V_{\mathrm{e}y}}\sqrt{\frac{3(T_{\mathrm{i}}+T_{\mathrm{e}})}{4\pi n_0 e^2}}\,.\tag{7}$$

A distinguishing feature of the Harris solution is the identical functional dependence on the transverse coordinate z of the current density $j_y(z)$ and the plasma density $n(z)$, which follows from the form of solution (6). In the Harris model, the magnetic field lines on both sides of the neutral plane $z=0$ are parallel and oppositely directed, and hence the normal component of the magnetic field B_z vanishes. Plasma particles, on the one hand, travel along magnetic field lines, and on the other hand, drift transverse to them in the y direction due to diamagnetic drift and support the self-consistent current in the system.

Because the actual magnetic field in the magnetotail is nonuniform along the x coordinate (it decays in the direction from the Sun), great attention has been devoted to constructing two-dimensional current equilibria. There has been success in generalizing the Harris model taking inhomogeneity into account, which is achieved by adding an arbitrary slowly varying function $F(x)$ to solution (6) [27, 76, 77]:

$$\begin{aligned} B_{0x}(x,z) &= -B_0 F(x)\tanh\left(F(x)\,\frac{z}{L}\right), \\ n(x,z) &= n_0\left\{\frac{F(x)}{\cosh\left[F(x)(z/L)\right]}\right\}^2. \end{aligned} \tag{8}$$

With more information available on Earth's magnetosphere, it has become clear that the Harris model and its modifications do not take into account that a small 'residual' normal component B_z originating from Earth's dipole field is present in the magnetotail practically over all of its extent. It turns out that if the normal component is added to the Harris model, plasma equilibrium becomes impossible. In this case, system of equations (4) does not have a stationary solution. The reason is that in the presence of a normal B_z component of the magnetic field, the magnetic configuration structure changes topologically. In the Harris model, each particle in its gyromotion remains 'glued' to its field line; hence, no vertical plasma mixing. Accounting for the normal magnetic component radically modifies the topology of plasma flows: they move from the northern to the southern hemisphere experiencing mixing, as shown schematically in Fig. 3.

Magnetic field lines are anti-parallel in Fig. 3a in the upper and lower half-planes, whereas velocities of plasma flows are parallel to the neutral plane. Figure 3b demonstrates the classical picture of the magnetotail with a relatively small normal component B_z and a large component B_x, $B_x \gg B_z$, outside the CS. Figure 3b indicates that the B_x component changes sign in the neutral plane $z = 0$; such a field is also referred to as reversed.

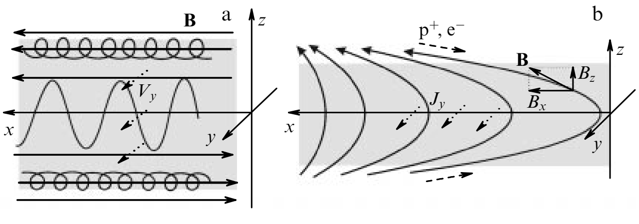

Figure 3. Comparison of one-dimensional Harris model (a) with a two-dimensional magnetic field model (b) where the transverse component B_z is taken into account. The gray color marks the current sheet region. Panel a shows characteristic trajectories of plasma particles, field lines, and plasma drift velocity V_y. The dashed arrows in panel b indicate the direction of magnetized plasma flows into the current sheet. The directions of vectors of local magnetic field $\mathbf{B} = \{B_x, B_z\}$ and current density J_y are shown. A comparison of current configurations indicates that in the one-dimensional Harris model Ampère's force along the x-axis is not balanced by other forces.

Further development of magnetotail models turned to constructing two-dimensional 'thick' equilibria. It was necessary to propose a simple and convenient model that would enable studying the main characteristics of the tail CS, its structure, and its stability. The question was primarily important in view of attempts to interpret magnetospheric substorms as an outcome of transient plasma processes developing in the tail CS as it loses stability. MHD models [78, 79] are noteworthy in this respect; they consider the plasma as a fluid moving in the y direction in accordance with the distributed velocity profile $V_y(z)$ given by the Lorentz function

$$V_y(z) = \frac{V_0 h^2}{z^2 + h^2}, \tag{9}$$

whereas self-consistent profiles of the magnetic field and the plasma and current density take the form

$$B_x(z) = B_0 \tanh\left(\frac{h}{L}\arctan\frac{z}{h}\right), \tag{10}$$

$$\begin{aligned} n(z) &= n_0\,\mathrm{sech}^2\left(\frac{h}{L}\arctan\frac{z}{h}\right), \\ j_y(z) &= \frac{B_0}{\mu_0 L}\,\frac{h^2}{z^2+h^2}\,\mathrm{sech}^2\left(\frac{h}{L}\arctan\frac{z}{h}\right). \end{aligned} \tag{11}$$

These solutions transform into the Harris solution as $h \to \infty$.

An important two-dimensional extension of the Harris model that accounts for the normal component is the Kan model [80] based on the solution of the Grad–Shafranov equation found earlier by Walker (1915) in the form of a generalized two-dimensional function $g(\zeta)$ ($\zeta = x + \mathrm{i}z$). The vector potential of the system $A_y(x,z)$ in the Kan model is the solution of the equation

$$\frac{\partial^2 A_y^*}{\partial x^{*2}} + \frac{\partial^2 A_y^*}{\partial z^{*2}} = \exp\left(-2A_y^*\right), \tag{12}$$

where $A_y^* = -A_y/(2B_0 L)$, $x^* = x/(2L)$, $z^* = z/(2L)$, and L is the characteristic thickness of a CS.

In models by Schindler and Birn [76, 77, 81, 82], solutions are sought of the Grad–Shafranov equation

$$\begin{aligned} \Delta A + \mu_0 j(A) &= 0, \\ j(A) &= \frac{\mathrm{d}p}{\mathrm{d}A}, \end{aligned} \tag{13}$$

where A is the vector potential, p is the plasma pressure, and μ_0 is the vacuum magnetic permeability in the International System of Units (SI). The boundary conditions for pressure are taken far from the current sheet and are identified with the conditions on the magnetopause (the boundary between the magnetosphere and solar wind), which allows controlling the CS structure. The asymptotic solution of Eqn. (13) is

$$a(x) - z = \int_{A(x,z)}^{A_\mathrm{b}} \frac{\mathrm{d}A}{\sqrt{2\mu_0\left(p_0(x) - p(A)\right)}}, \tag{14}$$

where

$$\int_{A_0(x)}^{A_\mathrm{b}} \frac{\mathrm{d}A}{\sqrt{2\mu_0\left(p_0(x) - p(A)\right)}}$$

defines the shape of the magnetopause ($A = A_{\mathrm{b}}$, $A_0 = A(x, 0)$) in the system. Solution (14) can be written as the dependence

$$a(p_0) = -\frac{1}{\sqrt{2\mu_0}} \int_{p_{\mathrm{b}}}^{p_0} \frac{1}{\mathrm{d}p/\mathrm{d}A} \frac{\mathrm{d}p}{\sqrt{p_0 - p}}\,, \qquad (15)$$

where $p_{\mathrm{b}} = p(A_{\mathrm{b}})$ is the pressure on the magnetopause. It is shown in [83] that the function $a(p)$ controls the structure and stability of this plasma equilibrium (open and closed magnetospheres), with the particular case $a(p_0) = \mathrm{const}$ being the already known Harris equilibrium.

The stability of CS models was explored in the framework of the two-dimensional (2D) model of a quasineutral sheet with a small transverse magnetic field B_z taken into account [27]. Electrons were treated as trapped, in agreement with a thick sheet configuration. A linear analysis of the energy balance in a CS showed that the tearing instability can be fully suppressed through the effect of 'electron compressibility', because the compression energy of magnetized electrons is borrowed from the free energy of a CS perturbed by the tearing mode. It turns out that electrons play the role of an 'elastic medium' suppressing the development of instability. Thus, from a theoretical standpoint, the development of the tearing mode, triggering the disruption of CSs and launching reconnection processes in the tail, proved to be impossible. Paper [27] prompted a long discussion as to exactly which instability can destroy the magnetotail CS during substorm perturbations (see review [19] and the references therein). This problem remained unsolved until the discovery and study of collisionless thin current structures in space.

We note that the models of 'thick' sheets described above agree well with observations of the magnetotail CS within relatively quiet geomagnetic periods, but fail to properly describe TCSs that are embedded and multi-scale. The first studies on modeling the TCS appeared at the time when nothing was known about their real existence. In 1965, Speiser [18, 67] described a new type of current sheet in which protons are demagnetized upon reaching the neutral sheet, draw semicircles in the magnetic field B_z, are then magnetized, and escape to infinity. Today, such trajectories are called by the name of their discoverer. Later, quasi-trapped particles were described [19, 36]. In 1972, Eastwood [84], based on the work by Speiser [67], showed, using a numerical model, that it is possible to maintain a self-consistent current in a TCS through protons in the Speiser orbits.

Because TCSs can be viewed as plasma quasi-equilibria [70], the magnetic tension tensor should be balanced in them by the anisotropy of the pressure tensor [85]. Here lies the main difference between TCSs and relatively thick CSs (measuring many proton gyroradii in thickness) in the magnetotail, where the tension of magnetic field lines is balanced by the radial pressure gradient. Models with an anisotropic pressure tensor evolved into a separate class of plasma equilibria, and this area has been actively developed over the two last decades. The first attempt to construct a self-consistent analytic model of 'thin' plasma equilibrium (with the electron component ignored) was undertaken in Ref. [86], where an inverse problem was solved on the reconstruction of the plasma distribution function based on a given magnetic field profile.

A self-consistent equilibrium solution of the Vlasov–Maxwell equations for a one-dimensional anisotropic current sheet was first found in Ref. [87] in the case of strong flow anisotropy and a small normal component B_z; the electrons were assumed to be a cold background and electrostatic effects were ignored. The solution in Ref. [87] for the profile of a magnetic field maintained by Speiser ions differs from the known Harris solution by the fact that the current density profile is embedded into the plasma density profile, whereas these profiles coincide in the Harris model.

A detailed study of the TCS structure was carried out in Refs [88–91]. It has been shown that the structure is determined by a superposition of competing para- and diamagnetic currents [89]. Processes of scattering of transient ions bear a diffusive character and can be the cause of accumulation of quasi-trapped plasma in the CS, followed by slow evolution and formation of split current density profiles [92]. It was also found that the cause of CS disruption can be not only the instabilities but also the accumulation of trapped ions up to a concentration exceeding some critical value [93]. Electrostatic effects were taken into account for the first time in a self-consistent model of anisotropic CSs [90] and weak splitting of the current density profile was explained by the motion of electrons under the action of an ambipolar electric field. An explanation was proposed for the narrow peak of embedded CSs having an electron scale [90]. The multi-component character of plasma enriched by heavy ions was taken into account, and the contribution of heavy particles to the current transversing the tail was estimated in [94]. Nonsymmetric current configurations were also explored and it was shown that there are at least two mechanisms influencing the formation of asymmetric CSs: the asymmetry of plasma sources [95] and the presence of a B_y component in the magnetic field [96]. The two-dimensional structure of TCSs was treated in Ref. [91] with the longitudinal inhomogeneity in the magnetic field along Earth's magnetotail taken into account.

The stability analysis of an anisotropic CS in the framework of linear perturbation theory and analysis of substorm dynamics revealed that metastable behavior is characteristic of this current structure. The estimate of marginal stability regions with respect to parameters also pointed to a fundamental difference between the properties of anisotropic CSs and those of the Harris type [30]. If the Harris CS is always unstable with respect to the tearing mode, the TCSs are unstable only in narrow ranges in the system parameter space, which in essence underlies their property of metastability. The estimate of wavelengths of different plasma modes and their increments in TCSs agrees with real scales for substorm processes in the magnetotail [30, 97, 98].

The main conclusions from theoretical models of thin CSs were compared with the data of satellite observations in Earth's magnetotail [99]. It was shown that the current density profiles and values of the main plasma parameters in thin CSs derived from the data of the Cluster mission can be approximated by the model of anisotropic CSs with an accuracy of about 80% in a wide range of measurements. On the other hand, not only the general geometry but also the kinetic structure of the proton distribution over velocities in CSs measured in Earth's magnetosphere is similar to the structure of the phase space of the TCS model [99].

The results in Refs [89, 95] were verified in numerical simulations based on the macroparticle method [100]. The results obtained helped to resolve a contradiction, called *the thermal catastrophe of current sheets* in [101] — the absence of equilibrium solutions for moderately anisotropic plasma sources. With the assistance of numerical simulations, the force balance of TCSs was studied in detail [100], and an interesting regime of dynamic oscillations in solutions close to equilibrium was found [93].

In Section 2, we consider the dynamics of charged particles in TCSs for different values of system parameters and the mechanisms of TCS structure formation in a collisionless cosmic plasma. Along with models based on solving the Vlasov–Maxwell equations, which can be loosely called semianalytic (an analytic solution can typically be obtained in the simplest cases, and the common approach is the numerical one), a class of models exists for which the Vlasov–Maxwell equations are solved with the macroparticle method [100, 102] or with hybrid codes [103]. An essential advantage of such models is the possibility of exploring not only statistical characteristics but also dynamical properties of plasma systems. They also offer a possibility of estimating and comparing the roles played by various parts of Earth's magnetosphere in general plasma dynamics. This review extends those on TCSs published by *Plasma Physics Reports* and *Physics–Uspekhi* [19, 104]; it presents results that were not considered earlier, including the newest advances in TCS research on cosmic plasma.

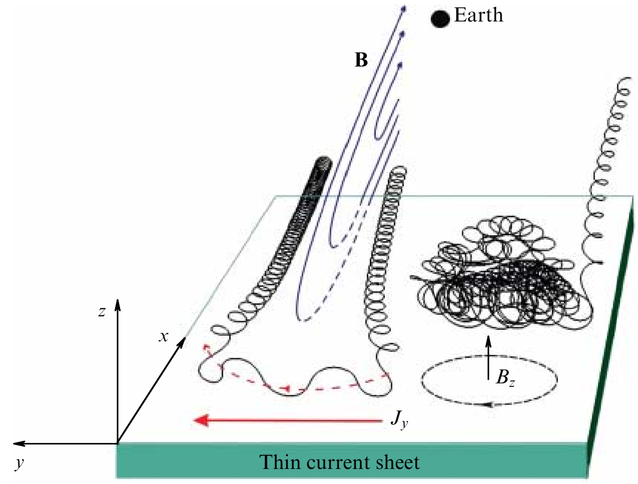

Figure 4. Two typical ion trajectories in the TCS: a transient (Speiser) trajectory and a quasi-trapped trajectory (performing many rotations around the current sheet). Shown are the plane of the TCS, magnetic field lines of the magnetotail going from Earth (its location is given by the black dot), the direction of the normal magnetic field component B_z at the CS center, and the direction of the local current J_y carried by particles in the solar-magnetospheric frame.

2. Dynamics of charged particles and the structure of thin current sheets

2.1 Quasi-adiabatic approach

It is shown in [36] that particle dynamics in the field reversals of TCSs in the magnetotail are almost entirely determined by the adiabatic parameter κ that characterizes the ratio of the magnetic field minimal curvature radius R_c to the maximum Larmor radius ρ_L in the vicinity of the neutral plane,

$$\kappa = \sqrt{\frac{R_c}{\rho_L}}\,. \tag{16}$$

For $\kappa \gg 1$, protons and electrons are fully magnetized, their magnetic moments are preserved, and their motion can be described in the guiding center approximation. For $\kappa \ll 1$, the gyroradii of particles are comparable to or greater than the field line curvature. Particle motion in this case becomes highly nonlinear: becoming demagnetized near the neutral plane, the particles follow meandering orbits along semicircles in the xy plane, alternately crossing the northern and southern lobes of Earth's magnetotail (so-called serpentine trajectories), then leave the CS, becoming magnetized (Fig. 4) by a rather strong magnetic field outside the TCS. On serpentine trajectories, for $\kappa \ll 1$, the x- and z-degrees of freedom are nearly decoupled: the particle motion can be decomposed into two independent motions, fast vertical oscillations in the z direction and relatively slow rotation in the field B_z along the x axis [36]. Magnetic moments of particles in this configuration are not conserved, but for $\kappa \ll 1$ the invariant of motion (action integral) $I_z = (2\pi)^{-1} \oint p_z \, dz$ is approximately conserved [36]. On the change from magnetized to meandering motion, the invariant can experience a jump $\Delta I_z \ll I_z$ in the vicinity of the neutral sheet. The jump magnitude is estimated as [105–107]

$$\Delta I_z \approx \mp \frac{3}{2} \kappa \sqrt{1 - I_z^{4/3}} \, \ln 2 |\cos \theta_{\text{sep}}| \,, \tag{17}$$

i.e., ΔI_z is proportional to the adiabatic parameter κ and depends on the phase angle θ_{sep} at which the particle arrived at the separatrix (the border line where the motion type changes). The jump averaged over an ensemble of particles is exactly zero,

$$\langle \Delta I_z \rangle_{\theta\,\text{sep}} \equiv \frac{1}{2\pi} \int_0^{2\pi} \Delta I_z \, d\theta = 0 \,, \tag{18}$$

but its rms value differs from zero:

$$\left\langle (\Delta I_z)^2 \right\rangle_{\theta_{\text{sep}}} \equiv \frac{1}{2\pi} \int_0^{2\pi} (\Delta I_z)^2 \, d\theta = \frac{3\pi}{16} \kappa^2 \left(1 - I_z^{4/3}\right). \tag{19}$$

This means that the change in the adiabatic invariants of ions as they traverse the CS can be described as a diffusive process with the characteristic diffusivity coefficient [36, 92]

$$D_{I_z I_z} = \frac{\left\langle (\Delta I_z)^2 \right\rangle}{T_{\text{QT}}} \,, \tag{20}$$

where T_{QT} is the approximate period for the full cycle of a quasi-trapped particle along the x coordinate. As can be seen from Eqns (17)–(20), the parameter κ is the key one for particle dynamics. For $\kappa \ll 1$, the ion motion is regular almost everywhere outside narrow separatrix regions where the invariants undergo changes described by Eqn (17). Such a regime of motion, as well as the invariant I_z, is referred to as quasi-adiabatic. Owing to the jumps ΔI_z, the quasiperiodic motion of quasi-trapped particles around the current sheet can be accompanied by slow chaotization (on the time scale of large-scale oscillations around the neutral plane) of the motion of quasi-trapped particles and the trapping of transient Speiser particles to closed trajectories. This process, studied in Ref. [92], was called the 'aging' of CSs.

For $\kappa \sim 1$, particle trajectories are such that gyroradii are comparable to the scale of the magnetic field inhomogeneity.

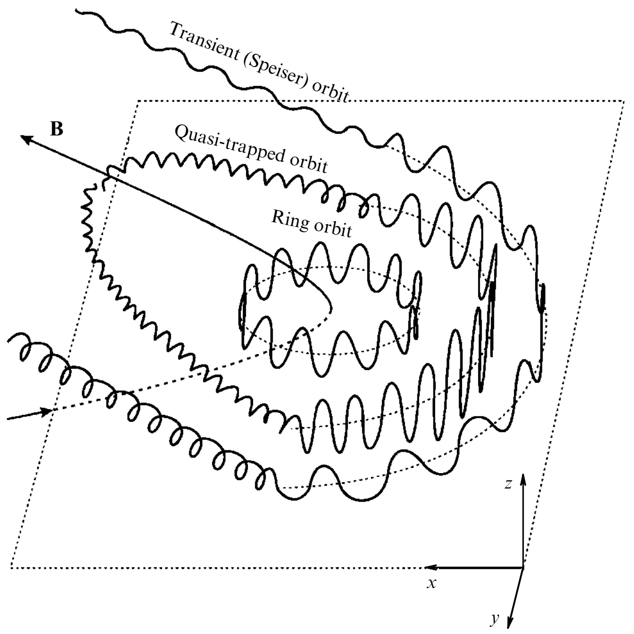

Figure 5. Types of trajectories of quasi-adiabatic particles in a TCS. Particles in open Speiser orbits are the main cross-sheet current carriers; quasi-trapped protons repeatedly cross the CS plane and move in quasi-closed orbits; ring orbits are inside the CS and do not cross the separatrix.

Particle motion is essentially chaotic ($\Delta I_z \sim I_z$), and the quasi-adiabatic approximation fails. As geomagnetic perturbations — substorms — start to evolve, during the so-called phase of magnetic flux accumulation in the tail, the tail CS narrows in the transverse direction substantially, from approximately 10,000 km to 250–2000 km; in this case, the adiabatic parameter for protons decreases by an order of magnitude. For electrons, $\kappa_e \sim 2-3$, but this parameter is an order of magnitude smaller for ions: $\kappa_i \sim 0.1-0.2$ [20, 108]. This makes the dynamics of plasma populations fundamentally different and eventually determines the structure and stability of CSs. The motion of magnetized electrons in the magnetotail follows the field lines, whereas the motion of ions becomes quasi-adiabatic (Fig. 5). In a model of current equilibrium, the motion of two plasma components cannot be described within the same approach, and hybrid models are mostly used, where electrons are described as anisotropic conducting fluid and ions are treated in the framework of the kinetic approximation. A detailed description of the equations of the TCS hybrid model, with account for the quasi-adiabatic one-dimensional (1D) model of the Speiser CS, is given in the Appendix. We refer to this model as the *basic* one below.

2.2 Properties of thin current sheets in the simplest model of plasma equilibrium: embedding and multi-scale character. Solving basic equations

The self-consistent system of equations for the 1D hybrid TCS model, described in detail in the Appendix, was first solved numerically in Refs [88–90]. The electrostatic effects were discarded for simplicity. Figure 6 displays profiles of dimensionless quantities (see the Appendix) in the direction transverse to the CS: the tangent magnetic field (Fig. 6a), the current density in the y direction (Fig. 6b), and the plasma density (Fig. 6c). The profiles were obtained for various values of the flow anisotropy parameter $\varepsilon = v_T/v_D$ of plasma sources [88], which, according to the figure, greatly influences the CS internal structure. As the ratio of thermal to drift velocities is increased, the maximal current density decreases.

In Fig. 6, self-consistent profiles of the densities of current and plasma (with the normalization described in the Appendix) are displayed as functions of the dimensionless coordinate ζ in the direction transverse to the sheet for different values of the flow anisotropy parameter $\varepsilon = v_T/v_D$. As follows from their comparison, the current density J_y tends to zero outside the CS, whereas the plasma density n tends to a constant value equal to unity in the normalized variables. This illustrates the fundamental property of a TCS, the embedding of a CS into a plasma sheet. Accounting for numerous additional factors that are lacking in the basic model [88, 89] but are present under real conditions (electrostatic effects [90, 91], heavy ions [94], a large concentration of quasi-trapped plasma [93, 109]) may lead to additional levels of embedding. For example, in the

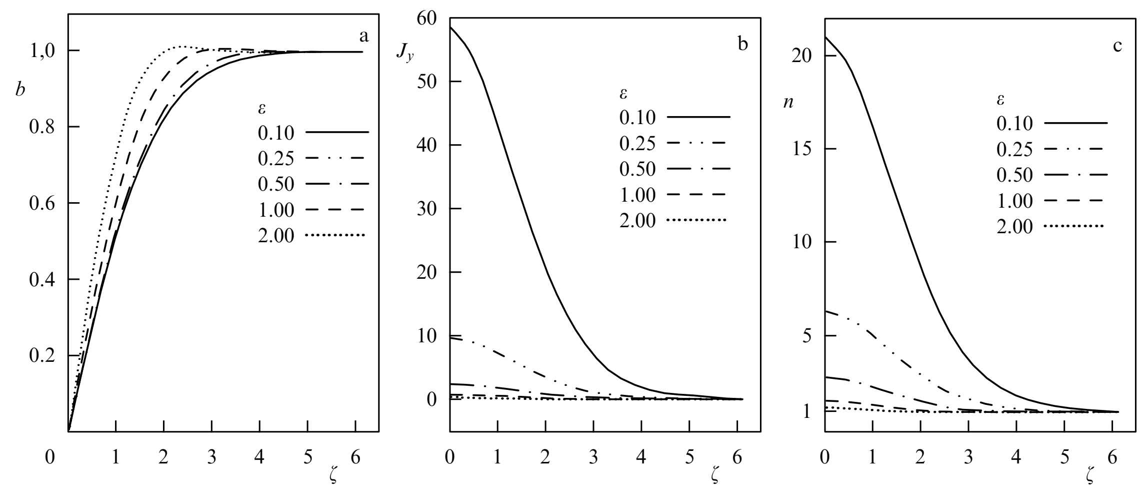

Figure 6. Profiles of (a) the magnetic field b, (b) the current density J_y, and (c) the plasma density n in a TCS as functions of the dimensionless coordinate $\zeta = z\omega_0/(\varepsilon^{4/3} V_D)$ in the cross-sheet direction (see the Appendix) for various values of the flow anisotropy parameter $\varepsilon = v_T/v_D$, where v_T and v_D are the thermal and drift plasma velocities at TCS boundaries [88]. The values of the parameter ε are given in the legends.

'matryoshka' (Russian doll) model [94], a narrow electron current is embedded in the proton CS, which is in turn is inside a CS formed by oxygen ions, whereas all this configuration lies inside a broader plasma sheet. A triple-split TCS embedded into a plasma sheet in which a positive central current is surrounded by two negative currents at the periphery is found in [109]. It is noteworthy that even such unusually complex structures can be observed by Cluster satellites as they traverse the magnetotail.

Thus, together with embedding, an important property of TCSs is their multiscale character. The dependence on the flow parameter ε is largely predictable: the larger the thermal velocity is compared with the drift velocity, the greater the number of particles with high values of the quasi-adiabatic motion invariant, i.e., quasi-trapped particles. The last do not carry net current across the sheet, because their trajectories are closed; hence, the current density should decrease proportionally to the concentration of quasi-trapped particles, or inversely proportional to the value of ε.

The structure of CSs is schematically shown in Fig. 7. As shown in [89], the contributions to the current density can come from (1) the current of Speiser particles in meandering orbits; (2) the gradient current; (3) the centrifugal current related to the drift of curvature; (4) the magnetization current. The current of Speiser particles is an analog of boundary paramagnetic current and flows in the positive y direction, while currents 2–4 are the drift or diamagnetic ones, flowing in the negative direction [in particular, Eqn (44) from the Appendix is applicable to describing them]. The current density at the boundaries of a CS (Fig. 7a) is predominantly determined by the Larmor rotation of particles (the regime without crossing the neutral plane $z = 0$); it is a manifestation of plasma diamagnetism. The segments of meandering (serpentine) orbits in the vicinity of the neutral plane (Fig. 7b) (the regime when the neutral plane is crossed) form when proton motion is demagnetized and protons alternately enter the northern and southern parts of the tail. As is seen from Fig. 7, the competition of dia- and paramagnetic currents inside the CS determines the final current profile in the CS and its vicinity. The directions of para- and diamagnetic currents are opposite, as indicated by arrows with labels.

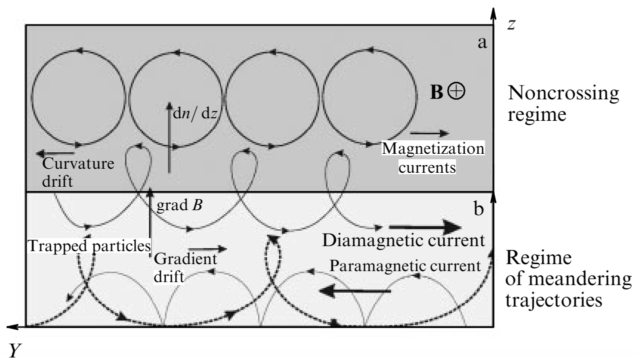

Figure 7. Mechanisms of current formation in the vicinity of the equatorial plane [89]. (a) The region where trajectories do not cross the neutral plane and where the guiding center approximation is applicable. Schematically shown are the Larmor rotation and the directions of gradient drift, curvature drift, and magnetization current. The net current in this region is negative, which illustrates the natural diamagnetism of magnetized plasma. (b) The region of meandering (serpentine) motion where the guiding center approximation is not applicable.

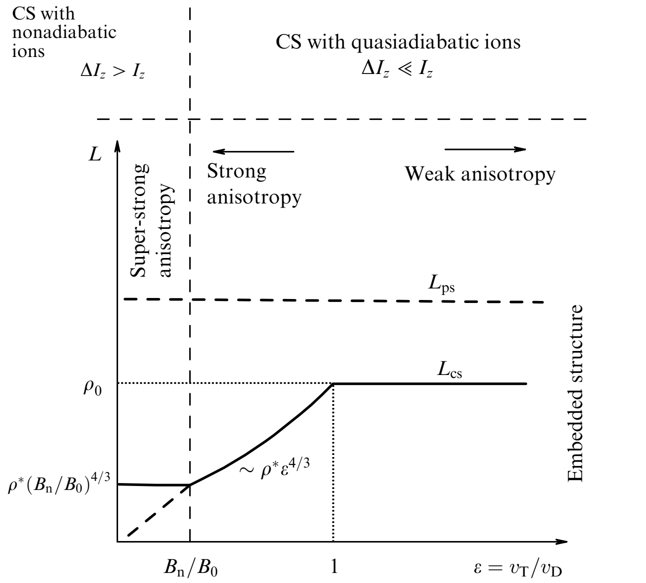

Figure 8. General schematic of the relation between thicknesses of proton current sheets L for various values of the source anisotropy ε. Here, $\rho_0 = v_{\rm T}/\omega_0$, $\rho^* = v_{\rm D}/\omega_0$, and $\omega_0 = eB_0/(mc)$. $L_{\rm ps}$ and $L_{\rm cs}$ are the thicknesses of plasma and current sheets.

2.3 Scales of current equilibria. Thin and super-thin current sheets

Figure 8 displays the dependence of the thickness L of thin current sheets on the flow anisotropy parameter $\varepsilon = v_{\rm T}/v_{\rm D}$ [89]. The thin dashed lines separate the three main regimes in the TCS that correspond to different dependences of thicknesses on external parameters: (1) a 'quasi-adiabatic' CS with a strong flow anisotropy $B_{\rm n}/B_0 \leqslant \varepsilon \leqslant 1$ and the thickness $L \approx \rho(v_{\rm T}/v_{\rm D})^{4/3}$; (2) a CS with a weak flow anisotropy $\varepsilon \geqslant 1$, and the thickness $L \approx \rho_0$, where ρ_0 is the thermal Larmor radius; (3) nonadiabatic current sheets with $\varepsilon < B_{\rm n}/B_0$ and $L \approx \rho^*(B_z/B_0)^{4/3}$, which are characterized by super-strong flow anisotropy with the particle velocities directed practically along the magnetic field lines at the TCS boundaries.

As can be seen from Fig. 8, the transition from the regime of moderate anisotropy $B_{\rm n}/B_0 \leqslant \varepsilon \leqslant 1$ to that with the highest source anisotropy with $\varepsilon < B_{\rm n}/B_0$ is sharp. In the quasi-adiabatic regime, the TCS thickness behaves as $L \sim \varepsilon^{4/3}$ [88, 89]. In the regime of super-strong flow anisotropy, according to the estimates in Refs [89, 90], $L^* = \rho^* b_{\rm n}^{4/3}$. The CS thickness in this case depends on the normalized value of the normal magnetic component $b_{\rm n} = B_z/B_x^0$, but is practically independent of ε. On passing to the regime of weak flow anisotropy, the TCS thickness becomes comparable to the thermal proton gyroradius $L \sim \rho_{\rm T}$, and then the dependence on the flow parameter disappears [111].

2.4 Estimate of the effect of an electric field on the transverse thickness of thin current sheets

We estimate the effect of a large-scale electric field on the CS thickness. Passing from the laboratory coordinate system at rest, in which an electric field E_y exists, to a moving de Hoffmann–Teller coordinate system where the electric field vanishes, we easily find that for a one-dimensional configuration with $B_z = $ const, the problem reduces to the one solved in Section 2.3. The velocity of the de Hoffmann–

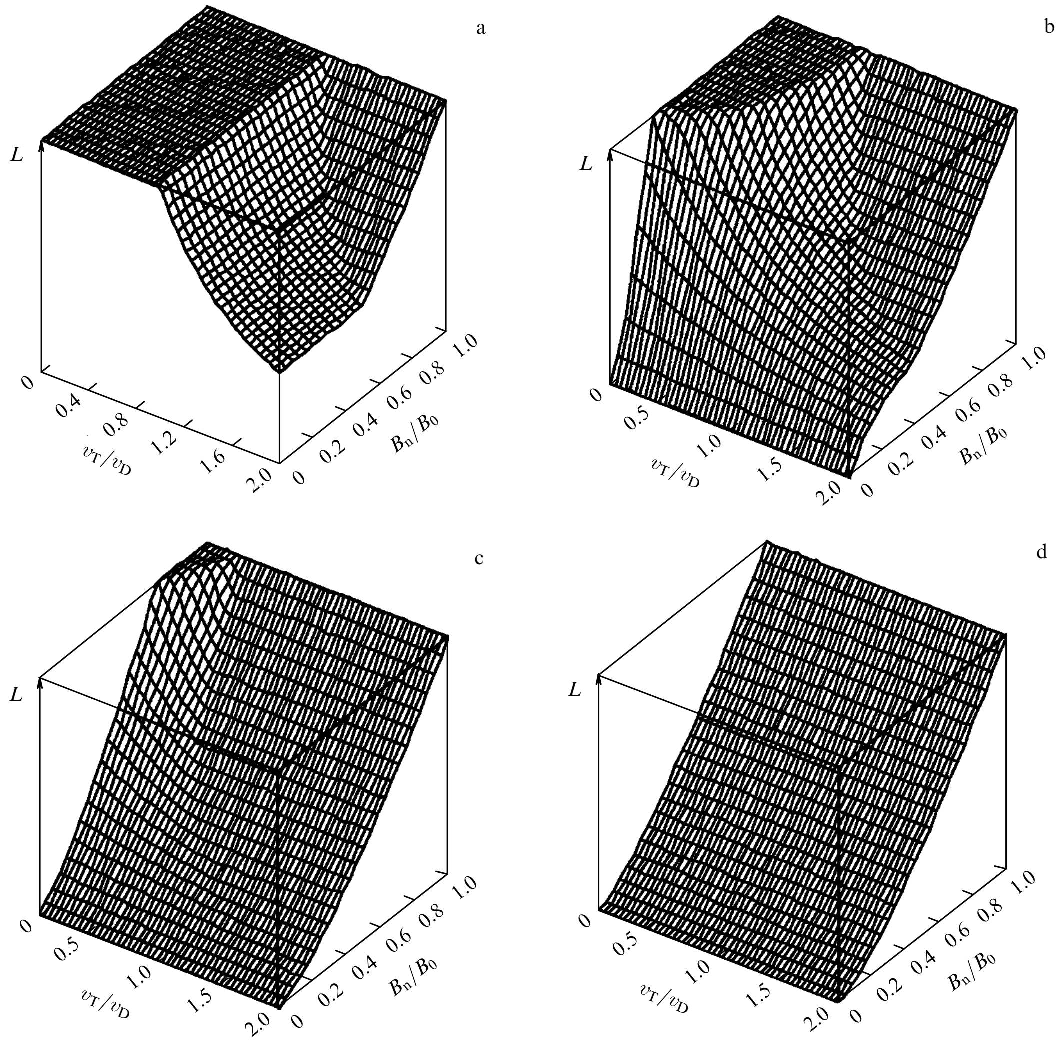

Figure 9. Dependence of the sheet thickness L on B_n/B_0 and $\varepsilon = v_T/v_D$ for different values of the normalized electric field: (a) $E_y^* \equiv cE_y/(v_D B_0) = 0$; (b) $E_y^* = 0.25$; (c) $E_y^* = 0.70$; and (d) $E_y^* = 1.00$.

Teller coordinate system in the x direction cE_y/B_z must therefore be added to the particle flow velocities v_D, which are also directed along the x coordinate at the boundaries of the CS. The plasma velocity in this coordinate system $\tilde{V}_d = v_D + cE_y/B_z$ depends on the external electric field (we here ignore a small correction due to the tilt of the field line relative to the equatorial plane). Substituting the expression for $\tilde{V}_d$ obtained above in the estimate for the TCS thickness in the quasi-adiabatic regime gives $L \approx \rho(v_T/\tilde{V}_d)^{4/3}$.

The dependence of the current sheet thickness $L \sim \varepsilon^{4/3} v_D/\omega_0$ on the parameters B_n/B_0 and $\varepsilon = v_T/v_D$ for different values of the dimensionless electric field E_y^* (which corresponds to the distribution of thicknesses in Fig. 8) is shown in Fig. 9 adapted from Ref. [89]. Figure 9a corresponds to the zero electric field. Figures 9b–d demonstrate the change in scales for several values of the dimensionless electric field E_y^*. By comparing them, we can see that the addition of the de Hoffmann–Teller translation velocity to the flow velocity increases the plasma flow anisotropy (the velocity along the magnetic field at the boundaries of the CS), which makes the CS thinner. This result agrees with the generally accepted concept of substorms, according to which the rotation of the B_z component of the IMF to the south facilitates the induced reconnection of magnetic field lines on the diurnal side, propagating to the nocturnal side. The increase in the convective electric field in the dawn–dusk direction in the magnetotail contributes to making a relatively thick CS thinner, with the formation of a TCS. Figure 9 agrees with such a scenario, showing several 'snapshots' of varying CS thickness for the increasing electric convective field E_y^*.

2.5 Mechanism of the formation of asymmetric equilibria

2.5.1 Asymmetry of plasma sources. Measurements by the satellites ISEE-1, ISEE-2,[1] Geotail, and Cluster have shown that TCSs in the magnetotail can have a complex multiscale structure and exhibit nonlinear temporal dynamics [19, 63, 65, 69, 72]. Statistical analyses based on data from four satellites of the Cluster mission after 30 crossings of a CS at the distance of $19 R_E$ from Earth in July–October 2001 helped to identify three main types of CS profiles: central, bifurcated, and asymmetric [112]. In many observations of 'single-peaked' CSs, the maximum of the current density does not coincide with the magnetic field minimum. Similar nonsymmetric magnetic field profiles were recorded for the magnetosphere of Mercury when Mariner-10 passed through it in 1975 [113].

Given the observational data that point to the lack of north–south symmetry in the magnetic field and current

[1] ISEE stands for the International Sun–Earth Explorer.

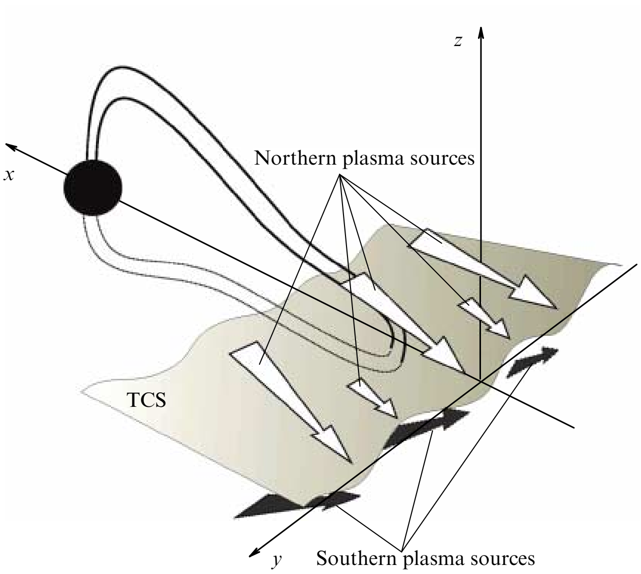

Figure 10. Schematic of the mechanism of vertical motions of a TCS caused by natural variations of the intensity of plasma sources along the y coordinate in the magnetotail [95].

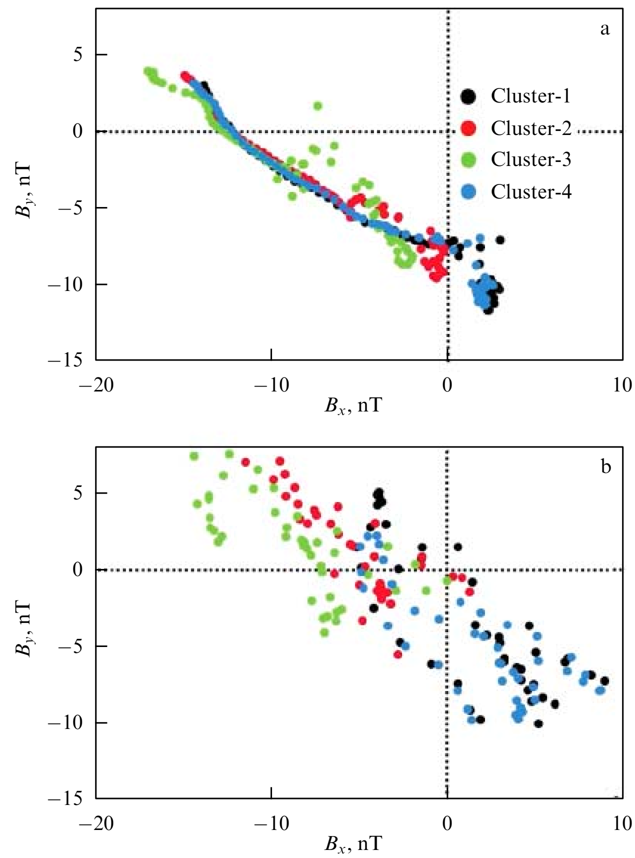

Figure 11. Spatial profiles of the shear component B_y observed by Cluster spacecraft during two subsequent crossings of the CS tailwards from the near X-line: (a) a bell-shaped spatial profile of $B_y(B_x)$ was observed at some distance from the X-line at 03:42–03:46:40 UT (the data of measurements on 22.09.2006); (b) an antisymmetric profile of $B_y(B_x)$ was observed close to the X-line at 03:46:40–03.49:30 UT. Under the assumption that the CS is horizontal, the magnitude of the B_x component is an indirect indicator of the separation of the satellite from the neutral plane ($B_x = 0$). Thus, the profiles of $B_y(B_x)$ can be considered spatial distributions of the B_y component across the CS [129].

density profiles in a TCS, we must answer questions about factors that are responsible for the profile asymmetry. As one mechanism, the asymmetry in the plasma density in the northern and southern plasma sources has been proposed, which may stem from natural fluctuations of a large-scale magnetic field or the deviation of the dipole magnetic moment direction from the planet rotation axis [95]. It was shown that disagreement between magnetic field zeros and current density maxima, which can reach one and a half Larmor radii, is a characteristic property of asymmetric TCSs. The deformation of such a CS occurs as a result of a shift in the vertical pressure balance $p_{zz} + B^2/(8\pi) = \text{const}$, when, because of the asymmetry of plasma sources, the plasma becomes denser on the side of the source and rarefied on the opposite side. Such a vertical deviation in the case of natural fluctuation of sources feeding the northern and southern tail lobes can lead to vertical (flapping) oscillations, as shown in Fig. 10.

2.5.2 Presence of a shear magnetic field component in the CS of the magnetotail. The majority of contemporary models of the tail CS allow the presence of a small normal component of the magnetic field but commonly disregard the shear component B_y directed along the current lines in the sheet. However, spacecraft-based observations indicate that a rather strong shear component (up to 50% of the field magnitude in the high-latitude part of the tail) might exist in the tail CS [114]. In [115], observations of a tilted CS in the presence of a shear magnetic field in the vicinity of the reconnection region and the influence of this field on the Hall current system are discussed. In this configuration, the electric current crossing the tail in the y direction becomes longitudinal, which should influence the dynamics of charged particles in the CS [116–119] and the process of magnetic reconnection [120–122].

The question of the origin of the shear component in the magnetic field within the tail is thus far open. Previous research showed the presence of a correlation between the B_y component of the magnetic field in the tail and the corresponding component of the interplanetary magnetic field [123–126]. It seems plausible that the shear magnetic field in the tail CS is due to the penetration of the IMF into the magnetosphere. However, it is shown in Refs [115, 127, 128] that substantial variations of B_y are not always connected to corresponding variations of the IMF and are frequently a result of internal dynamics in CSs. For example, the case where the y component of the magnetic field in the tail CS has the opposite sign to the B_y component of the IMF is discussed in [128]. The reconstruction of profiles of the shear component B_y in the tail CS based on multi-point measurements performed by the Cluster spacecraft indicates that in some cases the spatial distribution of this component along the normal to the CS plane is bell-shaped [128]. In other words, the field B_y is strongest in the vicinity of the neutral plane (the plane $B_x = 0$), decaying away from it. However, the mechanism governing this amplification of the shear component near the neutral plane was not discussed by the authors of Ref. [128].

The spatial distribution of the B_y component in the CS tailward from the near X-line was explored in [129] based on multi-point measurements of the Cluster spacecraft. It was demonstrated that the spatial distribution of this component varies as a spacecraft approaches or recedes from the X-line (Fig. 11). Far from the X-line, the distribution of the B_y component in space has a bell-shaped profile with a

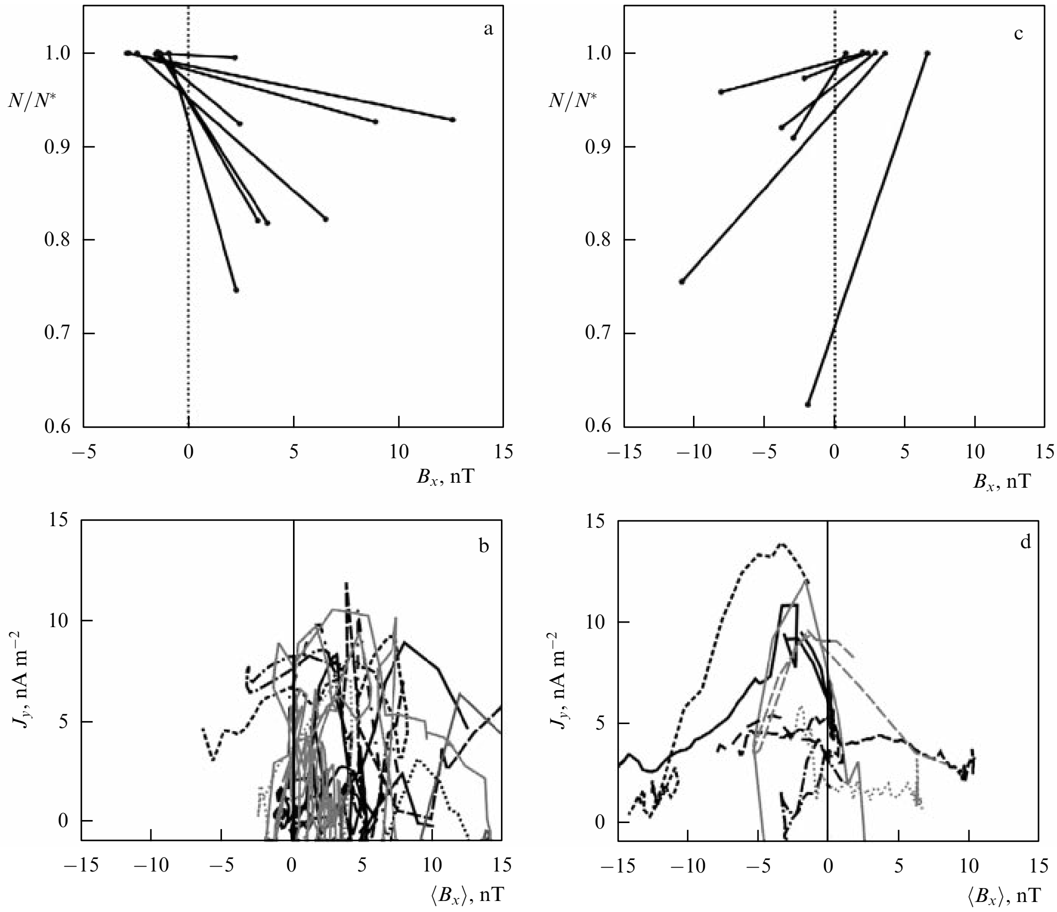

Figure 12. (Color online.) Spatial distributions of the normalized ion density $N^*(B_x)$ and the $J_y(B_x)$ current density component observed in intervals when a CS with magnetic configurations (a, b) $B_z > 0$, $B_y < 0$ or $B_z < 0$, $B_y > 0$ and (c, d) $B_z > 0$, $B_y > 0$ or $B_z < 0$, $B_y < 0$ is crossed. The ion density N for each CS crossing is normalized by the magnitude of the maximum ion density N^* observed in this crossing. The ordinates of each pair of points connected by lines show values of N/N^* averaged for the given crossing over the northern ($B_x > 0$) and southern ($B_x < 0$) parts of the plasma sheet (PS). The connecting lines show a tendency to the ion density increase in the direction of the northern or southern parts of the PS. Spatial profiles of the current density $J_y(B_x)$ are given by separate curves for each crossing [131].

maximum of B_y in the neutral plane (Fig. 11a). When a Cluster spacecraft approaches the X-line, the spatial distribution of B_y becomes antisymmetric: the B_y component changes its sign when the neutral plane is crossed and increases in absolute value toward the CS boundaries. Such a distribution of the shear field close to the magnetic reconnection region is related to the formation of the Hall system of electric currents as a result of spatial charge separation in the ion diffusive region (see, e.g., Refs [22, 130]).

The question of the mechanism governing the formation of a bell-shaped spatial profile of the magnetic shear component in a CS long remained unsolved. As shown in Ref. [129], such a magnetic configuration is stable enough and can be observed for about 7.5 min. It is plausible to assume that the amplification of B_y at the sheet center can be related to the presence of oppositely directed electric currents J_x flowing at the CS boundaries.

By analyzing 17 CS crossings by Cluster spacecraft, it is shown in Ref. [131] that the system of oppositely directed currents J_x in the CS of the tail is observed simultaneously with the bell-shaped profile for the shear component of the magnetic field. The analysis of ion velocity distribution functions observed in the CS in these periods indicates that the J_x currents are generated by quasi-adiabatic ions. Kinetic analysis of trajectories of quasi-adiabatic ions interacting with a CS characterized by a weak initial shear component B_{y0} indicates that a north–south asymmetry in the vicinity of a CS should accompany the process of reflection/refraction of ion trajectories [96, 129]. As a result, a concomitant asymmetry in the ion density can form in the northern and southern hemispheres. In order to maintain the pressure balance, the CS must displace as a whole; besides, an asymmetric current density profile should form in the direction normal to the sheet [96]. Such nonsymmetric profiles with displaced current density maxima were recorded by the Cluster spacecraft in the course of observations of the amplified shear component at the CS center [129, 131, 132] (Fig. 12).

To form a current loop, it is required that the oppositely directed currents J_x close somewhere. It is shown in [129] that the amplification of the shear component of the magnetic field at the CS center tailward from the X-line is observed inside a plasmoid. In this case, the currents J_x can close along the closed magnetic configuration of the plasmoid or magnetic island, thus contributing to the amplification of the shear field B_y near the neutral plane of a plasmoid CS (Fig. 13). The question of closing the currents J_x earthward from the X-line remains open. If these currents were closed through the ionosphere, the shear field B_y in the tail CS would be amplified on large spatial scales, up to the CS boundary

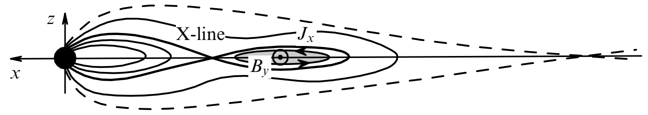

Figure 13. The mechanism of maintenance/amplification of the shear field at the CS plasmoid center (the region of field amplification $B_y > 0$ is shaded) tailward of the X-line owing to the formation of a current loop by oppositely directed currents J_x flowing in the northern and southern parts of the PS.

that is closest to Earth. The other possibility is that the currents J_x close along a magnetic island that can form between two X-lines if multiple X-lines form in the tail [133, 134]. Both hypotheses call for experimental verification, which we plan to carry out in our future work.

We discuss in more detail theoretical aspects of kinetic features of ion dynamics in a TCS with a sheared magnetic field and the formation of self-consistent current equilibria with a nonzero shear magnetic field component. As shown above, the presence of the B_y component in the magnetic field can lead to deformations in a magnetospheric CS. Such deformed TCs are studied in Ref. [135]. Amplification of the shear component in a CS during substorms and its consequences are described in detail in Ref. [127]. The observations reported there are of importance because not only the quasi-equilibrium structure but also magnetospheric dynamics can substantially depend on the shear magnetic field component. Its presence can be one of the causes behind the formation of bent or twisted CSs [115, 135]. It can also strongly influence the dynamics of quasi-adiabatic particles in TCSs [36, 96, 117, 118, 135] and MHD waves [136]. Theoretical studies [116, 137–139] indicated that the development of tearing instability in the presence of a shear field possibly leads to reconnection and reconfiguration of the magnetotail (see, e.g., Refs [69, 140, 141]). The north–south asymmetry in the magnetotail accompanies cases where a shear component of the magnetic field is present [142].

The asymmetry of particle scattering in relatively 'thick' magnetic configurations with a nonzero B_y component was explore in Refs [143, 144] by tracing particles. Kaufmann et al. [145] and Holland et al. [146] explored the dynamics of particles in a TCS numerically and demonstrated that a shear field leads to the destruction of energetic resonances (see below) because of the change in the character of particle scattering in a flat CS. The authors of Ref. [147] described processes related to particle scattering in relatively thin CSs. The study in Ref. [147] encompasses a broad range of dynamical regimes of plasma particle motion, from quasi-adiabatic to magnetized. Theoretical studies of the motion of quasi-adiabatic particles in a TC with a constant shear magnetic field component and main particle motion regimes were described in Refs [96, 148]. Specific details of the motion of quasi-adiabatic particles in a self-consistent model of TCSs with a global shear field were analyzed and it was established that the TCS structure depends on the mutual arrangement of particle sources as well as on the relative directions of the normal and shear magnetic fields [131]. In particular, it was shown that the asymmetry of particle scattering due to the shear magnetic can lead to asymmetry in profiles of the current density, concentration, and magnetic fields, and hence to a change in the entire TC configuration. All this makes studying the properties of TCs with a shear magnetic field undoubtedly important. In a 'classical' TCS with $B_y = 0$, the magnetic field lines are orthogonal to the current in the sheet center. The presence of a shear component in the magnetotail facilitates the generation of a current along the magnetic field lines in the neutral plane (i.e., in the direction of the y axis) [128, 129].

As mentioned above, the presence of a large-scale magnetic field component B_y in the tail is frequently interpreted as the penetration of the interplanetary magnetic field B_y into Earth's magnetosphere [149], although the mechanism supporting this phenomenon is still not fully understood [127]. The hypothesis that the shear magnetic field component can be self-consistently supported by currents in the magnetotail, i.e., be of an endogenic nature, has beem put forward by a number of authors (see, e.g., Ref. [128]), whose experimental studies were discussed at the beginning of this section; however a common opinion on the mechanism of its emergence is still lacking. Cowley in [142] explained the asymmetry of a reconnected flow by the presence of an IMF with B_y in the northern and southerns lobes. Asymmetric convective cells 'pull' the ends of magnetic field lines differently, which leads to their tilt and an additional amplification of B_y [150]. According to Ref. [151], the distribution of a nonzero B_y component in the magnetotail is maintained by currents along the magnetic field lines. This effect was taken into account in models T96 and T01 by Tsyganenko (see Ref. [151] and the references therein). The authors of Ref. [152] also formulated a hypothesis that convection of plasma toward Earth can be the reason for the amplified B_y in the magnetospheric CS.

In their two-dimensional MHD model, Hilmer and Voigt [144] assumed that the shear field in a quiet magnetotail is composed of two components: a constant background and an internal, spatially inhomogeneous one that exists only in a plasma sheet. The inhomogeneous B_y component should influence the plasma parameter β (the ratio of plasma pressure to the magnetic field pressure) and the magnitude of the B_z component. Its profile typically has a maximum at the sheet center and decays monotonically toward the boundaries. A similar bell-shaped distribution for the shear component was first found in a two-dimensional MHD model of the CS [153]. It was shown that the shear component can form at the center of the CS if the longitudinal plasma pressure is larger than the transverse one: $p_\parallel > p_\perp$. In the opposite case $p_\parallel < p_\perp$, in contrast, the profile of B_y has a local minimum in the neutral layer and maxima at the periphery. Unfortunately, the MHD models are applicable only for the description of a 'thick' magnetotail in a quiet state and cannot be used to study mechanisms of the shear component in a TCS.

Along with studies of symmetric (with respect to the transverse coordinate z) shear field component of a TCS, there have been attempts to explore its asymmetric (odd) configurations (see, e.g., Refs [154, 155]). Such configurations are frequently observed in TCSs close to reconnection regions when the Hall currents support quadrupole magnetic configurations [156]. Under such conditions, the B_y component can be rather large. Efforts invested in self-consistent quasi-adiabatic models of TCSs [87–90] over the last two decades have made them more elaborate and helped to generalize them to the case of magnetic shear [96, 157]. A symmetric configuration (with respect to the neutral plane) is considered in [157] in the framework of the self-consistent hybrid model of TCSs in which both symmetric and antisymmetric shear

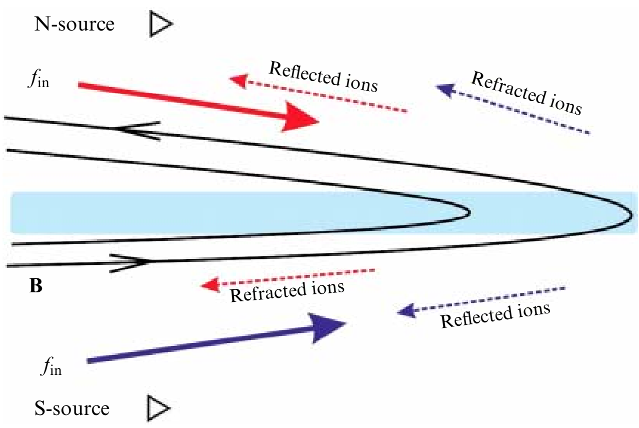

Figure 14. (Color online.) Streams of particles from the northern (N) and southern (S) sources are reflected from or refracted through the neutral sheet and pass to the other side (the respective stream directions are shown by blue and red arrows). An asymmetric configuration of the CS is formed because of the asymmetry of particle scattering.

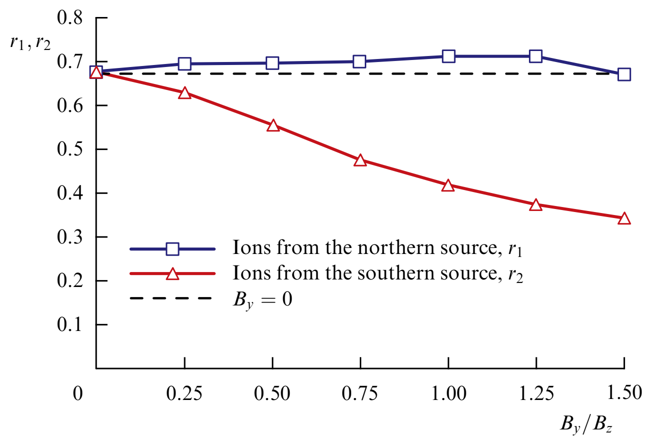

Figure 15. Coefficient of ion reflection from the CS depending on the ratio between the shear and normal magnetic field components and the plasma source position in the northern and southern hemispheres. Computations were performed for $B_{z0}/B_{x0} = 0.2$.

field configurations are explored, although the mechanism of their formation is not studied.

We consider the main features of the one-dimensional model of a CS with a constant magnetic shear. All three magnetic field components are taken into account: $\mathbf{B} = \{B_x(z), B_y, B_z\}$ ($B_x(z)$ changes sign in the plane $z = 0$, whereas the other components are constant). Plasma equilibrium in the CS is maintained through the balance between the tension of magnetic field lines and the finite inertia of ions [89]. This model is constructed under assumptions 1–6 on the quasi-adiabatic character of ion motion formulated in the Appendix; its schematic is given in Fig. 14, which shows how protons from the northern (N) and southern (S) sources enter the CS [96]. After interaction with the CS, the streams of ions can be reflected or pass through it (be refracted), which is shown by arrows in Fig. 14. Asymmetry of particle scattering in the presence of the B_y component, depending on the source the particles come from, can result in the formation of asymmetric current and plasma density profiles in the TCS, as well as the displacement of the TCS as a whole from the symmetric state (for $B_y = 0$).

The interaction of the plasma flow with a CS in the presence of a constant B_y component can be characterized by the coefficients of reflection r and refraction $n = 1 - r$ of the particle stream. To estimate the coefficients, 2×10^4 protons were released in the magnetic field of the TCS with $B_y = B_z = \mathrm{const}$ [96]. Their energies had the Maxwellian distribution. The transverse component B_z was taken positive and constant ($B_z = B_{z0} = 2$ nT), in agreement with its mean direction and magnitude in Earth's magnetotail. The ratio B_y/B_z was a parameter, and the value of the tangent component at the sheet boundaries was selected as $B_{x0} \approx 20$ nT. The dependence of the particle reflection coefficient on the plasma source position in the northern and southern hemispheres is shown in Fig. 15. As can be seen, in the absence of the shear component ($B_y = 0$), the reflection coefficients for particles coming from the northern and southern plasma sources are practically identical: $r \approx 0.67$.

If the shear component is nonzero, the reflection coefficient r_1 for ions coming from the northern source is practically independent of the ratio B_y/B_z, whereas the coefficient r_2 for particles from the southern source decreases inversely proportionally to B_y/B_z, reaching 0.3 at $B_y/B_z \approx 1.5$. Thus, the dynamics of ions coming from the northern and southern sources are different. As the shear component increases, ions from the northern hemisphere are scattered quasi-adiabatically, as in the case $B_y = 0$, whereas particles coming from the southern hemisphere cross the CS without being scattered or trapped, and continue to the opposite hemisphere. This indicates that the presence of the shear magnetic field in a CS inevitably leads to the formation of an asymmetric structure. In [105], particle scattering asymmetry was explored in configurations where the guiding center approximation is applicable to the description of plasma particle motion. Later, the perturbation of particle motion was explained in Ref. [147] by the action of a pulsed centrifugal force in the vicinity of the neutral plane. A nonzero value of B_y in the CS causes a turn of the pulsed centrifugal force in the rotation plane. As a result, the nonadiabatic behavior of particles either weakens or is amplified, depending on the hemisphere from which the particle came.

Thus, ions coming from opposite hemispheres behave differently, experiencing smaller or larger jumps in magnetic moments depending on the propagation direction. Furthermore, as follows from modeling results for a TCS with magnetic shear, particle dynamics in such TCSs fundamentally differ from those in relatively thick CSs, where they can be described in the framework of guiding center approximation.

The model of TCSs with a shear magnetic field [96] used the dependence of the ion reflection coefficient $r_{1,2} = r_{1,2}(B_y/B_z)$ shown in Fig. 15. The reflection coefficient for plasma from the northern source r_1 was taken to be constant, equal to 0.7 in all computations. The coefficient r_2 for the southern source was varied linearly from 0.7 for $B_y/B_z = 0$ to $r_2 = 0.3$ for $B_y/B_z = 1.5$. Figure 16 demonstrates self-consistent profiles of normalized quantities (see the Appendix): the field component $b_x(z)$, the current $j_y(z)$, and the plasma density for various values of b_y computed in the framework of models (9)–(14) with electrostatic effects taken into account.

Several physical effects can be singled out. The first is the asymmetry in plasma density profiles in the north–south direction, which depends on the magnitude of the shear

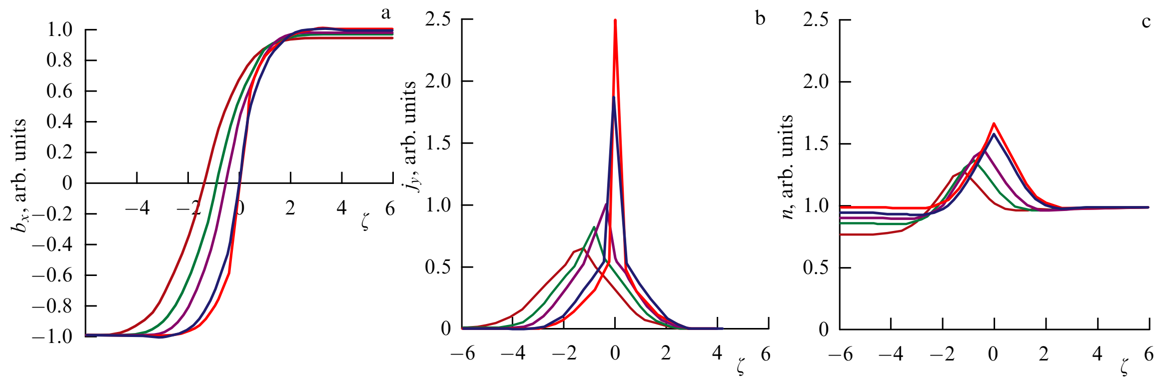

Figure 16. (Color online.) Profiles of (a) a dimensionless magnetic field and the densities of (b) current and (c) plasma as functions of the dimensionless coordinate ζ (the variables are described in the Appendix) in a TCS for various magnitudes of the shear magnetic field B_y for the parameter $\varepsilon = 0.1$ [96]. The profiles are given for $b_y = B_y/B_0 = 0$ (red), $b_y = 0.1$ (blue), $b_y = 0.2$ (violet), $b_y = 0.3$ (green), and $b_y = 0.4$ (brown).

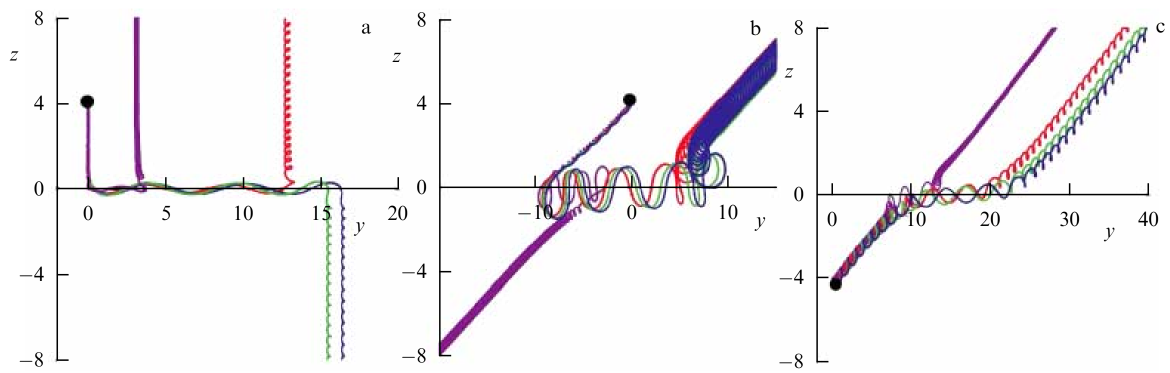

Figure 17. (Color online.) Projections of trajectories of four protons in a TCS on the yz plane (a) in the absence of magnetic shear, $B_{y0}/B_{x0} = 0$ ($\kappa = 0.12$), and also in its presence with the relative magnitude $B_{y0}/B_{x0} = 0.2$ for particles from (b) the northern and (c) southern sources. Spatial variables are normalized by the proton gyroradius at the CS boundaries; particles have the same initial energies and the initial pitch angles are $\theta = 0.15, 0.36, 0.65$, and 1.35 rad (the respective blue, green, red, and violet lines).

magnetic field component. The difference in plasma densities is explained by the difference in plasma reflection coefficients for different values of b_y. The current density and magnetic field profiles in the TCS are asymmetric. Owing to the meandering motion of ions in the neutral plane, the Speiser ions maintain a practically symmetric bell-shaped current density profile. At the boundaries of the CS, particles become magnetized and experience substantial diamagnetic drift in the negative y direction. This is accompanied by weak negative currents observed at the boundaries of the CS, the so-called diamagnetic wings [89]. In the Northern Hemisphere ($\zeta > 0$), the plasma density is larger than in the southern one; therefore, the net current is partly compensated by considerable negative diamagnetic currents, which creates an asymmetry in the current density. The second effect is related to electron currents, which are linked to the curvature current and greatly depend on the magnitude of b_y at the center of the TCS, where the curvature of magnetic field lines is smaller in the presence of the shear component. The electron currents practically disappear for $B_y/B_{x0} \geqslant 0.3$; the current density profile in the TCS thickens and becomes smoother for large values of the shear component. When electron currents are practically equal to zero, the effects of CS broadening and ion current dominance are observed in the TCS [96]. The effect of CS thickening is driven by a geometrical factor: in the presence of magnetic shear, the neutral plane becomes 'tilted', while ions become unmagnetized earlier than they reach the neutral plane $z = 0$. As a consequence, the width of the current density profile in projection on the z axis increases.

The influence of magnetic shear on quasi-adiabatic trajectories of protons in a TCS is also illustrated in Fig. 17. As an example, it shows trajectories of four particles launched at different pinch angles in configurations without a shear component, $B_{y0} = 0$ (Fig. 17a), with it, $B_{y0} > 0$ (Fig. 17b), and the particle source in the northern hemisphere, and with the source in the southern hemisphere (Fig. 17c). The relative magnitude of the shear component in Fig. 17b is $B_{y0}/B_{x0} = 0.2$ (B_{x0} is the tangent component of the magnetic field at the CS boundaries). The figure shows projections of particle motion on the yz plane in dimensionless coordinates (see the Appendix); the initial particle positions are labeled by black dots. The figure demonstrates essential differences in particle dynamics. In the absence of shear, the trajectories of particles launched from the northern and southern hemispheres are practically identical (Fig. 17a). For $B_{y0} \neq 0$, scattering of particles acquires asymmetry on their interaction with the CS. The character of particle motion depends on the source position: it remains quasi-adiabatic for the northern source; in this case, jumps of the quasi-adiabatic invariant are on average larger than in the case $B_{y0} = 0$, and the particles can be reflected back to the source or pass to the

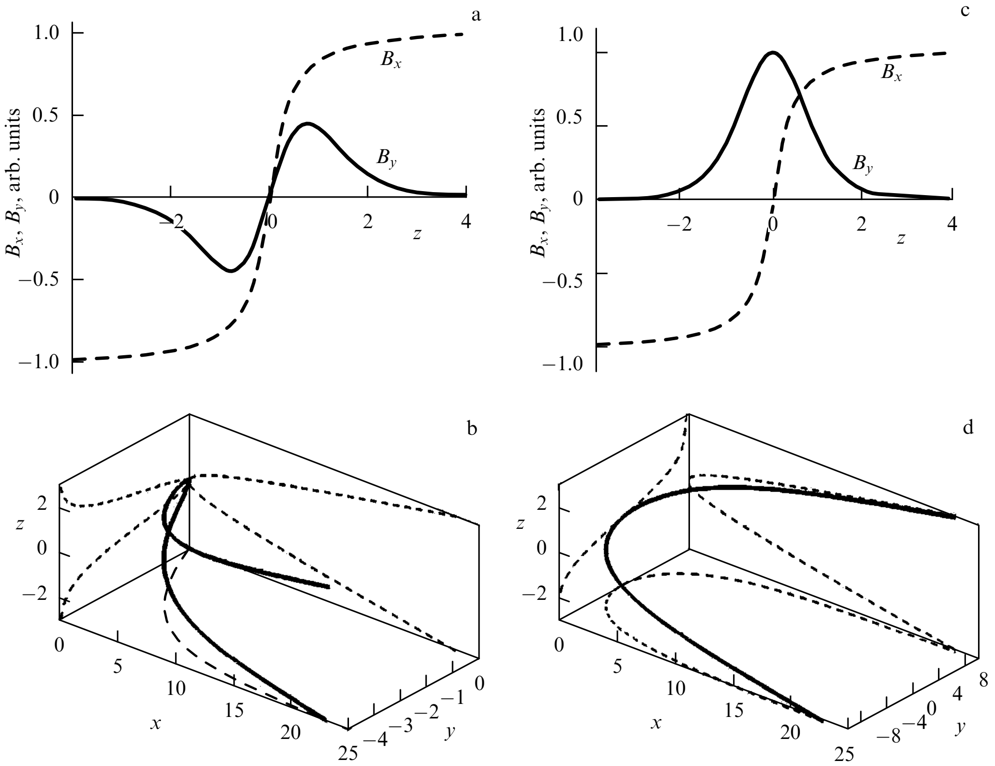

Figure 18. Geometry of magnetic field lines in Earth's magnetotail [157]. (a) Profiles of the antisymmetric component $B_y(z)$ (solid line) and the tangent component $B_x(z)$ (dashed line); (b) the related shape of the field line and its projections on coordinate planes. (c) The z profiles of the symmetric shear (solid line) and tangent (dashed line) magnetic field components, (d) the related shape of the field line. The coordinates $\{x, y, z\}$ are normalized by the ion Larmor radius at the CS boundary.

opposite hemisphere on interaction with the TCS (Fig. 17b). In contrast, protons from the southern hemisphere have a tendency to magnetize along the magnetic field lines (Fig. 17c) and move to the opposite hemisphere practically without being scattered. The difference in proton dynamics can be the cause of weak asymmetry in the plasma and current densities in the TCS with a shear component. A slope of the plane of meandering trajectories relative to the plane $z = 0$ (geometric factor) can be discerned from Fig. 17b. Another effect is more prominent: because of the difference in the scattering of protons arriving from both sources, the concentration of particles in the northern hemisphere exceeds that in the southern one. The new pressure balance forces the CS to move to the side of lower plasma density, i.e., toward the southern hemisphere, which is seen in Fig. 16. If the shear component is negative, $B_{y0} < 0$, all the effects mentioned above become mirror-reflected in the plane $z = 0$. Properties of quasi-adiabatic particle motion in a magnetic configuration with shear are explored in Ref. [148].

Below, we consider a more complex magnetic configuration where the shear component is no longer constant but depends on the coordinate z transverse to the current sheet.

2.5.3 Self-organization of the shear magnetic component in a TCS and mechanisms for the formation of asymmetric configurations. In a CS without magnetic field shear, all field lines lie in planes orthogonal to the neutral plane xy. If a constant shear component is present in the system, the planes with field lines turn through the same angle with respect to the neutral plane. If the shear component acquires a dependence on the z coordinate, the geometry of the field line can take two main configurations: the magnetic field $B_y(z)$ can be either symmetric or antisymmetric with respect to the plane $z = 0$.

Figures 18a, b schematically show the characteristic profiles of the tangent $B_x(z)$ and shear $B_y(z)$ components, and Figs 18c, d plot the respective three-dimensional field lines and their projections. In all cases, the magnetic field lines are reversed in the neutral plane, but in the cases in Fig. 18a, c the magnetic field line are twisted, and in the cases in Fig. 18b, d the deformation of the field line is of the type of bending, i.e., the field line lies on a smooth curved surface [157].

Together with the 'semianalytic' approach to the problem described in the Appendix, to verify the results obtained for the equilibrium structure of a TCS and various dynamical regimes, numerical modeling of TCSs was carried out by tracing macroparticles in magnetic and electric fields, with a subsequent step of making the currents ($j(z)$ and $j_x(z)$) and magnetic fields ($B_x(z)$ and $B_y(z)$) self-consistent [100, 102]. The main assumptions of the numerical model correspond to those in the Appendix. In some of the computations, the shear component $B_y(z)$ was taken to be the sum of a self-consistent part $B_y^{\mathrm{S}}(z)$ and an external constant field B_y^{E}: $B_y(z) = B_y^{\mathrm{S}}(z) + B_y^{\mathrm{E}}$. Above and below the region $|z| < L$, where L is the CS thickness, the magnetic field was taken to be constant,

$$\begin{aligned} \mathbf{B}\big|_{z \geqslant L} &= B_x(L)\mathbf{e}_x + B_y^{\mathrm{E}}\mathbf{e}_y + B_z\mathbf{e}_z\,, \\ \mathbf{B}\big|_{z \leqslant -L} &= B_x(-L)\mathbf{e}_x + B_y^{\mathrm{E}}\mathbf{e}_y + B_z\mathbf{e}_z\,. \end{aligned} \tag{21}$$

The distribution function $f_0(z, \mathbf{v}, n_{(\pm)}, T_0, V_{\mathrm{D}})$ was taken as a shifted Maxwellian distribution on the CS boundary and was implemented by the generation of $N_{\mathrm{g}} = 3 \times 2^{17}$ model

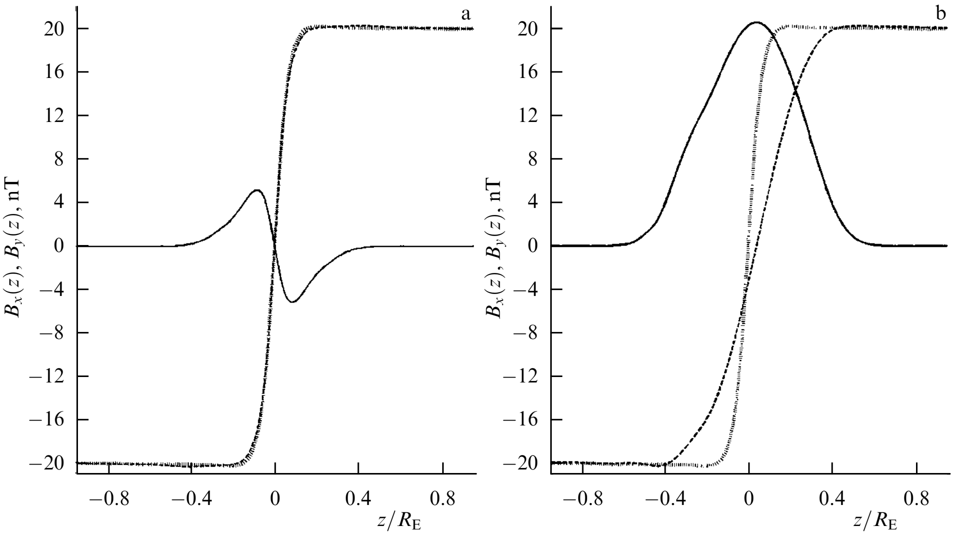

Figure 19. Magnetic field components in a current sheet for $B_y^\mathrm{E} = 0$: (a) antisymmetric and (b) bell-shaped components $B_y(z)$ (solid lines). The dashed lines show the components $B_x(z)$, and light dotted lines depict profiles of $B_x^0(z)$ in the case where the field has no shear ($B_y(z) \equiv 0$). The spatial coordinate z is normalized by Earth's radius R_E here and in Figs 20 and 21.

macroparticles with 16 energy levels. In the course of modeling, the concentration $n(z)$, components of the proton current $\mathbf{j}(z)$, and self-consistent components of the magnetic field $B_x(z)$ and $B_y(z)$ were computed. The input parameters were selected as follows: the temperature $T_0 = 4$ keV, which gives $V_\mathrm{T} = \sqrt{eT_0/m_\mathrm{p}} \approx 619$ km s^{-1} for thermal velocity of protons, $V_\mathrm{D} = 2V_\mathrm{T}$, $\Delta B_x = 40$ nT, and $B_z = \Delta B_x/20 = 2$ nT.

Modeling results can be subdivided into three main groups, in which the shear magnetic field component $B_y(z)$

(1) is absent;

(2) is fully self-consistent and takes two main forms, symmetric or antisymmetric with respect to the coordinate z;

(3) has two components $B_y(z) = B_y^\mathrm{S}(z) + B_y^\mathrm{E}$, one of which, $B_y^\mathrm{S}(z)$, is self-consistently maintained by the current component $j_x(z)$ (which corresponds to the symmetric or antisymmetric mode), and the other, $B_y^\mathrm{E} = \mathrm{const}$, is external, caused by the global effect of the solar wind.

The case with a zero shear component $B_y(z) \equiv 0$ is a basic configuration in which $j_x(z) \equiv 0$, and the tangent magnetic field component is an odd function, $B_x(-z) = -B_x(z)$ [96, 100, 102].

Figure 19 demonstrates self-consistent profiles for the two components of the magnetic field in a TCS for antisymmetric (Fig. 19a) and bell-shaped (Fig. 19b) distributions of $B_y(z)$. The basic profile $B_x^0(z)$ is plotted with the gray dashed line. We note that profiles of the tangent magnetic field $B_x(z)$ have a shape characteristic for CSs: they vanish in the neutral plane $z = 0$ and tend to a constant value (saturation) with the distance from it. In the case of an antisymmetric $B_y(z)$ (Fig. 19a), the $B_x(z)$ component saturates at $|z|/R_\mathrm{E} \approx 0.2$, and in the case of a 'bell-shaped' $B_y(z)$ (Fig. 19b), at $z/R_\mathrm{E} \approx 0.4$; hence, the thickness of the CS with the current along the y axis is twice as large as in Fig. 19a. Interestingly, in the first case, the amplitude of the self-consistent shear field is small (5 nT), and in the second case it is comparable to the amplitude of the tangent field (21 nT). A comparison of Figs 19a and b allows concluding that the effect of the shear component $B_y(z)$ with a shape that is close to a symmetric bell leads to the broadening of the CS and to some weak violation of the antisymmetry in $B_x(z)$ and the symmetry in $B_y(z)$. This is related to the scattering asymmetry for particles from the northern and southern sources as they interact with the CS.

Figure 20 illustrates the distribution of the densities of longitudinal and transverse currents. In the antisymmetric case (Fig. 20a), the current is concentrated in the center of a narrow region $|z|/R_\mathrm{E} \leqslant 0.2$ and exhibits a sharp maximum, whereas in the symmetric case, the spatial region occupied by the current is approximately twice as broad, $|z|/R_\mathrm{E} \leqslant 0.4$, and the amplitude is approximately one third as high. The comparison with the profile that corresponds to the basic configuration of the TCS (the gray dashed line), points to a substantial broadening of the CS with a symmetric mode. We note that the tangent fields maintained by longitudinal currents in the model have approximately equal amplitudes in both configurations (see Fig. 19). Figure 20 also shows that the longitudinal currents $j_x(z)$ are local, because the components $B_y(z)$ maintained by them tend to zero outside the TCS. The dashed-dotted lines in Fig. 20 plot the profile of the longitudinal current $j_x^0(z)$ for the basis configuration. It can be seen that $j_x^0(z)$ is much smaller in absolute value than the basic current component $j_y^0(z)$ and the self-consistent component $j_x(z)$ for two configurations with the $B_y(z)$ component. Thus, in the numerical model, the absence of $B_y(z)$ in the basic configuration is fully relevant. We note that for all three configurations displayed in Figs 19 and 20, the z component of the current density $j_z(z)$ is only a very weak discrete noise. Hence, with high accuracy the model can be considered spatially one-dimensional.

We now discuss how the equilibrium configuration of a TCS is modified by a constant external magnetic field B_y^E, which coexists with the self-consistent shear component $B_y^\mathrm{S}(z)$, i.e., the full shear field is $B_y = B_y^\mathrm{S}(z) + B_y^\mathrm{E}$. As a result of numerical computations, a family of stationary configurations of a TCS is obtained for two different distributions of the shear field in the presence of a constant B_y^E component.

Figure 21 displays profiles of self-consistent magnetic field components for several values of B_y^E. It can be seen

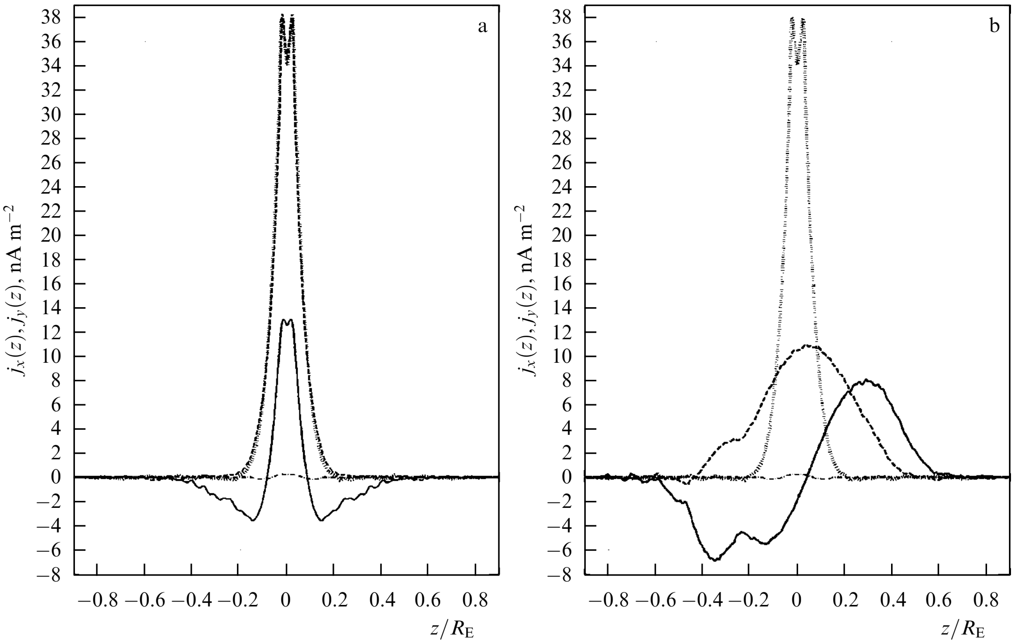

Figure 20. Current density components in the CS for the external shear magnetic field $B_y^E = 0$ in the cases of (a) an antisymmetric and (b) a bell-shaped component $B_y(z)$. The dashed line corresponds to $j_y(z)$ and the solid one to $j_x(z)$. In both panels, the gray curves correspond to the case $B_y(z) \equiv 0$, with $j_y^0(z)$ given by the dotted line and $j_x^0(z)$ by the dashed-dotted one.

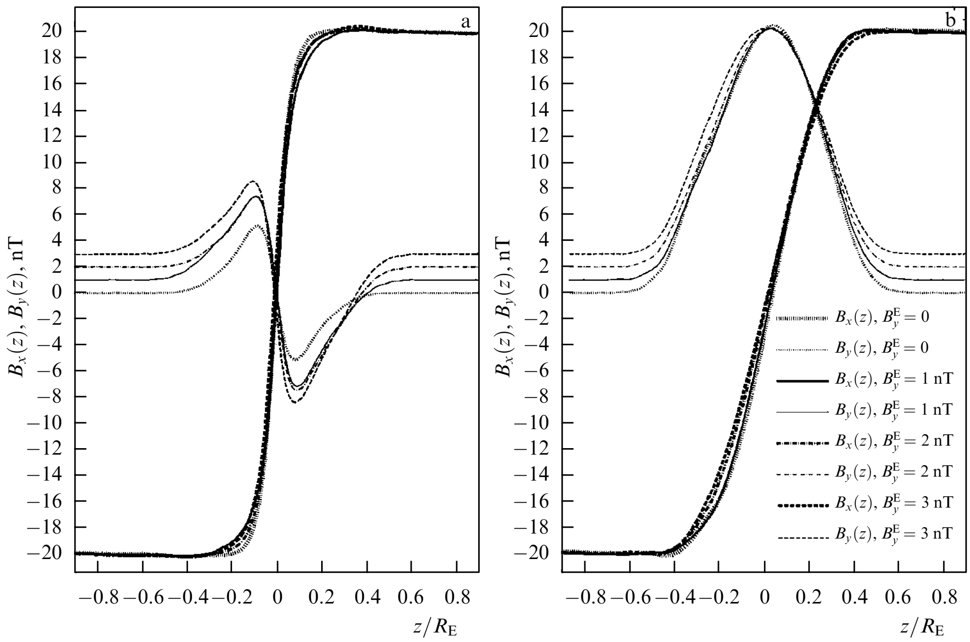

Figure 21. Magnetic field component in the CS for various B_y^E in the cases of (a) an antisymmetric $B_y(z)$, (b) a bell-shaped $B_y(z)$. For $B_y^E = 0$, the light dotted line plots $B_y(z)$ and the thick dotted line plots $B_x(z)$. For $B_y^E = 1$ nT, the light solid line plots $B_y(z)$ and the thick one $B_x(z)$. For $B_y^E = 2$ nT, dashed-dotted lines are used, and for $B_y^E = 3$ nT the lines are dashed.

that with the increase in B_y^E, the current profiles for both configurations with magnetic shear vary only slightly compared with those for $B_y^E = 0$, i.e., the presence of external shear neither changes the thickness of the CS nor deforms it. This implies that the main mechanism of the TCS formation under the action of a shear magnetic field is the action of longitudinal currents and the related self-consistent shear component. The external magnetic field does not deform the CS and leaves its thickness intact.

2.6 Solutions in the parameter space

The model of TCSs was explored in the parameter range characteristic of Earth's magnetosphere. The range of the initial perturbation amplitudes $B_y(0) = B_y^A$ was 0–20 nT and of the normal magnetic component B_z, 0–3 nT with a step of 1 nT. We note that in all numerical experiments, the initial shear perturbation had a symmetric shape with respect to the z coordinate and a positive amplitude B_y^A. Numerical simulations revealed two main classes of self-consistent

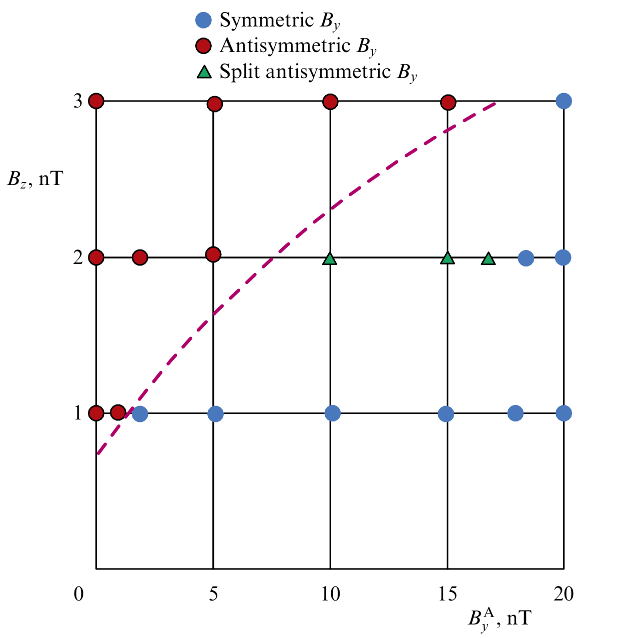

Figure 22. (Color online.) Types of self-consistent current sheet configurations in the parameter domain $\{B_y^A, B_z\}$.

solutions: (1) with a symmetric profile of the shear component B_y (Fig. 19b), (2) with an asymmetric profile of $B_y(z)$ (Fig. 19a). Additionally, several configurations were found with a transient, asymmetric distribution of B_y (the slopes of profiles in the northern, $z > 0$, and southern, $z < 0$, hemispheres being different) and the weakly split current density profile, realized for a narrow parameter region on the boundary between the two main configurations.

Figure 22 displays the parameter plane of solutions, in which the symmetric configurations are located in a triangle-shaped parameter subdomain $\{B_y^A, B_z\}$ with the boundary approximately described as $B_z \approx \xi B_y^A$, where ξ is a positive number. When the normal magnetic field component B_z is increased, the region where antisymmetric solutions $B_y(z)$ are observed becomes wider, and for $B_z = 4$ nT practically all solutions become antisymmetric, even though the initial perturbation amplitude B_y^A is large and comparable in magnitude to the tangent component $B_x(L)$. The intermediate current configurations, characterized by an asymmetric distribution of the shear component and a split profile of the current density $j_y(z)$, are located at the boundary between symmetric and asymmetric current sheets with a shear magnetic field; their appearance can hence be explained by the influence of the antisymmetric configuration of the CS on the symmetric configuration for large values of B_z.

To clarify the physics of processes maintaining such a structure of equilibrium solutions, we consider the dynamics of charged particles in a TCS with a shear magnetic field. Figure 23 presents results of tracing four particles with equal energies and different pitch angles $\theta_j = 0.15$, 0.35, 0.65, and 1.45 rad $(j = 1, 2, 3, 4)$ in the magnetic field $\mathbf{B} = (B_0 \tanh(z/L); B_y^A/\cosh^2(z/L); B_z)$ introduced above. The trajectories of particles are shown in the yz plane for three values of the normalized field $B_y^A/B_0 = \{0; 0{,}4; 0{,}8\}$ in Figs 23a, d; 23b, e; and 23c, f. Figures 23a–c correspond to particles starting from the northern hemisphere, and Fig. 23d–f correspond to particles starting from the southern hemisphere. Particle trajectories in the absence of the magnetic field shear component are presented in Fig. 23a, d: particles are magnetized outside the CS; entering the sheet, they become unmagnetized and drift in the positive y direction. Analysis of a large number of trajectories confirms that the coefficients of particle reflection on interaction with the CS are practically equal for both sources.

In the presence of a local shear component (Fig. 23b, c, e, f), the asymmetry in scattering for particles coming from the northern and southern hemispheres can clearly be seen. Similar asymmetric scattering in the interaction with a CS can be seen in Fig. 17, where protons move in the CS with a global shear component ($B_y = \text{const}$). Thus, all ions coming from the southern hemisphere (Fig. 23e, f) cross the CS and enter the northern hemisphere. Furthermore, their averaged trajectory nearly repeats the shape of the magnetic field line in the yz plane because ions are magnetized in the center of

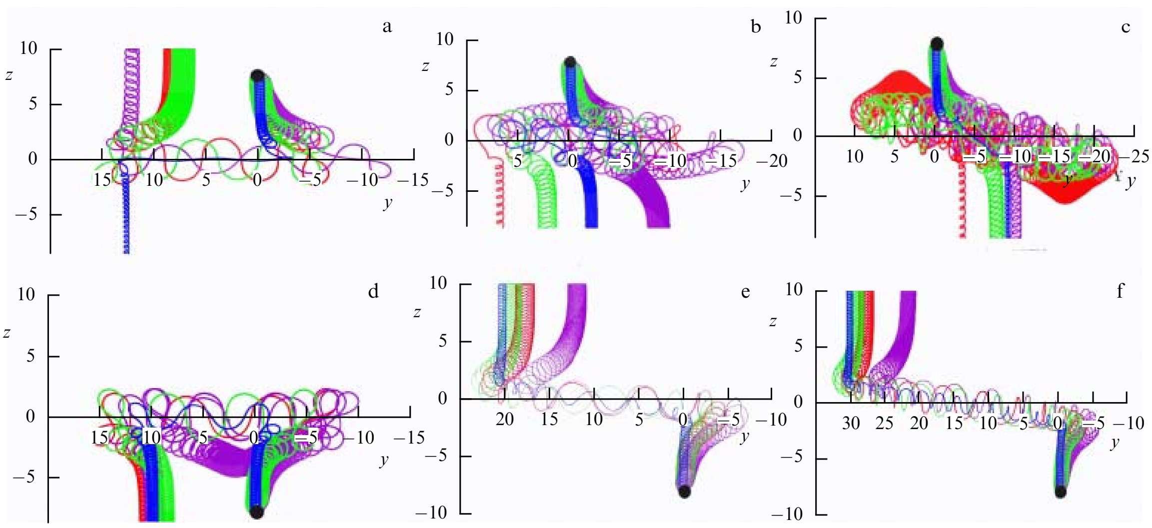

Figure 23. Tracing four particles from the (a–c) northern and (d–e) southern sources in a field reversal region with a local shear. Spatial variables are normalized by the ion gyroradius at the CS boundaries. The initial pitch angles of particles are $\theta_1 = 0.15$, $\theta_2 = 0.35$, $\theta_3 = 0.65$, and $\theta_4 = 1.45$. The ratio B_y^A/B_0 ($B_0 = 20$ nT) is 0 (a, d), 0.4 (b, f), and 0.8 (c, e).

the CS for the values of the B_y component being considered. Particle motion can be decomposed into a superposition of two independent motions: meandering motion and Larmor rotation (close to the center of the TCS, where the amplitude of the shear field is large). Both motions are directed along magnetic field lines, and become aligned in the center of the sheet and oriented along the coordinate $y > 0$. Because the magnetic field lines turn around the TCS, magnetized ions maintain the longitudinal current density $j_x(z) \sim \sin(\pi z/L)$.

The study of ion scattering in a TCS with magnetic shear leads to the following conclusion. The formation of a symmetric shear component $B_y(z)$ is related to the fact that the initial deformation of magnetic field lines modifies the dynamics of particles in a CS. This modification is such that the scattering of protons traversing the sheet substantially depends on the location of plasma sources. On magnetized intervals of their orbits, particles from the southern hemisphere carry a longitudinal current j_x along the magnetic field lines. Its direction is negative in the southern hemisphere and positive in the northern one, i.e., $j_x(z) \sim \sin(\pi z/L)$. But the ions from the northern hemisphere experience strong scattering in the sheet plane. The current density maintained by them is opposite in direction to the current density of the 'southern' particles, being much smaller in amplitude. As a result, the contribution of southern particles to the current $j_x(z)$ becomes dominant and is not compensated by the contribution from the 'northern' ions. This leads to a self-consistent amplification and maintenance of the shear field component inside the CS.

Thus, the main mechanism leading to the formation of the symmetric shear magnetic component in a TCS is the asymmetry of ion scattering in the north–south direction as they interact with the TCS, if there is some initial deformation of the sheet.

3. Thin current sheets with a longitudinal inhomogeneity in the antisolar direction in Earth's magnetotail

The development of CS models demonstrated that the kinetic models are most interesting, and that the MHD approximation is not quite applicable to the description of configurations with a small thickness $\rho_{\mathrm{L}} \sim L$. The earliest well-known kinetic model of CSs is the self-consistent model of Harris [74] mentioned in Section 1, dealing with a one-dimensional CS with a zero transverse magnetic field component. In Section 2, we considered a class of one-dimensional TCS models with a transverse magnetic field, in which the tension of magnetic field lines is balanced by the inertia force of ions crossing the sheet [86–89]. It is worth noting that all these models of TCSs ignore the inhomogeneity of the transverse magnetic component B_z along the tail, originating from the planetary dipole magnetic field. It is known that the B_z component decays on average with the distance x from Earth as $(L_x/x)^{0.8}$ [76, 157]. The gradient of the magnetic component B_z creates a large-scale longitudinal inhomogeneity of the CS in the antisolar direction. The longitudinal inhomogeneity was taken into account in Ref. [96]. The model developed there is a two-dimensional generalization of the one-dimensional kinetic model of TCSs proposed previously [90].

In what follows, we turn to specific features of particle dynamics in an inhomogeneous CS, because these features determine the characteristics and fine structure of TCSs. We consider the main assumptions under which this model is applicable and present the main modeling results [19, 90, 91].

The first numerical studies of the effect of a longitudinal inhomogeneity of the magnetotail on particle motion were carried out in the framework of a global model of the magnetosphere in Ref. [85], where it was shown that solar wind ions can be trapped in the vicinity of the neutral sheet and perform large-scale oscillations around it. The convection electric field E_y, crossed in the neutral layer with the transverse magnetic field B_z, enforces the drift of plasma particles toward Earth with the convective velocity $\mathbf{V}_{\mathrm{c}} = c\mathbf{E}_y \times \mathbf{B}_z/B_z^2$. It was also shown that particle motion preserves the quasi-adiabatic invariants of motion I_z and the longitudinal quasi-adiabatic invariant $I_x = (m/2\pi)\oint v_x\,\mathrm{d}x$ [158] (v_x is the particle velocity along the magnetotail and $\mathrm{d}x$ is the displacement increment along the x axis), which are analogs of longitudinal invariants in the guiding center theory. Thus, in a two-dimensional configuration of a CS, along with exact integrals of motion, such as the total energy $W_0 = mv_0^2/2 + e\varphi$ (v_0 is the initial particle velocity, e is the charge, and φ is the electrostatic potential) and the generalized momentum $P_y = mv_y + (e/mc)A_y(x,z)$, the motion of ions can be characterized by approximate adiabatic invariants I_z and I_x. Here, $A_y(x,z) = -\int B_x(z)\,\mathrm{d}z + \int B_z(x)\,\mathrm{d}x$ is the vector potential of the system.

The model of TCSs with a longitudinal magnetic inhomogeneity relies on general assumptions 1–6 in the Appendix and the following additional assumptions [159].

(1) The magnetic field in the TCS is orthogonal to the current direction and has two self-consistent components $B_x(z)$ and $B_z(x)$ in the GMS coordinate system, which satisfy the condition $\operatorname{div}\mathbf{B} = 0$. The shear component is ignored in this model, i.e., $B_y = 0$.

(2) The magnetic field B in the CS is practically homogeneous in the dawn–dusk direction (y), weakly inhomogeneous in the Earth–Sun direction (x), and strongly inhomogeneous in the direction perpendicular to the sheet (z), such that the following relations hold between the scales: $L_\beta \sim B/(\partial B/\partial x_\beta) \gg L_z$, where L_β, $\beta = x, y$, are the characteristic scales of the magnetic field in the magnetotail in the x and y directions, and L_z is the TCS thickness. Because the tangent field component is zero in the neutral plane, the inhomogeneity scale is determined by the 'slowness' of the change of the normal component $B_z(x)$. All quantities in the model depend only on the coordinates x and z (there is no dependence on y because of translation invariance).

The distribution functions of transient $f_{\mathrm{trans}}(\mathbf{v})$ and quasi-trapped $f_{\mathrm{trap}}(\mathbf{v})$ plasma components are taken in the form

$$
\begin{aligned}
f_{\mathrm{trans}}(\mathbf{v}) &= \frac{n_1}{(\pi v_{\mathrm{Ti}})^3 (1 + \operatorname{erf}\varepsilon^{-1})} \\
&\quad\times \exp\left\{-\frac{1}{v_{\mathrm{T}}^2}\left[\left(\sqrt{v_0^2 - \frac{\omega_0}{m} I_z} - v_{\mathrm{D}}\right)^2 + \frac{\omega_0}{m} I_z\right]\right\}, \\
f_{\mathrm{trap}}(\mathbf{v}) &= \frac{n_1}{(\pi v_{\mathrm{Ti}})^3 (1 + \operatorname{erf}\varepsilon^{-1})}\, K_{\mathrm{trap}} \\
&\quad\times \exp\left[-\frac{v_{\mathrm{D}}^2 + v_0^2 + (\omega_0/m) I_x}{v_{\mathrm{T}}^2}\right],
\end{aligned}
\tag{22}
$$

where we use a free parameter K_{trap} that characterizes the density of trapped particles (their source can be independent of transient particles). The quasi-adiabatic invariants are

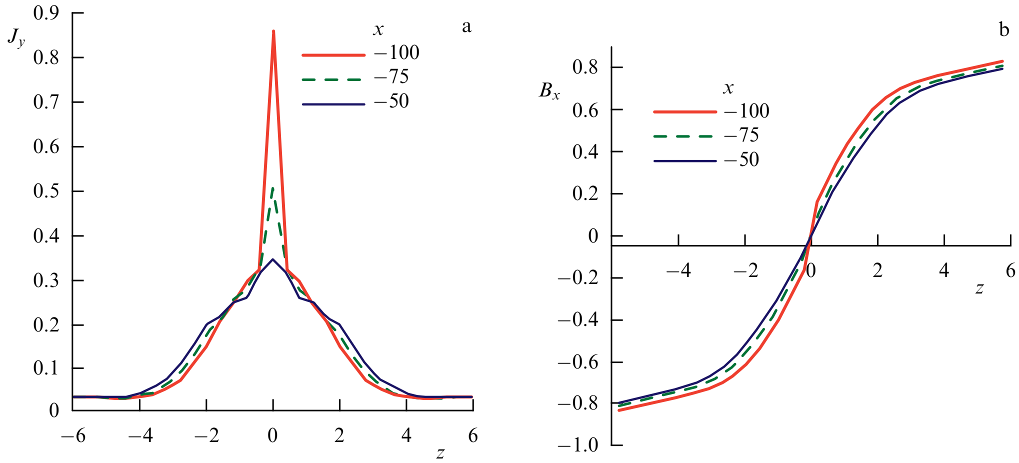

Figure 24. Profiles of (a) the currents and (b) the magnetic field along the TCS in cross sections $x = -100$ (gray solid line), $x = -75$ (dashed line), and $x = -50$ (black solid line) [159].

computed as

$$I_z = \frac{m}{2\pi} \int_{z_0}^{z_1} \left\{ v_0^2 - v_x^2 - \left[m v_y + \frac{e}{mc} \left(A_y(x, z) - A_y(x, z') \right) \right]^2 + \frac{2e}{m} \left(\varphi(x, z) - \varphi(x, z') \right) \right\}^{1/2} \mathrm{d}z' ,$$

$$I_x = \frac{m}{2\pi} \oint v_x \, \mathrm{d}x = \frac{m}{2\pi} \oint \left\{ v_0^2 - v_z^2 - \left[v_y + \frac{e}{mc} \left(A_y(x, z) - A_y(x', z) \right) \right]^2 + \frac{2e}{m} \left(\varphi(x, z) - \varphi(x', z) \right) \right\}^{1/2} \mathrm{d}x' . \quad (23)$$

The model of self-consistent TCSs is roughly given by an open three-dimensional box with the reversed magnetic field. Streams of transient plasma particles enter the box along field lines through the top and bottom faces. Interacting with the neutral sheet, these particles maintain the current in the system and create a self-consistent magnetic field. Quasi-trapped particles are redistributed in the longitudinal direction in agreement with the change in the normal magnetic field and contribute to the local redistribution of currents and fields in the system. Magnetized electrons perform large-scale oscillations in the vicinity of the neutral layer. The most important component in the motion of electrons is their strong drift due to curvature of the magnetic field lines, which is inversely proportional to the curvature radius [90]. Thus, electron drift currents are localized in the region where the curvature of field lines is minimal, the neutral plane.

The model is based on the system of Vlasov–Maxwell equations for the densities of currents, particles, and the vector potential. The plasma is assumed quasineutral. The ion part of the currents is described by the equations [159]

$$\Delta A_y = -\frac{4\pi}{c} (j_{y\mathrm{i}} + j_{y\mathrm{e}}) ,$$

$$j_{y\mathrm{i}} = e \int_{V^3} v_y \left[f_{\mathrm{trans}}(W_0, I_z) + f_{\mathrm{trap}}(W_0, I_x) \right] \mathrm{d}^3 v ,$$

$$\frac{\mathrm{d} f_{\mathrm{trans}}}{\mathrm{d}t} = 0 , \qquad \frac{\mathrm{d} f_{\mathrm{trap}}}{\mathrm{d}t} = 0 ,$$

$$A_y(x_0, z) = a_{\mathrm{l}}(z) ,$$

$$A_y(x_1, z) = a_{\mathrm{r}}(z) ,$$

$$A_y(x, -L_{\mathrm{a}}) = \psi_0(x) ,$$

$$A_y(x, L_{\mathrm{a}}) = \psi_1(x) . \quad (24)$$

Here, $j_{y\mathrm{i}}$ and $j_{y\mathrm{e}}$ are the densities of ion and electron currents ($n_{\mathrm{e}} = n_{\mathrm{i}}$), $a_{\mathrm{l}}(z)$, $a_{\mathrm{r}}(z)$, $\psi_0(x)$, and $\psi_1(x)$ are the given distributions of the vector potential on the left/right and top/bottom box boundaries, which are varied in agreement with the specific form of the system to be explored. In the case of a two-dimensional CS, the hybrid equations for the vector potential take the form

$$\frac{\partial^2 A_y(x, z)}{\partial x^2} + \frac{\partial^2 A_y(x, z)}{\partial z^2} + \frac{4\pi}{c} \left\{ \int_{V^3} v_y \left[f_{\mathrm{trans}}\left(W_0, I_z(z, \mathbf{v}) \right) + f_{\mathrm{trap}}\left(W_0, I_x(x, \mathbf{v}) \right) \right] \mathrm{d}^3 v + j_{\mathrm{e}} \right\} = 0 , \quad (25)$$

where the distribution functions are given by expressions (22) and the adiabatic invariants are computed by Eqns (23). A detailed description of electron motion and computations of the electrostatic potential are given in the Appendix (see also Ref. [96]).

The Vlasov–Maxwell system of equations (24) with boundary conditions and distribution functions (22) was solved numerically. The self-consistent profiles of dimensionless densities of plasma and current, and the magnetic field were found for a two-dimensional TCS.

The profiles of the current and magnetic field in cross sections $x = -100$, -75, and -50 (in units of the Larmor radius ρ_{L} at the boundary of the TCS, at $x = x_0$ of the box considered) of the magnetotail are plotted in Fig. 24. All variables are given in dimensionless form: $J_y = j_y / (e n_0 v_{\mathrm{D}} \varepsilon^{2/3})$, $\mathbf{r} = \mathbf{R} / \rho_{\mathrm{L}}$, $n = N(x, z) / n_0(x, L)$, and $B_x = \tilde{B}_x / B_0(x_0, L)$. As follows from the figure, in the TCS region that is closer to Earth ($x = -50\rho_{\mathrm{L}}$), the current density is bell-shaped, which points to the dominance of the transient ion current. The thickness of such a CS stays practically constant along the x axis, equal to several Larmor radii, which coincides with estimates made previously in Refs. [20, 157]. With the distance from Earth, a narrow electron current embedded into a wider ion current begins to prevail in the

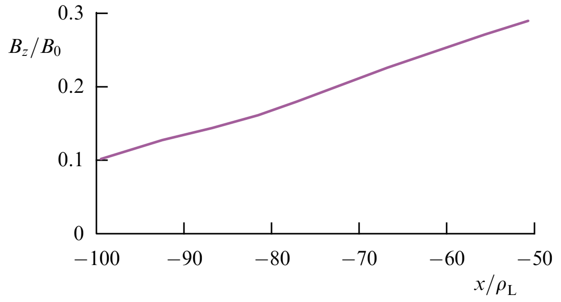

Figure 25. Profile of the normalized magnetic field component B_z along a CS.

neutral plane. The corresponding magnetic field profiles become steeper there, as can be seen by comparing the magnetic field profiles shown for $x = (-75, -100)\rho_L$ (ρ_L is the Larmor proton radius far from the CS on the earthward face of the model box).

The self-consistent profile of the magnetic field component B_z along the CS is depicted in Fig. 25. In the first iteration of the solution algorithm, this profile is taken as a linear one, increasing toward Earth. In the final solution, its distribution is determined by electron currents, but the linear dependence on x is preserved.

We now consider the contributions to the net current from different particle populations. Figure 26 demonstrates the current density distribution maintained by transient ions in various tail cross sections. We see that the role of transient ions amounts to maintaining a practically one-dimensional CS that is independent of the longitudinal inhomogeneity of the magnetic field and the jump of B_z along it. However, the density of quasi-trapped particles turns out to be sensitive to the longitudinal inhomogeneity of the sheet: their concentration increases in the region where the transverse magnetic field is larger (see Fig. 26) and, accordingly, the amplitudes of their local currents are the higher, the closer they are to Earth.

The plasma density profiles in different cross sections of the magnetotail (Fig. 27) show that just as in the real case, the plasma density increases in the direction toward Earth. This happens owing to the quasi-trapped particles, whose distribution is sensitive to the distribution of the transverse magnetic field component B_z. Furthermore, the plasma density profiles tend to a constant at the boundaries of the CS, whereas the current density tends to zero there. Hence, we conclude that the CS is confined inside a much wider plasma sheet, which agrees with experimental observations of Earth's magnetotail. Quasi-trapped ions contribute to an effective increase in the CS width, which on average becomes wider as their concentration increases [159].

As regards the electron currents, their amplitude is inversely proportional to the curvature radius of magnetic field lines [90], and it is therefore natural to expect that they reach a maximum at the locations where the magnetic component B_z is minimal, i.e., at the CS boundary that is the farthest from Earth, as illustrated in Fig. 28.

The shape of current density profiles in TCSs was explored for different densities of quasi-trapped protons in the magnetotail. Figure 29 plots two-dimensional current density surfaces (in the xy plane). Figure 29a shows a classical bell-shaped current density profile maintained by transient protons and electrons, in which case the density of quasi-trapped plasma is much smaller than the density of the main current carriers. The increase in the density of this population in the magnetotail, shown in Fig. 29b, can result in a noticeable splitting of the current density profile in the region of the CS nearest to Earth, whereas splitting is small in the more distant part, and an embedded profile of the proton current with a peak of the electron density at the center is apparent. As a result, the structure with three current density maxima is formed, which was described previously, e.g., in Refs [90, 94]. Figure 29c shows an essentially split structure of TCSs for a high density of plasma, quasi-trapped in the CS (for $K_{\text{trap}} = 200$, the number of quasi-trapped particles is greater than the number of transient ones by approximately a factor of 1.4).

To summarize, the effect of longitudinal inhomogeneity on the CS structure helps to reveal important differences in the dynamics of electrons and the transient and quasi-trapped ions. The generalization of the quasi-adiabatic model to configurations with a weak inhomogeneity along x when the additional longitudinal quasi-adiabatic integral I_x is still preserved offers an opportunity to treat a TCS distributed along the magnetotail. Three main effects through which the nonadiabatic dynamics of ions and electrons influence the CS structure were identified.

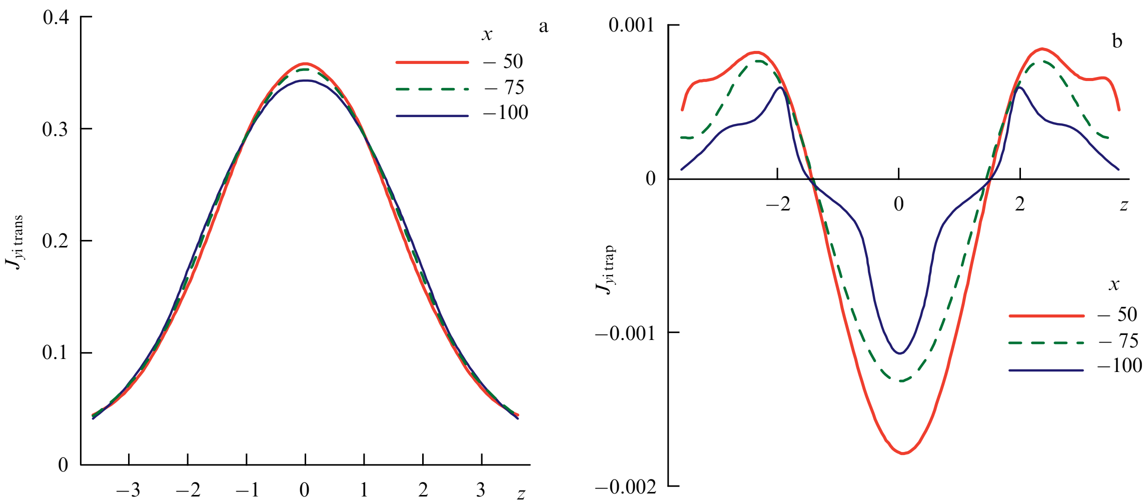

Figure 26. Distribution of partial current densities for (a) transient and (b) quasi-trapped particles in the CS at different distances to Earth.

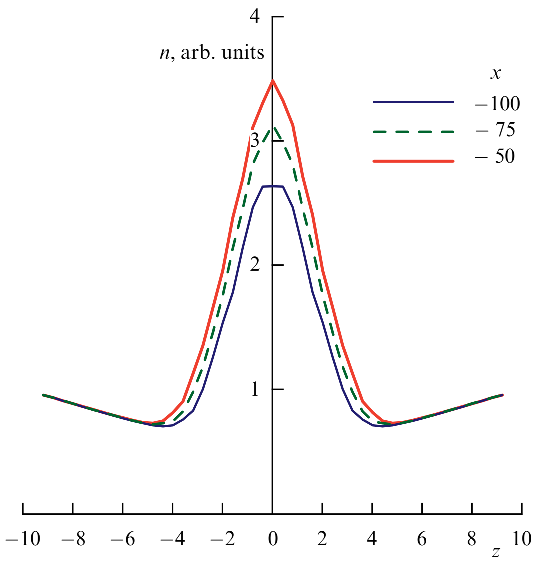

Figure 27. Plasma density in the CS in three cross sections at different x.

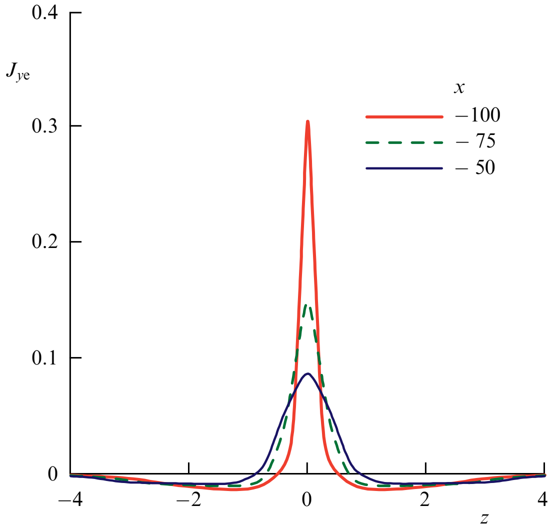

Figure 28. Partial electron current densities in three CS cross sections.

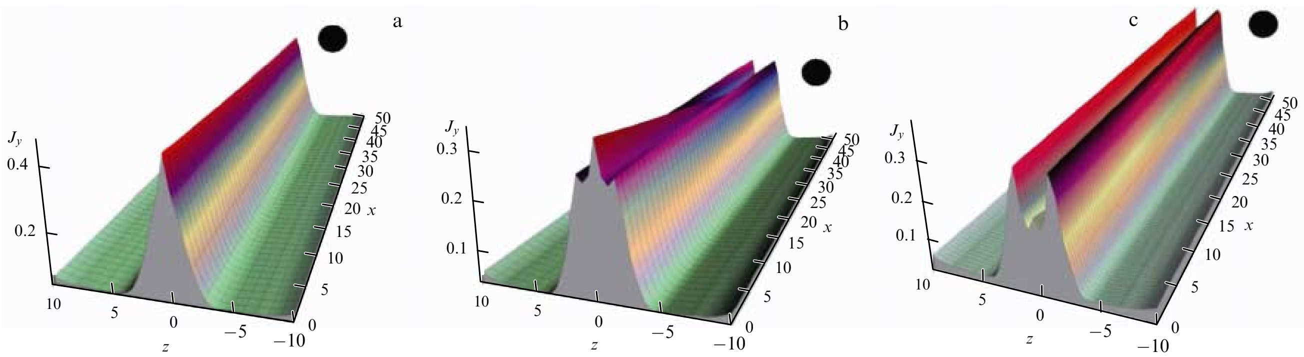

Figure 29. Two-dimensional current density structure in a TCS for different concentrations of quasi-trapped plasma: (a) the coefficient $K_{trap} = 1$ in a system where the density of quasi-trapped particles is small compared with the nontrapped ones; (b) $K_{trap} = 100$, the densities are comparable; (c) the density of quasi-trapped particles is 1.4 times larger, $K_{trap} = 200$. The black dots show Earth's position in the selected reference frame.

(1) Transient ions together with electrons are the main current carriers. However, in contrast to electrons, transient ions maintain a practically one-dimensional current density distribution in the sheet.

(2) Owing to the preservation of the longitudinal quasi-adiabatic invariant I_x of slow oscillations, quasi-trapped ions are redistributed in the CS such that their density increases in the direction of the increasing B_z component, i.e., toward Earth. As a consequence, in the region where their density is higher, the redistribution of the current density of the main carriers can occur, causing expansion of the CS.

(3) The motion of electrons depends in a sensitive way on the inhomogeneity of the magnetic field along the CS: the currents created by them increase in the antisolar direction, in agreement with the decrease in the normal magnetic field and the curvature radius of the field lines.

4. Nonadiabatic ion acceleration in a current sheet and structure formation

In Sections 2 and 3, we mainly considered solutions of the system of equations for plasma equilibria. The conservation of exact invariants of motion (energy, the full velocity, the generalized momentum along the y direction) and approximate ones (I_z and I_x) allowed transforming the distribution functions of transient and trapped protons into functions depending only on the integrals of motion, which could then be extended to the entire phase domain where the equations are integrated. However, this approach is approximate. The propagation of flows of charged particles in magnetic field reversals might be accompanied by exciting phenomena associated not with conservation but with violation of quasi-adiabatic invariants. One such phenomenon is the nonadiabatic acceleration of charged particles in the magnetotail. Below, we consider mechanisms leading to it and present data of related observations in space. Theoretical consideration of the problem in Refs [18, 36, 37, 85,111, 159–161] made it possible to clarify the main mechanisms generating the streams of accelerated particles in Earth's magnetotail and explain the main features of this phenomenon.

Syrovatskii and his colleagues in their early work [12–15, 18] already considered the possibility of strong acceleration of charged particles in a CS. In the presence of an electric field, particles can acquire substantial energy in the neutral plane of the CS, where the magnetic field is sufficiently weak and the first adiabatic invariant is not conserved. In this case, a charged particle 'loses' magnetization and moves along the electric field, accumulating energy owing to a mechanism similar to the Fermi mechanism, on reflection from a 'magnetic mirror' moving with the convection speed $V_c = E/B_z$, where E is the electric field in the CS oriented along the y axis (tangent to the plane of the sheet along the direction of the current) and B_z is a small component of the magnetic field along the normal to the sheet. According to Refs [18, 160, 162],

$$\Delta W \approx \frac{m}{2}(2V_c)^2 = \frac{m}{2}\left(\frac{2E}{B_z}\right)^2 . \tag{26}$$

If a particle in a CS is such that $\kappa < 1$, where κ is the parameter characterizing the degree to which the particle is nonadiabatic [see formula (16)], then its motion is nonadiabatic and cannot be described in the guiding center approximation. In this case, the particle follows a complex, meandering trajectory (see Section 2.1).

As discussed in Section 2.1, two components of nonadiabatic motion characterized by different temporal scales can be singled out based on the kinetic analysis of the trajectories of such particles: (1) a slow, quasi-Larmor particle rotation in a weak magnetic field B_z of the CS; (2) fast oscillations in the plane perpendicular to the CS plane (in the direction of z normal to the plane of the CS) (see Fig. 5).

The motion of nonadiabatic particles in the CS is chaotic in general: plasma particles are eventually scattered and the energy accumulated by them is transformed into heat [see formula (20)]. This invites a question regarding the mechanisms leading to the generation of strongly accelerated and collimated ion beams, which are frequently observed in satellite-assisted experiments in the vicinity of Earth's magnetotail [163–165].

Although the particle dynamics in a CS are chaotic, we have succeeded in answering the question of the generation of 'regular' strongly accelerated beams of charged particles by introducing a quasi-adiabatic invariant for the fast motion component of a nonadiabatic particle and analyzing its jumps when the particle crosses the neutral plane of the CS ($z = 0$). The quasi-adiabatic invariant for oscillatory motion of a particle along the normal to the CS plane (z) is described by the formula given in Section 2.1,

$$I_z = \frac{1}{2\pi}\oint p_z \, dz . \tag{27}$$

The quantity I_z is approximately conserved along the particle trajectory, but experiences noncompensated jumps on the first and last crossing of the neutral plane in general [18, 166]. In [36], general expression (27) for I_z is adapted to the magnetic configuration of the magnetotail and the net jump ΔI_z^{Σ} occurring in the quasi-adiabatic invariant on crossing the magnetic separatrix (i.e., on the first and the last crossings of the plane $z = 0$) is computed. The net jump of the invariant ΔI_z^{Σ} is given by the sum of jumps in I_z on entering and leaving the CS:

$$\Delta I_z^{\Sigma} = \Delta I_z^{\text{in}} + \Delta I_z^{\text{out}} ,$$

where each of the jumps is determined by the value of the fast motion phase θ on crossing the separatrix. If the phase has an arbitrary value θ_S at the entrance to the CS, then on leaving it the phase is $\theta_S + \Delta\theta$, where $\Delta\theta$ is the phase shift depending on the local sheet parameters and on particle motion in the regime of fast meandering oscillations around the layer. Summing the values of jumps, after simple trigonometric calculations, we find that ΔI_z^{Σ} is extremely sensitive to the increment $\Delta\theta$ in the fast-oscillation phase of the nonadiabatic particle,

$$\Delta I_z^{\Sigma} = -\frac{3}{2}\,\kappa(x)\ln|\cos\Delta\theta + \theta_S \sin\Delta\theta| . \tag{28}$$

For certain values of $\Delta\theta$ in the 'ocean of chaos' arising already after several crossings of the CS neutral plane by particles, there are islands of regularity in the parameter space, in which the motion of a nonadiabatic particle stays practically regular. Indeed, if

$$\Delta\theta = N\pi , \tag{29}$$

where N is an integer, ΔI_z vanishes, i.e., the jump of the quasi-adiabatic invariant is fully compensated, irrespective of the initial particle phase θ_S on entering the CS. The 'chaos-generating' dependence of jumps on θ_S disappears under these conditions.

Condition (29) is known as the resonance acceleration condition, and the integer N as the resonance number. The regions of the CS where condition (29) is satisfied are called the regions of resonance acceleration or simply resonances. The resonance number N, in addition to its mathematical meaning, also has a physical meaning, being the ratio of the period of relatively slow quasi-Larmor motion of a particle in the CS plane to the period of fast oscillations in the plane perpendicular to the CS.

Thus, if the local parameters of the CS in the interaction region are such that resonance condition (29) is satisfied, stochastic jumps of the quasi-adiabatic invariant on entering and leaving the CS are mutually compensated, and the motion of a nonadiabatic particle becomes regular. In this case, almost all energy (26) gained by the particle is transformed into the kinetic energy of its directed motion along magnetic field lines. Such particles escape from the CS and move along a separatrix (separating open and closed field lines) at small pitch angles, forming narrow beamlets propagating along the magnetic field. Depending on whether the resonance number N is even or odd, particles can go into the upper (northern) or lower (southern) half-planes (Fig. 30).

In Earth's magnetotail, the magnetic separatrix divides open magnetic field lines of high-latitude tail regions going into the solar wind and closed (reconnected) field lines populated by hot and practically isotropic (over pinch angles) plasma of the plasma sheet (PS). In a finite-width layer near the separatrix (Fig. 31a), we often observe beamlets accelerated to energies that are several hundred or thousand times larger than the initial energies of charged particles entering the CS. This region is known as the boundary plasma sheet (BPS).

Figure 31b presents an example of beamlet observation by the Geotail satellite at a distance of about 280,000 km from Earth. The satellite moved from the southern part of the PS to the high-latitude part of the tail and for almost 21 min (from approximately 13:34:30 to 13:55:20 UT) stayed in the BPS, registering a beamlet propagating toward Earth along the magnetic field line at the mean speed $V_{\parallel} \approx 1000$ km s^{-1}. The beamlet was collimated over both energy and pitch angles (see the ion velocity distribution functions in Fig. 31b).

In contrast to ions, electrons observed in the BPS have an isotropic distribution function, similar to that in the PS.

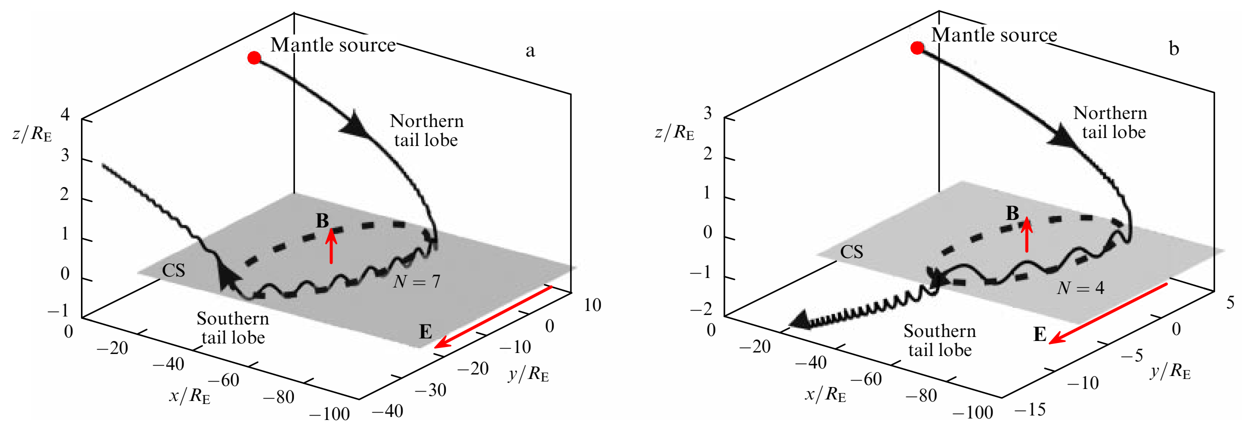

Figure 30. Example of two trajectories of nonadiabatic ions on their resonance interaction with a CS in Earth's magnetotail. The ions enter the CS from the source in the magnetosphere mantle. (a) Ion acceleration in a resonance source with the odd number $N = 7$. (b) The same, but for the even number $N = 4$ [167].

Isotropic electron distribution functions observed in the BPS simultaneously with accelerated collimated ion beams indicate that the sources of resonance ion acceleration in the CS are in the region where the field lines are already closed and the magnetic field has a small but nonzero B_z [161, 169]. In other words, the resonance acceleration of ions in the CS is not linked to the process of magnetic reconnection and can occur far enough from the X-line. For beamlet acceleration, only the nonadiabaticity condition ($\kappa < 1$) and resonance condition (29) must be satisfied.

The BPS is of immense significance for magnetospheric physics because the velocity distribution functions of charged particles observed there reflect the processes of energy transformation occurring in the distant regions of the CS. Additionally, the BPS region serves as a 'transport channel' carrying plasma energy and momentum from distant regions of the CS toward Earth. In particular, accelerated beams of charged particles precipitate in the high-latitude auroral region [170–172] and can contribute to the intensification of auroras.

Although the appearance of a resonant acceleration region hinges on fairly 'fine' kinetic effects of particle interaction with the CS, this phenomenon is sufficiently stable in practice. Numerous satellite-based observations indicate that the lifetime of beamlets in the tail BPS can be several dozen minutes, i.e., their acceleration bears a quasistationary character [162, 169, 173]. It is shown in [174] that the sources of resonance ion acceleration in the CS are indeed rather stable to magnetic field perturbations: the resonance conditions are preserved even for high-amplitude fluctuations with $\Delta B/B \sim 1.0$.

Simulation of the nonadiabatic interaction of ions with a CS in a broad vicinity of the far X-line is considered in [161] based on a large-scale kinetic model. It is found that resonance interaction condition (29) holds only in localized regions of the CS located at various distances from Earth (x). The energies ΔW of beamlets generated in resonance sources located at various radial distances from Earth differ, according to Eqn (26), due to the radial dependence of the magnetic field component $B_z(x)$ in the CS. Propagating to Earth, beamlets accelerated in different resonance sources are displaced toward the CS neutral plane (along the z direction) owing to the drift in crossed electric (E_y) and magnetic (B_x) fields. As a result, the intersection of beamlets with different energies is possible at some point (x, z) in the BPS (Fig. 32). This phenomenon is indeed repeatedly observed in the tail BPS [175].

One such example is given in Fig. 32a. The energy–time spectrogram of protons measured by CIS/CODIF (Cluster Ion Spectrometry/COmposition and DIstribution Function analyzer) [176] installed on the Cluster-4 satellite clearly reveals two beamlets propagating to Earth along magnetic field lines, with energies of approximately 5 and 30 keV, which are observed for approximately 2.5 min. Two isolated maxima correspond to these beamlets in the velocity space (see one-dimensional cross sections of proton distribution functions along the magnetic field direction). Such a 'multiplet' structure in the BPS, consisting of two or possibly several beamlets with essentially distinct energies, can only be formed due to the simultaneous action of several resonance acceleration sources in the CS.

Thus, the region of the CS where the magnetic field component perpendicular to the sheet (B_z) is small enough to satisfy the nonadiabaticity condition $\kappa < 1$ is inhomogeneous if judged by the kinetic features of trajectories of nonadiabatic ions, and consists of spatially localized regions of strong scattering and heating of ions and regions of resonance ion acceleration from where the collimated beamlets are injected into the BPS, practically without scattering. If the region of nonadiabatic ion dynamics in the CS is sufficiently large, several localized resonance acceleration regions that are isolated from each other can simultaneously function there.

For at least two isolated sources of resonance ion acceleration to exist, the characteristic spatial scale L of the magnetic field gradient $\Delta B_z(x)$ in the CS where these sources are located must exceed the maximal Larmor radius ρ_M of ions accelerated in the source with the normal magnetic field component B_z,

$$B_z \left(\frac{\Delta B_z}{L}\right)^{-1} > \rho_M \,. \tag{30}$$

In Earth's magnetotail, the condition for ions to be nonadiabatic is usually satisfied together with condition (30) in the presence of a 'long tail', where the magnetic X-line is

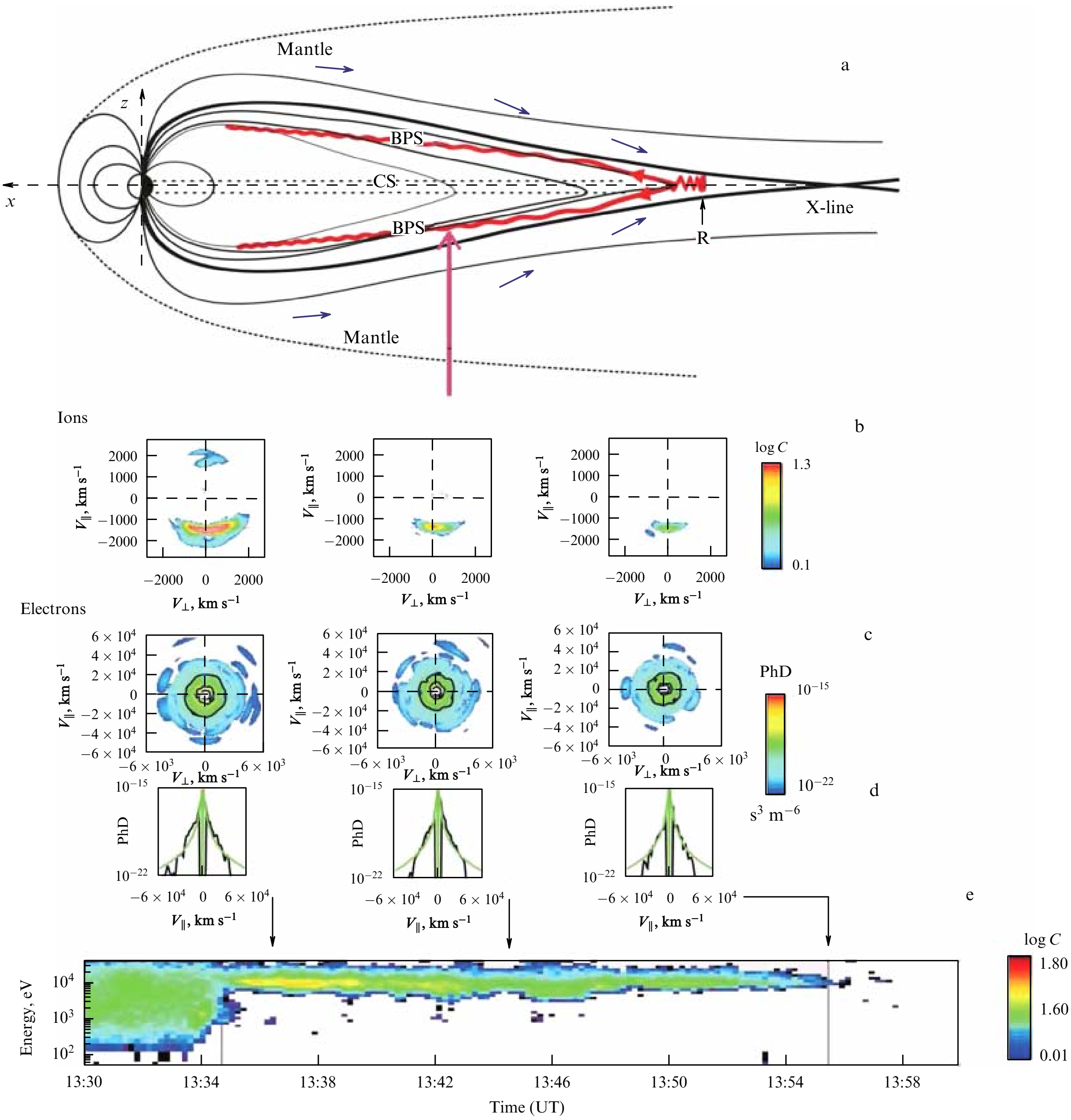

Figure 31. (Color online.) Schematic of ion acceleration in a resonance source R located in the tail CS far from the X-line. Cold ions entering the CS from the mantle (indicated by blue arrows) are accelerated in the source R and injected into the BPS, forming a beamlet collimated over energies and pitch angles (red curve), which moves toward Earth along the field lines. The magnetic separatrix is shown by the thick black line. (b–e) An example of beamlet observation by the Geotail satellite (12.12.1994): (b) Two-dimensional ion velocity distribution function (C is the number of readings for the single spectrum measurement time; the horizontal dotted line indicates that the parallel beamlet velocity does not vary over the measurement time); (c) two-dimensional electron velocity distribution functions in the plane $(V_\perp, V_\parallel)$; and (d) their one-dimensional sections along the magnetic field (PhD stands for phase distribution); (e) energy–time ion spectrogram [169] with the beamlet observation period indicated by vertical dashed lines.

formed in its far domain (at radial distances greater than 600,000 km from Earth) [169, 177] (Fig. 33a). Such a magnetic configuration is commonly encountered during quiet or weakly perturbed geomagnetic periods.

With the decrease in L, neighboring resonance sources of beamlet acceleration come closer to each other, and if condition (30) is violated, the neighboring resonance acceleration sources coalesce (Fig. 33b). If L is reduced even further, all resonances coalesce and form one common source of ion acceleration in which a beam that is broad over parallel velocities is formed because of the strong gradient of $B_z(x)$. The presence of a strong gradient in $B_z(x)$ is characteristic of a CS in the vicinity of a near X-line (Fig. 33c), which is typically formed during perturbed geomagnetic conditions [178, 179].

Thus, the change in the large-scale configuration of the magnetotail (the transition from a configuration with a far X-line to the magnetic topology with a near X-line) is reflected in the kinetic features of the dynamics of ions and their acceleration in the CS: the resonance regime of acceleration in multiple localized sources of the CS is transformed into the well-known regime of acceleration of an energetic ion beam, which is broad over parallel velocities, in the vicinity of magnetic reconnection.

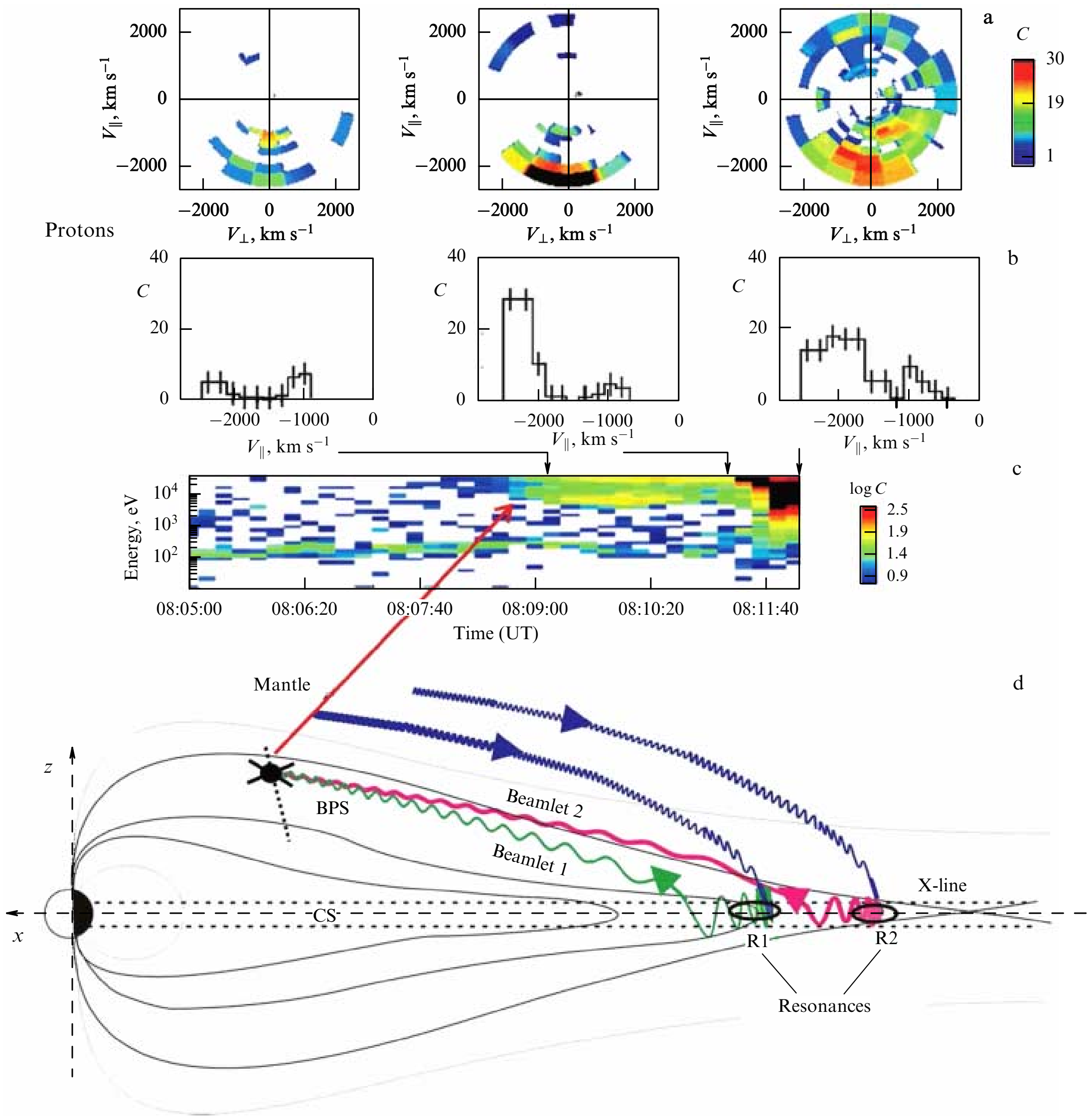

Figure 32. (Color online.) Observational example showing the intersection of two beamlets in the tail BPS by Cluster satellites (01.09.2003). (a) 2D proton velocity distribution functions in the plane ($V_\perp$, $V_\parallel$); (b) their 1D along-field cross sections measured by the CIS/CODIF instrument [176] of Cluster-4 at the time moments indicated by the red arrows (C is the number of readings for the duration of a single energy spectrum measurement); (c) energy–time spectrogram of protons [175]; (d) schematic of the intersection in the tail BPS of two beamlets accelerated in two isolated resonance sources R1 and R2 located in the far tail CS region with closed field lines.

5. Conclusion

We have discussed the main recent advances in the theory and observational studies of relatively thin current sheets in a magnetospheric plasma [19, 20–22, 43, 65, 69, 104, 112]. In reality, TCSs represent universal structures with different localizations sharing a number of properties, such as a multi-scale, multi-component, and metastable character independent of their localization, which can be the solar corona, magnetotails of planets in the Solar System, or astrophysical plasmas [6–10, 19, 32–35]. TCSs are invariably formed on the boundaries between plasmas and magnetic fields with different properties, being responsible for dynamical diversity and variability of magnetoplasma structures in space driven by instabilities evolving in them and magnetic reconnection, accompanied, in turn, by plasma turbulence, transport, and the heating of plasma particles.

We note that studies of TCSs in cosmic plasmas in many respects rely on the first studies by Syrovatskii on MHD modeling of the reconnecting current sheet in the solar corona [12–16]. These studies were foundational for clarifying the nature of flare activity on the Sun and offered an explanation of the observed behavior. Ginzburg, although not directly dealing with the problem of solar flares, was fully aware of its importance and fostered research on magnetic reconnections [11] in a CS in the theoretical department of FIAN, which he headed for almost two decades.

Knowledge on the nature of boundary current structures has deepened profoundly over recent decades. Multi-satellite missions such as Cluster helped to explore the fine structure of TCSs in Earth's magnetotail [20–22]. In parallel with observational studies, the theory of TCSs was further advanced in the 2000s [19, 80–84, 88–98]. A new hybrid model of thin current equilibria was proposed, contributing to detailed studies of the fine structure of TCSs, particle dynamics in them, and estimates of instability regions in the parameter space. A solution was proposed to the CS absolute stability paradox, which contradicted the available views on

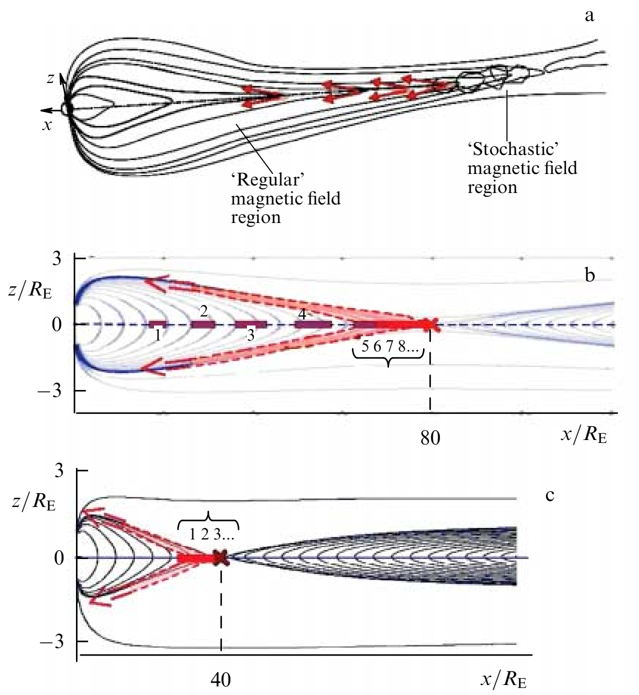

Figure 33. (Color online.) Schematics of the mechanism leading to coalescence of resonance acceleration sources in a magnetotail CS. (a) The tail magnetic configuration with the reconnection region (possibly stochastic) located in the far CS. In an extended domain L with a weak magnetic field gradient $B_z(\Delta B_z/L)^{-1} \gg \rho_M$ located on the Earth side of the reconnection region, several isolated resonance acceleration sources function simultaneously. (b) The approach of the magnetic X-line to Earth and increase in the field gradient $B_z(\Delta B_z/L)^{-1} \sim \rho_M$ trigger the coalescence of neighboring resonance acceleration sources (shown by red rectangles). (c) The tail magnetic configuration with a near X-line is associated with a strong field gradient $B_z(\Delta B_z/L)^{-1} < \rho_M$. All beamlet resonance acceleration sources merge into a single one close to the X-line, accelerating a powerful ion beam with a distribution function that is broad over parallel velocities.

the development of explosive instability as a trigger of global perturbations in Earth's magnetosphere, magnetic substorms. With the help of the hybrid model, an explanation was found for the metastable behavior of TCSs, when the instability and reconnection processes occur spontaneously in a relatively stable quasi-equilibrium background [30]. The development of the theory of TCSs helped to relate the main characteristics of the internal TCS structure to the laws of particle dynamics in this structure and kinetic plasma properties. In this review, we tried to present this aspect of TCS structure research, and in particular to show that the mechanisms of intriguing phenomena such as accelerated beamlets, complex nonmonotonic profiles of the current density and magnetic field in TCSs, and self-organization of the magnetic shear component in them are consequence of the CS kinetic features related to the complex nonlinear dynamics of charged particles.

The authors are indebted to O V Mingalev and I V Mingalev for the fruitful discussions and shared figures. The work by H V M was supported by the RFBR grants 14-02-01269 and 14-02-00769, and also by the P-9 program of the RAS; the work by E E G was supported by the Program of the Presidium of RAS (I.P7); the work by V Yu P was supported by the RFBR grants 16-02-00479 and 14-05-91000 ANF-a; and the work by L M Z was supported by the RFBR grant 16-52-16009 NTsNIL_a.

6. Appendix. Details of the model of one-dimensional current sheets and systems of equations of current equilibria

We consider equations of a simple one-dimensional model of TCSs, which deals with three components of the magnetic field $\mathbf{B} = \{B_x(z), B_y, B_z\}$ depending only on the transverse z coordinate. The tangent component of the magnetic field $B_x(z)$ changes sign in the equatorial plane $z = 0$. The spatial scale of inhomogeneities in the shear B_y and normal B_z components of the magnetic field can frequently be global in the magnetotail. Plasma equilibrium in the TCS can be maintained through the balance between the tension of magnetic field lines and finite inertia of ions [88–90]. The following general assumptions, relying on observational data for the magnetotail, are taken in constructing the model.

(1) The current layer is maintained by mutually permeating plasma flows coming from the northern and southern plasma sources (magnetospheric mantle). A schematic of the CS and directions of flows of plasma particles injected into it are depicted in Fig. 34.

(2) The magnitude of the tangent magnetic field B_x on the CS boundaries varies sufficiently slowly along the magnetotail; it can therefore be taken as constant at the sheet boundary in the model, $B_x(L) = \text{const}$. The normal magnetic field component in the tail is assumed to be uniform in space and small compared to the tangent component: $B_z/B_x(L) \approx 0.1$. In the configuration with an external shear magnetic field, its magnitude B_y^{E} is assumed to be smaller than $B_x(L)$ at the outer sheet boundaries; as a result, the magnetic field in the neutral plane is insufficiently strong to fully magnetize the ions.

(3) The TCS is considered in the de Hoffmann–Teller coordinate system [89] moving uniformly toward Earth at the speed $V_{\mathrm{d}} = cE_y/B_z$, in which the electric field in the magnetotail E_y (in the dawn–dusk direction) is equal to zero.

(4) The proton population consists of two main types of particles: Speiser particles, i.e., protons in open orbits, and quasi-trapped ions moving along quasi-closed orbits (fully

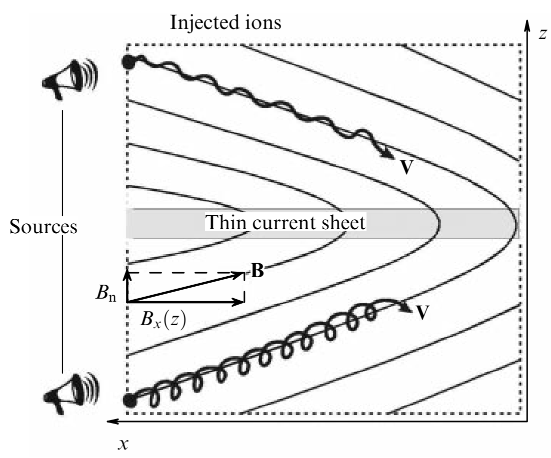

Figure 34. Schematic of the TCS model. Mutually penetrative plasma streams come to the CS neutral plane from plasma sources at infinity. Shown are the magnetic field lines, the decomposition of the magnetic field vector into tangent and normal components, and the trajectories of two protons coming from the northern and southern sources.

trapped particles are not taken into account); motion of both types of particles approximately preserves the quasi-adiabatic integrals of motion $I_z = (2\pi)^{-1}\oint p_z\,dz$ [36, 167, 181]. Quasi-trapped ions cannot carry the current entirely across the sheet, but can redistribute it locally such that the CS broadens, and the plasma profile evolves two crests, with a local current minimum in the neutral plane. The Speiser ions are considered to be the main carriers of the proton current.

(5) The TCS is 'thick' compared to the electron gyroradius, and hence the guiding center approximation can be used to describe the electron dynamics. It is assumed that electrons propagate along magnetic field lines sufficiently fast to ensure quasineutrality, such that their distribution can be taken as the Boltzmann one [90]. Drift motion of electrons is the fastest in the neutral plane because of the curvature drift (in the region with the minimal curvature of magnetic field lines).

(6) The system obeys the quasineutrality condition $n_i \approx n_e$, which allows taking electrostatic effects into account. The large-scale electric field E_y is eliminated from consideration by using the de Hoffmann–Teller coordinate system moving toward Earth at the speed $v_{dHT} = cE_y/B_z$. The component of the ambipolar electrostatic field $E_z(z)$, appearing because of the difference in dynamics of electrons and ions [90], is taken into account.

One of the most important questions for the solution of the Vlasov–Maxwell system of equations is the distribution function for the transient plasma particles. We let f_1 and f_2 denote the distribution functions of particles coming from the northern and southern hemispheres and r_1 and r_2 the particle reflection coefficients. Then the distribution of Speiser ions in the hemispheres becomes

$$f_{z>0} = \begin{cases} f_1\,, & v_\parallel < 0\,,\\ r_1 f_1 + (1-r_2) f_2\,, & v_\parallel > 0\,, \end{cases} \tag{31}$$

$$f_{z<0} = \begin{cases} r_2 f_2 + (1-r_1) f_1\,, & v_\parallel < 0\,,\\ f_2\,, & v_\parallel > 0\,. \end{cases} \tag{32}$$

The ion distribution functions at the CS boundaries are taken as shifted Maxwellian distributions,

$$f_{1,2}(\mathbf{v}) = \frac{n_{01,2}}{\left(\sqrt{\pi}\,v_{T1,2}\right)^3\left(1+\operatorname{erf}\varepsilon_{1,2}^{-1}\right)} \times \exp\left[-\frac{\left(v_\parallel \pm v_{D1,2}\right)^2 + v_\perp^2}{v_{T1,2}^2}\right] d\mathbf{v}\,. \tag{33}$$

We here set $\varepsilon_{1,2} = v_{D1,2}/v_{T1,2}$, where $v_{T1,2}$ and $v_{D1,2}$ are the respective thermal and flow plasma velocities in the northern and southern hemispheres; the plus and minus signs correspond to flows along negative ($v_\parallel < 0$) and positive ($v_\parallel > 0$) directions along the x coordinate. For simplicity, it can be assumed that the plasma sources are identical, i.e., $n_{01} = n_{02} \equiv n_0$, $v_{D1} = v_{D2} \equiv v_D$, $v_{T1} = v_{T2} \equiv v_T$, $\varepsilon_{1,2} \equiv \varepsilon$, and the coefficients r_1 and r_2 are different. The refraction coefficients are $1 - r_1$ and $1 - r_2$. The coefficients r_1 and r_2 are external to the model: their magnitudes can be taken from the results of tracing a proton beam in a model with field reversal by determining the population-mean coefficient of reflection from the CS [96]. The construction of the system of equations for thin current equilibrium is described in detail in Ref. [90]. Here, we present the main hybrid system of stationary Vlasov–Maxwell equations (with electrons and ions respectively considered within the semi-hydrodynamic and kinetic approaches) in the form

$$\begin{aligned} &\frac{df_{1,2}(\mathbf{v},z)}{dz} = 0\,,\\ &\frac{dB_x}{dz} = \frac{4\pi}{c}\left[\int v_y\left(f_{z>0}(\mathbf{v},z) + f_{z<0}(\mathbf{v},z) + f_{\text{trap}}(\mathbf{v},z)\right) d^3v + j_e(z)\right],\\ &B_x(z)\Big|_{z=L} = B_0\,,\qquad \varphi(z)\Big|_{z=L} = 0\,, \end{aligned} \tag{34}$$

where B_0 is the magnetic field outside the CS, φ is the electrostatic potential, and j_e is the electron current density. The distribution function of quasi-trapped plasma $f_{\text{trap}}(\mathbf{v},z)$ can be taken independent of the source position, in the form of the thermal Maxwellian distribution

$$f_{\text{trap}} = \frac{n_0}{\left(\pi^{1/2} v_T\right)^3\left[1+\operatorname{erf}\left(v_D/v_T\right)\right]}\exp\left(-\frac{v_D^2+v_0^2}{v_T^2}\right). \tag{35}$$

This function must match the distribution functions of Speiser ions (33) for the quasi-adiabatic invariant value $I_z = mv_0^2/\omega_0$ that separates the transient ($I_z \leqslant mv_0^2/\omega_0$) and quasi-trapped ($I_z > mv_0^2/\omega_0$) particles in the phase space of invariants I_z [97, 167]. The effect of the quasi-trapped plasma was studied in [92, 93] by introducing a weight coefficient before the function f_{trap} in Eqn (34). The third and fourth equations in (34) are boundary conditions for the magnetic and electrostatic potentials.

With the integrals of motion taken into account, the quasi-adiabatic invariant I_z takes the form

$$I_z = \frac{m}{2\pi}\oint v_z\,dz = \frac{m}{2\pi}\oint\sqrt{v^2 - \frac{2e}{m}\,\varphi - v_x^2 - v_y^2}\;dz\,.$$

Outside the TCS, it can be written as

$$I_z = \frac{2m}{\pi}\int_{z_0}^{z_1}\left[v^2 + \frac{2e}{m}\left(\varphi(z) - \varphi(z')\right) - \left(v_x - \frac{e}{mc}\,B_y(z-z')\right)^2 - \left(v_y + \frac{e}{mc}\int_{z'}^{z} B_x(z'')\,dz''\right)^2\right]^{1/2} dz\,. \tag{36}$$

The integration limits over z in Eqn (36) are the vanishing points of the integrand:

$$-\frac{e}{mc}\int_z^{z_{0,1}} B_x(z'')\,dz'' = v_y \pm \left\{v^2 + \frac{2e}{m}\left(\varphi(z) - \varphi(z_{0,1})\right) - \left[v_x + \frac{e}{mc}\,B_y(z - z_{0,1})\right]^2\right\}^{1/2}. \tag{37}$$

An additional condition must also be imposed: if a solution $z_0 < 0$ is obtained, it must be replaced with zero ($z_0 = 0$) in Eqn (34).

Using the relation between the magnetic moment of the particle $\mu \equiv mv_\perp^2/(2B_0)$ and the adiabatic invariant I_z outside the TCS, $\mu = (e/2mc)I_z$, the source distribution function can be written in terms of the invariants of motion $\{v_0, I_z\}$ ($v_0 = \sqrt{2W_0/m}$, where W_0 is the total energy of particles) and extrapolated over the entire space with the help of the

Liouville theorem [89]:

$$f_{1,2}(\mathbf{v}) = \frac{n_0}{(\pi v_{\mathrm{T}})^3 \left(1 + \operatorname{erf} \varepsilon^{-1}\right)} \times \exp\left\{ -\frac{1}{v_{\mathrm{T}}^2} \left[\left(\sqrt{v_0^2 - \frac{\omega_0}{m} I_z - \frac{2e}{m} \varphi} \pm v_{\mathrm{D}} \right)^2 + \frac{\omega_0}{m} I_z \right] \right\}. \tag{38}$$

A similar approach is used to transform the distribution function of quasi-trapped plasma (35). The second equation in (34) can be transformed into the form

$$\frac{\mathrm{d}B_x}{\mathrm{d}z} = \frac{4\pi}{c} \left\{ \int v_y \left[f_{z>0}\left(W_0(\mathbf{v}), I_z(\mathbf{v}, z)\right) + f_{z<0}\left(W_0(\mathbf{v}), I_z(\mathbf{v}, z)\right) + f_{\mathrm{trap}} \right] \mathrm{d}^3 v + j_{\mathrm{e}}(z) \right\}. \tag{39}$$

Electrons in the TCS, in contrast to ions, are fully magnetized and can therefore contribute to the current across the tail through their drift.

We now outline the basic derivation of the corresponding equations of the semi-hydrodynamic approximation. In the general form, the equation of motion of an electron in the hydrodynamic approximation with the mirror force taken into account is

$$m_{\mathrm{e}} \frac{\mathrm{d}\mathbf{u}_{\mathrm{e}}}{\mathrm{d}t} = -e\left(\mathbf{E} + \frac{1}{c}[\mathbf{u}_{\mathrm{e}} \times \mathbf{B}]\right) - \frac{\operatorname{div} \hat{\mathbf{P}}_{\mathrm{e}}}{n_{\mathrm{e}}} - \mu \nabla B\,, \tag{40}$$

where m_{e} and e are the mass and charge of the electron, $\mathbf{u}_{\mathrm{e}}$ and n_{e} are the electron hydrodynamic velocity and concentration, $B = |\mathbf{B}|$, μ is the mean magnetic moment of electrons, and $\hat{\mathbf{P}}_{\mathrm{e}}$ is the electron pressure tensor. We consider electrons to be a fluid with the gyrotropic pressure tensor

$$\hat{\mathbf{P}}_{\mathrm{e}} = p_{\mathrm{e}\perp} \hat{\mathbf{I}} + (p_{\mathrm{e}\parallel} - p_{\mathrm{e}\perp})\, \mathbf{b} \otimes \mathbf{b}\,, \tag{41}$$

where $\hat{\mathbf{I}}$ is the unit tensor and $\mathbf{b} \otimes \mathbf{b}$ is the diadic tensor formed by a unit vector along the magnetic field $\mathbf{b} = \mathbf{B}/B$ [102]. Then

$$\operatorname{div} \hat{\mathbf{P}}_{\mathrm{e}} = \nabla_\perp p_{\mathrm{e}\perp} + (p_{\mathrm{e}\parallel} - p_{\mathrm{e}\perp})(\mathbf{b}, \nabla)\, \mathbf{b} + (p_{\mathrm{e}\parallel} - p_{\mathrm{e}\perp})\, \mathbf{b} \operatorname{div} \mathbf{b} + (\mathbf{b}, \nabla p_{\mathrm{e}\parallel})\, \mathbf{b}\,, \tag{42}$$

and from the equation of motion, using the equality $\operatorname{div} \mathbf{b} = -(\mathbf{b}, \nabla B)/B$, we arrive at the equation of motion along the magnetic field lines

$$m_{\mathrm{e}} \frac{\mathrm{d}\mathbf{u}_{\mathrm{e}\parallel}}{\mathrm{d}t} = -e\mathbf{E}_\parallel - \frac{\nabla_\parallel p_{\mathrm{e}\parallel}}{n_{\mathrm{e}}} + \frac{1}{n_{\mathrm{e}}}(p_{\mathrm{e}\parallel} - p_{\mathrm{e}\perp}) \nabla_\parallel (\ln B) - \mu \nabla_\parallel B\,, \tag{43}$$

where $\mathbf{E}_\parallel = -\nabla_\parallel \Phi(z)$ and $\Phi(z)$ is the electrostatic potential. According to the drift theory in the case under consideration, the current density of magnetized electrons in the direction orthogonal to the magnetic field is written in the zeroth approximation as

$$\mathbf{j}_{\mathrm{e}\perp} = -e n_{\mathrm{e}} c\, \frac{\mathbf{E} \times \mathbf{b}}{B} + \frac{c}{B}[\mathbf{b} \times \nabla_\perp p_{\mathrm{e}\perp}] + \frac{c}{B}(p_{\mathrm{e}\parallel} - p_{\mathrm{e}\perp})\left[\mathbf{b} \times (\mathbf{b}, \nabla)\, \mathbf{b}\right]. \tag{44}$$

Assuming the equilibration process to be isothermal, we use the equation of state

$$p_{\mathrm{e}\parallel} = n_{\mathrm{e}} T_{\mathrm{e}\parallel}\,, \qquad p_{\mathrm{e}\perp} = n_{\mathrm{e}} T_{\mathrm{e}\perp}\,. \tag{45}$$

Neglecting electron inertia, Eqns (42) and (43) can be written as

$$T_{\mathrm{e}\parallel} \nabla_\parallel (\ln n_{\mathrm{e}}) = e \nabla_\parallel \Phi + (T_{\mathrm{e}\parallel} - T_{\mathrm{e}\perp})\, \nabla_\parallel (\ln B) - \mu \nabla_\parallel B\,. \tag{46}$$

Integrating Eqn (46) from z to $+\infty$ with the quasineutrality condition

$$n_{\mathrm{e}}(z) = n_{\mathrm{i}}(z)\,, \tag{47}$$

the condition at infinity in Eqn (8), and the assumption $\mu = \mathrm{const}$ leads to the equality

$$T_{\mathrm{e}\parallel} \ln \frac{n_0}{n_{\mathrm{e}}(z)} = e\left(\Phi_0 - \Phi(z)\right) + (T_{\mathrm{e}\parallel} - T_{\mathrm{e}\perp}) \ln \frac{B}{B(z)} - \mu\left(B_0 - B(z)\right), \tag{48}$$

which can be rewritten in a form analogous to the Boltzmann distribution for isothermal electrons:

$$\frac{n_{\mathrm{e}}(z)}{n_0} = \left(\frac{B(z)}{B_0}\right)^{1 - T_{\mathrm{e}\perp}/T_{\mathrm{e}\parallel}} \exp\left[\frac{e\left(\Phi(z) - \Phi_0\right) - \mu\left(B(z) - B_0\right)}{T_{\mathrm{e}\parallel}}\right]. \tag{49}$$

Thus, in the model, electrons are assumed to be a fluid in the direction parallel to the magnetic field, but are treated in the guiding center approximation in the perpendicular direction. We refer to such an approach as 'semihydrodynamic'. Under the assumptions made, the electrons satisfy the Boltzmann approximation. To account for them, three additional input parameters must be introduced: $T_{\mathrm{e}\perp}$, $T_{\mathrm{e}\parallel}$, and μ.

We note that the distribution functions in the right-hand side of Eqn (39) depend only on the particle integrals of motion, and the electron current is obtained in the Boltzmann approximation [90] (34)–(49) with regard for the anisotropy of the electron pressure. Recalling that $\mathbf{B} = -\mathrm{rot}\, \mathbf{A}$, where $\mathbf{A}$ is the vector potential, Eqn (39) can be rewritten as the Grad–Shafranov equation $-\mathrm{rot}\, \mathbf{A} = (4\pi/c)\, j\,(\mathbf{A})$, a peculiar feature of which is the presence of nonlocal (integral) constraints related to the quasi-adiabatic invariants of motion.

Introducing the dimensionless variables $(x, y, z) = (x^*, y^*, z^*)\omega_0/\varepsilon^{4/3} v_{\mathrm{D}}$, where x^*, y^*, and z^* are dimensional coordinates (in this review, the dimensionless coordinate z is sometimes denoted as ζ), $b_{x,y,z} = B_{x,y,z}/B_0$, and $n = \tilde{n}/n_0$ (where $\omega_0 = eB_0/(mc)$ is the proton gyrofrequency, $B_0 = (B_{x0}^2 + B_{y0}^2 + B_{z0}^2)^{1/2}$ is the full magnetic field at the TCS boundary, J_y is the current density through the sheet, $\varepsilon = v_{\mathrm{T}}/v_{\mathrm{D}}$, and v_{T} and v_{D} are the thermal and drift velocities of plasma at the TCS boundaries), we see that system of equations (34)–(49) depends on several free parameters [90], in particular, on the flow asymmetry ε and the normal magnetic field component b_z. Some parameters can be determined from the boundary conditions, which for the TCS can be conveniently specified far from the neutral plane. It has been shown that the boundary conditions for system of equations (34) for a TCS imply the marginal firehose condition [88, 89, 101, 182]

$$p_{\parallel 0} - p_{\perp 0} = \frac{B_0^2}{4\pi}\,, \tag{50}$$

where $p_{\parallel 0}$ and $p_{\perp 0}$ are the parallel and perpendicular components of the plasma pressure tensor outside the TCS.

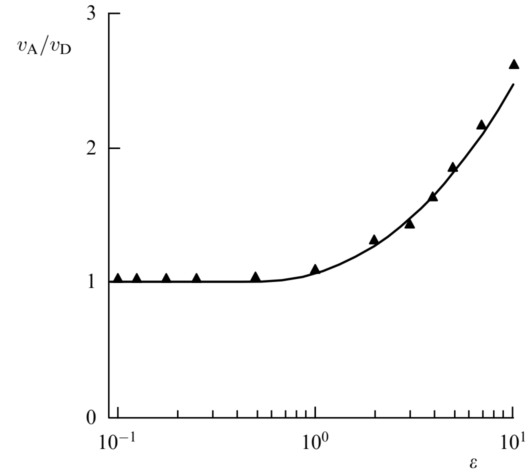

Figure 35. Test of the marginal firehose condition for a TCS [88]: the solid line plots the analytical dependence of the ratio of the Alfvén velocity to drift velocity v_A/v_D on the parameter $\varepsilon = v_T/v_D$, and the triangles correspond to numerical computations.

As shown in Refs [88, 101, 182], this condition is a direct consequence of the balance of forces acting along the magnetotail symmetry axis x. Furthermore, it is shown in Ref. [101] that for the Maxwellian distribution of form (33), condition (50) reduces to

$$\frac{v_A}{v_D} = \sqrt{1 + \frac{\varepsilon}{1 + \operatorname{erf} \varepsilon^{-1}} \frac{\exp \varepsilon^{-2}}{\pi^{1/2}}} . \tag{51}$$

where $v_A = B_0/\sqrt{4\pi n_0 m}$ is the Alfvén velocity (or the speed of magnetoacoustic waves). Accordingly, the fulfillment of relations (50) and (51) can serve as a test for the correctness of a self-consistent numerical solution. In Fig. 35, we compare results of a numerical solution of Eqns (34)–(44) and the values of expression (51) and present a test of marginal firehose condition (50). As follows from the figure, theoretical and numerical results agree well with each other: the condition of marginal firehose stability in a one-dimensional equilibrium TCS, needed for equilibrium, is observed with high accuracy, which was confirmed later in Refs [88, 157].

References

1. Ginzburg V L *The Physics of a Lifetime. Reflections on the Problems and Personalities of 20th Century Physics* (Berlin: Springer, 2001); Translated from Russian: *O Fizike i Astrofizike. Stat'i i Vystupleniya* (Moscow: Nauka, 1992)
2. Ginzburg V L *Phys. Usp.* **42** 353 (1999); *Usp. Fiz. Nauk* **169** 419 (1999)
3. Ginzburg V L *Sov. Phys. Usp.* **15** 839 (1973); *Usp. Fiz. Nauk* **108** 749 (1972)
4. Ginzburg V L, Landau L D, in Landau L D *Collected Papers* (Oxford: Pergamon Press, 1965) p. 546; Translated from Russian: *Zh. Eksp. Teor. Fiz.* **20** 1064 (1950)
5. Ginzburg V L *Phys. Usp.* **40** 407 (1997); *Usp. Fiz. Nauk* **167** 429 (1997)
6. Ginzburg V L *Phys. Usp.* **47** 1155 (2004); *Usp. Fiz. Nauk* **174** 1240 (2004)
7. Ginzburg V L *Usp. Fiz. Nauk* **62** 37 (1957)
8. Ginzburg V L, Syrovatskii S I *Sov. Phys. Usp.* **3** 504 (1961); *Usp. Fiz. Nauk* **71** 411 (1960)
9. Ginzburg V L, Syrovatskii S I *Sov. Phys. Usp.* **9** 223 (1966); *Usp. Fiz. Nauk* **88** 485 (1966)
10. Ginzburg V L *Phys. Usp.* **36** 587 (1993); *Usp. Fiz. Nauk* **163** (7) 45 (1993)
11. Frank A G *Phys. Usp.* **53** 941 (2010); *Usp. Fiz. Nauk* **180** 982 (2010)
12. Syrovatskii S I *Usp. Fiz. Nauk* **62** 247 (1957)
13. Somov B V, Syrovatskii S I "Neutral current sheets in plasmas" *Proc. Lebedev Phys. Inst.* Vol. 74 (Ed. N G Basov) (New York: Consultants Bureau, 1976) p. 13; Translated from Russian: "Neitral'nye tokovye sloi v plazme" *Trudy Fiz. Inst. Akad. Nauk SSSR* Vol. 74 (Ed. N G Basov) (Moscow: Nauka, 1974) p. 14
14. Somov B V, Syrovatskii S I *Bull. Acad. Sci. USSR Phys. Ser.* **39** (2) 109 (1975); *Izv. Akad. Nauk SSSR Ser. Fiz.* **39** 375 (1975)
15. Syrovatskii S I *Vestn. Akad. Nauk SSSR* (10) 33 (1977)
16. Artemyev A V et al. *J. Geophys. Res. Space Phys.* **118** 2789 (2013)
17. Syrovatskii S I *Sov. Phys. JETP* **33** 933 (1971); *Zh. Eksp. Teor. Fiz.* **60** 1727 (1971)
18. Speiser T W *J. Geophys. Res.* **70** 4219 (1965)
19. Zelenyi L M et al. *Plasma Phys. Rep.* **37** 118 (2011); *Fiz. Plazmy* **37** 137 (2011)
20. Sergeev V A et al. *J. Geophys. Res.* **98** 17345 (1993)
21. McPherron R L et al., in *Quantitative Modeling of Magnetosphere-Ionosphere Coupling Processes* (Eds Y Kamide, R A Wolf) (Kyoto, Japan: Kyoto Sangyo Univ., 1987) p. 252
22. Runov A et al. *Geophys. Res. Lett.* **30** 1579 (2003)
23. Sun W-J et al. *Geophys. Res. Lett.* **42** 3692 (2015)
24. Halekas J S et al. *Geophys. Res. Lett.* **33** L13101 (2006)
25. Somov B V *Phys. Usp.* **53** 954 (2010); *Usp. Fiz. Nauk* **180** 997 (2010)
26. Arons J *Space Sci. Rev.* **173** 341 (2012)
27. Lembege B, Pellat R *Phys. Fluids* **25** 1995 (1982)
28. Pellat R, Coroniti F V, Pritchett P L *Geophys. Res. Lett.* **18** 143 (1991)
29. Lui A T Y *Space Sci. Rev.* **113** 127 (2004)
30. Zelenyi L et al. *J. Atmos. Solar Terr. Phys.* **70** 325 (2008)
31. Galeev A A, Zelenyi L M *Sov. Phys. JETP* **43** 1113 (1976); *Zh. Eksp. Teor. Fiz.* **70** 2133 (1976)
32. Lui A T Y et al. *J. Geophys. Res.* **97** 1461 (1992)
33. Pulkkinen T I et al. *J. Geophys. Res.* **99** 5793 (1994)
34. Somov B V, Verneta A I *Space Sci. Rev.* **65** 253 (1993)
35. Ledentsov L S, Somov B V *Phys. Usp.* **58** 107 (2015); *Usp. Fiz. Nauk* **185** 113 (2015)
36. Büchner J, Zelenyi L M *J. Geophys. Res.* **94** 11821 (1989)
37. Zelenyi L M, Grigorenko E E, Fedorov A O *JETP Lett.* **80** 771 (2004); *Pis'ma Zh. Eksp. Teor. Fiz.* **80** 771 (2004)
38. Edmondson J K et al. *Astrophys. J.* **707** 1427 (2009)
39. Baryshnikova Y et al. *Astron. Astrophys.* **177** 27 (1987)
40. Beck R et al. *Annu. Rev. Astron. Astrophys.* **34** 155 (1996)
41. Bykov A et al. *Mon. Not. R. Astron. Soc.* **289** 1 (1997)
42. Bykov A et al. *Acta Astron. Geophys. Univ. Comenianae* **19** 13 (1997)
43. Beskin V S *Phys. Usp.* **40** 659 (1997); *Usp. Fiz. Nauk* **167** 689 (1997)
44. Romanova M M et al. *Astrophys. J.* **588** 400 (2003)
45. Vasko I Yu, Popov V Yu *Moscow Univ. Phys. Bull.* **67** (1) 37 (2012); *Vestn. Mosk. Univ. Ser. 3 Fiz. Astron.* **67** (1) 38 (2012)
46. Priest E, Forbes T *Magnetic Reconnection MHD Theory and Applications* (Cambridge: Cambridge Univ. Press, 2000); Translated into Russian: *Magnitnoe Peresoedinenie: Magnitogidrodinamicheskaya Teoriya i Prilozheniya* (Moscow: Fizmatlit, 2005)
47. Forbes T G *J. Geophys. Res.* **105** (A10) 23153 (2000)
48. Pojoga S, Huang T S *Adv. Space Res.* **32** 2641 (2003)
49. Webb D F, Howard T A *Living Rev. Solar Phys.* **9** 3 (2012)
50. Somov B V, Syrovatskii S I *Sov. Phys. Usp.* **19** 813 (1976); *Usp. Fiz. Nauk* **120** 217 (1976)
51. Ginzburg V L et al. *Sov. Phys. Usp.* **23** 274 (1980); *Usp. Fiz. Nauk* **131** 73 (1980)
52. Parker E N *J. Geophys. Res.* **62** 509 (1957)
53. Petschek H E, in *The Physics of Solar Flares. Proc. of the AAS/NASA Symp. on the Physics of Solar Flares, 28–30 October, 1963, Greenbelt, MD* (Eds W N Hess) (Washington, DC: NASA Science and Technical Information Division, 1964) p. 425
54. Shibata K, Magara T *Living Rev. Solar Phys.* **8** 6 (2011)
55. Sturrock P A *Nature* **211** 695 (1966)
56. Hirayama T *Solar Phys.* **34** 323 (1974)
57. Kopp R A, Pneuman G W *Solar Phys.* **50** 85 (1976)
58. Bazilevskaya G A *Space Sci. Rev.* **186** 409 (2014)
59. Solanki S K *Astron. Astrophys. Rev.* **11** 153 (2003)

60. Buchner J *Space Sci. Rev.* **122** 149 (2006)
61. Bemporad A et al. *Astrophys. J.* **638** 1110 (2006)
62. Ness N F *J. Geophys. Res.* **70** 2989 (1965)
63. Petrukovich A A et al. *Space Sci. Rev.* **188** 311 (2015)
64. Tsurutani B T et al. *Earth Planets Space* **61** 555 (2009)
65. Sharma A S et al. *Ann. Geophys.* **26** 1 (2008)
66. Sanny J et al. *J. Geophys. Res.* **99** 5805 (1994)
67. Speiser T W *J. Geophys. Res.* **70** 1717 (1965)
68. Mitchell D G et al. *Geophys. Res. Lett.* **17** 583 (1990)
69. Runov A et al. *Ann. Geophys.* **23** 1 (2005)
70. Kropotkin A P, Lui A T Y *J. Geophys. Res.* **100** (A9) 17231 (1995)
71. Coppi B, Laval G, Pellat R *Phys. Rev. Lett.* **16** 1207 (1966)
72. Baker D N et al. *J. Geophys. Res.* **101** (A6) 12975 (1996)
73. Landau L D, Lifshitz E M *Mechanics* (Oxford: Butterworth-Heinemann, 1976); Translated from Russian: *Mekhanika* (Moscow: Fizmatlit, 2001)
74. Harris E G *Nuovo Cimento* **23** 115 (1962)
75. Galeev A A, in *Basic Plasma Physics* (Eds A A Galeev, R N Sudan) (Amsterdam: North-Holland, 1983); *Osnovy Fiziki Plazmy* (Eds A A Galeev, R Sudan) Vol. 1 (Moscow: Energoatomizdat, 1983) p. 331
76. Birn J, Sommer R R, Schindler K *J. Geophys. Res.* **82** 147 (1977)
77. Schindler K, in *Earth's Magnetospheric Processes. Proc. of a Symp., Cortina, Italy, August 30 – September 10, 1971* (Astrophysics and Space Science Library, Vol. 32, Ed. B M McCormac) (Berlin: Springer, 1972) p. 200
78. Yoon P H, Lui A T Y *J. Geophys. Res.* **109** A11213 (2004)
79. Lui A T Y, Chang C-L, Yoon P H *J. Geophys. Res.* **100** 19147 (1995)
80. Kan J R *J. Geophys. Res.* **78** 3773 (1973)
81. Schindler K, Birn J *J. Geophys. Res.* **107** (A8) 1193 (2002)
82. Birn J, Schindler K *J. Geophys. Res.* **107** (A7) 1117 (2002)
83. Birn J, Sommer R, Schindler K *Astrophys. Space Sci.* **35** 389 (1975)
84. Eastwood J W *Planet Space Sci.* **20** 1555 (1972)
85. Ashour-Abdalla M et al. *J. Geophys. Res.* **99** (A8) 14891 (1994)
86. Kropotkin A P, Domrin V I *J. Geophys. Res.* **101** 19893 (1996)
87. Kropotkin A P, Malova H V, Sitnov M I *J. Geophys. Res.* **102** 22099 (1997)
88. Sitnov M I et al. *J. Geophys. Res.* **105** 13029 (2000)
89. Zelenyi L et al. *Nonlin. Proc. Geophys.* **7** 127 (2000)
90. Zelenyi L M et al. *Nonlin. Proc. Geophys.* **11** 579 (2004)
91. Malova H V et al. *J. Geophys. Res.* **118** 4308 (2013)
92. Zelenyi L M et al. *Geophys. Res. Lett.* **29** 1608 (2002)
93. Zelenyi L M et al. *Cosmic Res.* **40** 357 (2002); *Kosmich. Issled.* **40** 385 (2002)
94. Zelenyi L M et al. *Geophys. Res. Lett.* **33** L05105 (2006)
95. Malova H V et al. *Geophys. Res. Lett.* **34** L16108 (2007)
96. Malova H V et al. *J. Geophys. Res.* **117** A04212 (2012)
97. Zelenyi L M et al. *Ann. Geophys.* **27** 861 (2009)
98. Zelenyi L M et al. *Cosmic Res.* **47** 352 (2009); *Kosmich. Issled.* **47** 388 (2009)
99. Artemyev A V et al. *Ann. Geophys.* **27** 4075 (2009)
100. Mingalev O V et al. *Plasma Phys. Rep.* **33** 942 (2007); *Fiz. Plazmy* **33** 1028 (2007)
101. Burkhart G R et al. *J. Geophys. Res.* **97** (A9) 13799 (1992)
102. Mingalev O V et al. *Plasma Phys. Rep.* **35** 76 (2009); *Fiz. Plazmy* **35** 85 (2009)
103. Kuznetsova M M, Hesse M, Winske D *J. Geophys. Res.* **101** 27351 (1996)
104. Zelenyi L M et al. *Phys. Usp.* **53** 933 (2010); *Usp. Fiz. Nauk* **180** 973 (2010)
105. Zelenyi L M et al. *Phys. Usp.* **56** 347 (2013); *Usp. Fiz. Nauk* **183** 365 (2013)
106. Cary J R, Escande D F, Tennyson J L *Phys. Rev. A* **34** 4256 (1986)
107. Neishtadt A I *J. Appl. Math. Mech.* **51** 586 (1987); *Prikl. Matem. Mekh.* **51** 750 (1987)
108. Lui A T Y *J. Geophys. Res.* **98** 13423 (1993)
109. Bykov A A, Zelenyi L M, Malova Kh V *Plasma Phys. Rep.* **34** 128 (2008); *Fiz. Plazmy* **34** 148 (2008)
110. Pritchett P L, Coroniti F V *J. Geophys. Res.* **97** 16773 (1992)
111. Ashour-Abdalla M et al. *J. Geophys. Res.* **101** 2587 (1996)
112. Runov A et al. *Ann. Geophys.* **24** 247 (2006)
113. Whang Y C *J. Geophys. Res.* **82** 1024 (1977)
114. Øieroset M et al. *Nature* **412** 414 (2001)
115. Nakamura R et al. *J. Geophys. Res.* **113** A07S16 (2008)
116. Buechner J, Kuznetsova M, Zelenyi L M *Geophys. Res. Lett.* **18** 385 (1991)
117. Zhu Z, Parks G *J. Geophys. Res.* **98** (A5) 7603 (1993)
118. Delcourt D C, Belmont G *J. Geophys. Res.* **103** 4605 (1998)
119. Shen C et al. *Ann. Geophys.* **26** 3525 (2008)
120. Paolo R et al. *Phys. Plasmas* **11** 4102 (2004)
121. Pritchett P L, Coroniti F V *J. Geophys. Res.* **109** A01220 (2004)
122. Pritchett P L, Mozer F S *J. Geophys. Res.* **114** A11210 (2009)
123. Fairfield D H *J. Geophys. Res.* **84** 1950 (1979)
124. Lui A T Y, in *Magnetospheric Currents. Chapman Conf., Irvington, VA, April 5 – 8, 1983, Selected Papers* (Washington, DC: American Geophysical Union, 1984) p. 158
125. Sergeev V A *Geomagn. Aeronom.* **27** 612 (1987)
126. Kaumaz Z et al. *J. Geophys. Res.* **99** 11113 (1994)
127. Petrukovich A A *J. Geophys. Res.* **116** A07217 (2011)
128. Rong Z J et al. *J. Geophys. Res.* **117** A06216 (2012)
129. Grigorenko E E et al. *J. Geophys. Res.* **118** 3265 (2013)
130. Eastwood J P et al. *J. Geophys. Res.* **112** A06235 (2007)
131. Grigorenko E E et al. *Plasma Phys. Rep.* **41** 88 (2015); *Fiz. Plazmy* **41** 92 (2015)
132. Wang R et al. *J. Geophys. Res.* **117** A07223 (2012)
133. Deng X H et al. *J. Geophys. Res.* **109** A05206 (2004)
134. Liu C et al. *J. Geophys. Res.* **118** 2087 (2013)
135. Shen C et al. *J. Geophys. Res.* **113** A07S21 (2008)
136. Lee K-W, Hau L-N *J. Geophys. Res.* **113** A12209 (2008)
137. Kuznetsova M M, Zelenyi L M *Geophys. Res. Lett.* **18** 1825 (1991)
138. Karimabadi H et al. *J. Geophys. Res.* **110** A03213 (2005)
139. Hau L-N, Voigt G-H *J. Geophys. Res.* **97** (A6) 8707 (1992)
140. Belehaki A et al. *Ann. Geophys.* **16** 528 (1998)
141. Kan J R *J. Geophys. Res.* **112** A01207 (2007)
142. Cowley S W H *Planet. Space Sci.* **29** 79 (1981)
143. Birn J, Hesse M *J. Geophys. Res.* **99** 109 (1994)
144. Hilmer R V, Voigt G-H *J. Geophys. Res.* **92** 8660 (1987)
145. Kaufmann R L, Chen L, Larson D J *J. Geophys. Res.* **99** 11277 (1994)
146. Holland D L, Chen J, Agranov A *J. Geophys. Res.* **101** 24997 (1996)
147. Delcourt D C, Zelenyi L M, Sauvaud J-A *J. Geophys. Res.* **105** 349 (2000)
148. Artemyev A V, Neishtadt A I, Zelenyi L M *Nonlin. Process. Geophys.* **20** 899 (2013)
149. Lemaire J, Roth M *Space Sci. Rev.* **57** 59 (1991)
150. Moses J J et al. *J. Geophys. Res.* **90** 11078 (1985)
151. Tsyganenko N A, Stern D P, Kaymaz Z *J. Geophys. Res.* **98** (A11) 19455 (1993)
152. Hau L-N, Erickson G M *J. Geophys. Res.* **100** (A11) 21745 (1995)
153. Cowley S W H *Planet. Space Sci.* **27** 769 (1979)
154. Richardson A, Chapman S C *J. Geophys. Res.* **99** 17391 (1994)
155. Chapman S C, Mouikis C G *Geophys. Res. Lett.* **23** 3251 (1996)
156. Hoshino M et al. *J. Geophys. Res.* **101** (A11) 24775 (1996)
157. Mingalev O V et al. *Plasma Phys. Rep.* **38** 300 (2012); *Fiz. Plazmy* **38** 329 (2012)
158. Zelenyi L M, Zogin D V *Cosmic Res.* **28** 369 (1990); *Kosmich. Issled.* **28** 430 (1990)
159. Malova H V et al. *J. Geophys. Res.* **118** 4308 (2013)
160. Nakamura R et al. *Space Sci. Rev.* **122** 29 (2006)
161. Shabanskii V P *Yavleniya v Okolozemnom Prostranstve* (Phenomena in the Near-Earth Space) (Moscow: Nauka, 1972)
162. Ashour-Abdalla M et al. *J. Geophys. Res.* **98** 5651 (1993)
163. Lyons L R, Speiser T W *J. Geophys. Res.* **87** 2276 (1982)
164. DeCoster R J, Frank L A *J. Geophys. Res.* **84** 5099 (1979)
165. Parks G et al. *Geophys. Res. Lett.* **25** 3285 (1998)
166. Grigorenko E E, Fedorov A O, Zelenyi L M *Ann. Geophys.* **20** 329 (2002)
167. Sonnerup B U O *J. Geophys. Res.* **76** 8211 (1971)
168. Zelenyi L M et al. *JETP Lett.* **85** 187 (2007); *Pis'ma Zh. Eksp. Teor. Fiz.* **85** 225 (2007)
169. Eastman T E et al. *J. Geophys. Res.* **89** 1553 (1984)
170. Grigorenko E E et al. *J. Geophys. Res.* **114** A03203 (2009)

171. Zelenyi L M, Kovrazhkin R A, Bosqued J M *J. Geophys. Res.* **95** 12119 (1990)
172. Bosqued J M et al. *J. Geophys. Res.* **98** 19181 (1993)
173. Sauvaud J-A, Kovrazhkin R A *J. Geophys. Res.* **109** A12213 (2004)
174. Grigorenko E E, Sauvaud J-A, Zelenyi L M *J. Geophys. Res.* **112** A05218 (2007)
175. Dolgonosov M S et al. *J. Geophys. Res.* **118** 5445 (2013)
176. Zelenyi L M et al. *Geophys. Res. Lett.* **33** L06105 (2006)
177. Rème H et al. *Ann. Geophys.* **19** 1303 (2001)
178. Grigorenko E E et al. *Space Sci. Rev.* **164** 133 (2011)
179. Borg A L et al. *Geophys. Res. Lett.* **32** L19105 (2005)
180. Sergeev V A et al. *Geophys. Res. Lett.* **34** L02103 (2007)
181. Sonnerup B U O *J. Geophys. Res.* **76** 8211 (1971)
182. Hill T W, Voigt G-H *Geophys. Res. Lett.* **12** 2441 (1992)